NONLINEAR ESTIMATION

APPLIED TO

^{13}C NMR STUDIES OF

MULTICOMPONENT EQUILIBRIUM

by

David George Naugler

B.Sc., University of Toronto, 1972

A THESIS SUBMITTED IN PARTIAL FULFILLMENT OF

THE REQUIREMENTS FOR THE DEGREE OF

MASTER OF SCIENCE

in the Department

of

Chemistry

SIMON FRASER UNIVERSITY

June 1979

APPROVAL

Name: David George Naugler

Degree: Master of Science

Title of Thesis: Nonlinear Estimation Applied to ^{13}C NMR Studies of Multicomponent Equilibrium

Examining Committee:

Chairman: Dr. T.N. Bell

Dr. R.J. Cushley
Senior Supervisor

Dr. G.L. Malli

Dr. E.J. Wells

Dr. I.D. Gay
External Examiner

Date Approved: June 1, 1979

PARTIAL COPYRIGHT LICENSE

I hereby grant to Simon Fraser University the right to lend my thesis, project or extended essay (the title of which is shown below) to users of the Simon Fraser University Library, and to make partial or single copies only for such users or in response to a request from the library of any other university, or other educational institution, on its own behalf or for one of its users. I further agree that permission for multiple copying of this work for scholarly purposes may be granted by me or the Dean of Graduate Studies. It is understood that copying or publication of this work for financial gain shall not be allowed without my written permission.

Title of Thesis/Project/Extended Essay

NONLINEAR ESTIMATION APPLIED TO ^{13}C NMR STUDIES OF MULTICOMPONENT EQUILIBRIUM

Author:

(signature)

DAVID G. NAUGLER

(name)

July 11, 1979

(date)

ABSTRACT

A. Two anhydropolyhydric alcohols, 1,4-anhydroerythritol and 1,4-anhydrothreitol, were synthesized from the corresponding tetratols via acid catalyzed dehydration, under vacuum, using H^+ cationic ion exchange resin. Comparison of temperature dependent ^{13}C NMR chemical shifts in aqueous and non-aqueous solvents demonstrated a significant molecular association interaction between 1,4-anhydroerythritol and water. Further experiments showed a dependence of the ^{13}C NMR chemical shifts of 1,4-anhydroerythritol on aqueous salts. A specific interaction between NH_4^+ and 1,4-anhydroerythritol was proven by varying the salts.

The stoichiometry of the interaction between 1,4-anhydroerythritol and solvent or solute (water or aqueous NH_4^+) was determined by nonlinear regression analysis applied to data obtained from ^{13}C NMR chemical shifts through variation of temperature, solvent activity, and solute activity.

The techniques of thermodynamics were used to calculate, at various temperatures, the activity coefficient of a strong 1:1 electrolyte in aqueous solution. A computer program to determine the activities, a_{H_2O} (c, T), a_{NH_4Cl} (c, T), as functions of concentration and temperature from various thermodynamic functions tabulated in the literature was constructed.

A general model with undetermined stoichiometry was constructed for the dependence of the ^{13}C NMR chemical shifts upon temperature and the activities of the two ligand species. The stoichiometry and free energy values, which optimized, in a least squares sense, the agreement with the data, are given as

$$E \underset{\leftarrow}{\overset{\rightarrow}{}} E.D_2O^{(1)} \underset{\leftarrow}{\overset{\rightarrow}{}} E.ND_4^{+(2)} \underset{\leftarrow}{\overset{\rightarrow}{}} E.ND_4^{+}.D_2O^{(3)} \underset{\leftarrow}{\overset{\rightarrow}{}} E.2D_2O^{(4)}$$

$\Delta G^{(1)}$ = .35 kcal/mole

$\Delta G^{(2)}$ = 1.3 kcal/mole

$\Delta G^{(3)}$ = 3.3 kcal/mole

$\Delta G^{(4)}$ = 3.4 kcal/mole

B. Formation of the N-oxide for several pyridine derivatives results in a large upfield shift of the 2-, 4-, and 6-carbons and a significant downfield shift of the 3- and 5-carbons. The chemical shifts ($\Delta\delta$) are consistent with a resonance and electric field mechanism. MO calculations using CNDO/2 show a qualitative correlation between excess charge density and $\Delta\delta$.

A Davidon-Fletcher-Powell optimization method was used to investigate the conformational manifold of oxolane and its derivatives using the MINDO/3 MO program. Oxolane was predicted to have the planar conformation.

To my late father, Ira

" It is a capital mistake to theorize before one has data. Insensibly one begins to twist facts to suit theories, instead of theories to suit facts."

Sherlock Holmes

ACKNOWLEDGEMENTS

This thesis was made possible by the support and patience of my supervising professor, Dr. R. J. Cushley. The author is grateful for the opportunity of having many enlightening discussions with him, as well as the privilege of being able to work in his research group. Recognition is also due to Dr. E. J. Wells and Dr. G. L. Malli as members of the supervisory committee.

The author is pleased to thank Dr. D. M. Eaves and Dr. R. D. Russell of the Department of Mathematics for helpful discussions of multivariate regression and splines and to also thank Dr. I. D. Gay and Dr. F.W.B. Einstein for discussions of activities and least squares.

The author would like to thank the Staff of the Computing Center for their help and advice and Mr. A. L. Brooke and Mr. G. L. Owen for their assistance.

The financial support of the Natural Science and Engineering Research Council of Canada, through research grants to Dr. R. J. Cushley, and the support of Simon Fraser University are gratefully acknowledged.

This thesis was patiently typed by Ms. M. P. Fankboner.

TABLE OF CONTENTS

BACKGROUND

EXPERIMENTAL

LIST OF TABLES

LIST OF FIGURES

1. INTRODUCTION

A. The structures I and II, 1,4-anhydroerythritol (oxalane 3,4-cis-diol) and 1,4-anhydrothreitol (oxalane 3,4-trans-diol) shown in Figure 1, form the central moiety of the biochemically important molecules given in Figure 1, III-VI. Adenosine triphosphate, ATP, III, provides the driving force for numerous biochemical coupling reactions due to the high Gibbs free energy of the hydrolysis of ATP. Ribonucleic acid, RNA, IV, serves as a transporter of genetic information. Adenosine 3', 5'-cyclic phosphoric acid, cyclic AMP, V, acts as a secondary messenger in the regulation of enzymatic processes. D-fructose-6-phosphate, VI, is an entry point in the glycolytic pathway. I is seen to represent the basic sugar backbone of structures III, IV, and V, and II that of VI.

The interactions of I and II with other species are governed by the lone pairs of electrons on the oxygen atoms, which may participate in the interactions one, two, or three at a time. The symmetry of I and II are C1h(m) and C2(2), respectively, and, in any interaction with a species of higher symmetry in solution, this symmetry will be preserved on the average. I and II are, to a first approximation, structurally rigid and measurement of Dreiding molecular models shows the O-O distance of the cis hydroxyls of I to be 2.5 Å; the O-O distance in I between hydroxyl and ether oxygen is 3.0 Å; the O-O distance of the trans hydroxyls of II is 3.5 Å. Thus, the symmetries and geometrical features of I and II permit the comparison of geometries of association complexes.

To date a considerable amount of work has been done on the interaction of various metal ions with sugars and related compounds in different solvent systems. Thus, the interaction of metal ions with various sugars has been studied by a number of techniques. ^{23}Na NMR has been used [1] for the study of sugar-sodium interactions in pyridine solution. Since it has been shown that the sodium cation coordinates on one face to three or more oxygen atoms

Figure 1. The structures of 1,4-anhydroerythritol (oxalane 3,4-cis, diol), I; 1,4-anhydrothreitol (oxalane 3,4-trans diol), II; Adenosine triphosphate, ATP, III; Ribonucleic acid, RNA, IV; Adenosine 3',5'-cyclic phosphoric acid, cyclic AMP, V; D-fructose-6-phosphate, VI. Many of the ring hydrogens have been left off for simplicity.

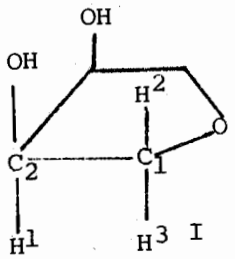

I

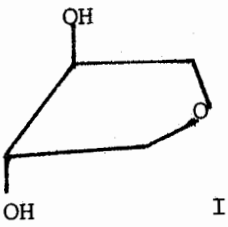

II

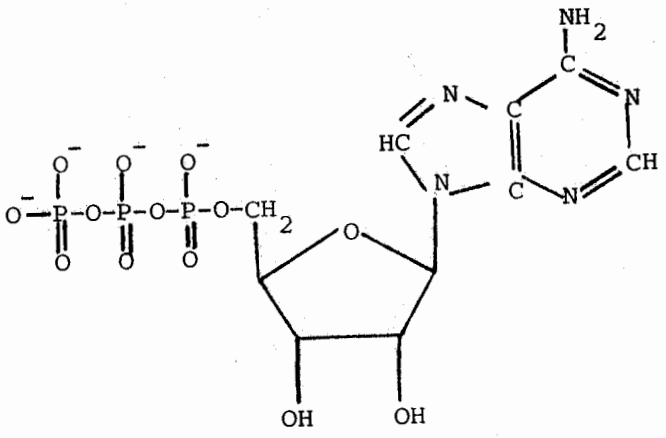

III

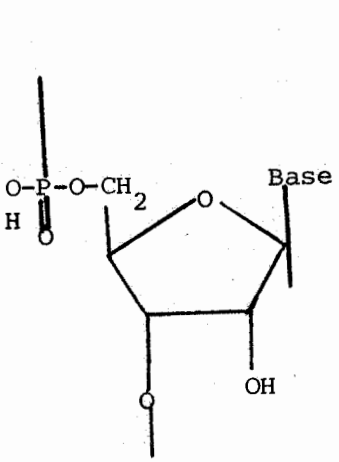

IV

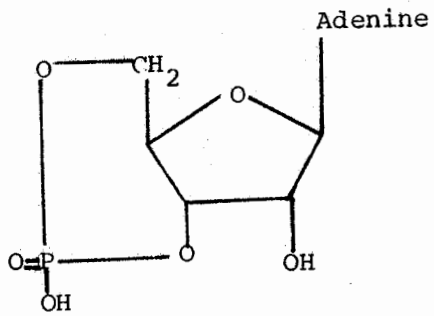

V

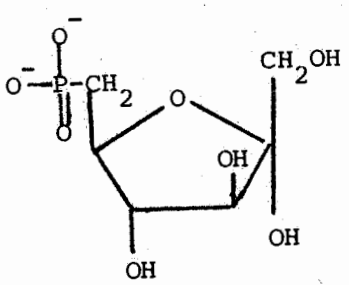

VI

from the sugar, and on the other face with nitrogen atoms from the solvent molecules, there is a substantial electrostatic field gradient at the quadrapolar nucleus. Line broadening can be analyzed to reveal details of this complexation.

Complexation of lanthanide ions with alditols and polyhydric alcohols have been used as model studies for the complexation of sugars with isosteric Ca(II) [2, 3]. It was shown that a lanthanide-sorbitol complex in D_2O solution, for example, was formed with the sorbitol adopting a normal zig-zag conformation while using O-2, O-3, and O-4 as ligands.

The interaction of carbohydrate derivatives with sodium ions in acetone-d_6 solution was studied by ^1H NMR [4]. All the proton resonances of 1,4-anhydroerythritol showed induced shifts, but of differing degrees. The chemical shift data for the three observed protons was analyzed by the Scott modification of the Benesi-Hildebrand method[41].The protons yielded equilibrium constants for complex formation of approximately 6,1 and 2.5 M^{-1}. The variation in these values is clearly the result of the non-validity of assumptions inherent in this treatment. This point will be discussed at greater length subsequently. It is of interest to note that $NaClO_4$ and NaSCN complexes of 1,4-anhydroerythritol may be crystallized. The $NaClO_4$ complex forms an orthorhombic crystal with space group $P\,2_1 2_1 2_1$, with unit cell dimensions a = 12.77, b = 7.28, and c = 17.69 Å and with eight complex units in the unit cell [5]. The distances from the sodium ion to the two hydroxyl and the ether oxygens of the sugar are 2.314 (11), 2.294 (12), and 2.550 (10), respectively, as shown by X-ray diffraction. It has been observed that compounds with two hydroxy groups on adjacent carbon atoms have markedly superior complexing properties to those of compounds with other spacings [6]. 1,4-anhydroerythritol possesses three such spacings.

5'-adenosine monophosphate, 5'-AMP, has three sites for the binding of metal ions: through the phosphate, through the adenine nitrogens or through the ribose oxygens. Metal binding to ribose is of some significance since metal ions appear to be capable of distinguishing between ribonucleotides and deoxyribonucleotides in enzymic reactions. Thus, whereas manganese(II)can replace magnesium ions in the DNA polymerase reaction, the selectivity of the reaction is modified by such a substitution. Magnesium ions permit the incorporation of only deoxyribonucleotides into DNA [7]. Manganese ions, on the other hand, permit the incorporation of both deoxynucleotides and ribonucleotides into the "DNA". Using potentiometric methods to study the adenosine complexes with copper ions, some authors have concluded that, at high pH, there exists a metal-ribose interaction [10]. Comparison of the effects in the titration curves were made with 9-methyladenine and deoxyadenosine. ^{1}H NMR studies of uranyl, UO_2^{2+}, ion binding with 5'-AMP has shown that the ions bind through the phosphate and the 2' and 3' oxygens on the ribose [11]. Using ^{31}P and ^{1}H NMR techniques to investigate the binding site of Cu^{2+} to ATP [12], binding was shown to be a function of pH. At high pH, neither the nitrogens of the base nor the phosphate group are still bound. The ribose moiety is then the coordination site of the metallic cation.

The metal ions discussed above are strongly coordinating. When weakly coordinating species are considered, competition with the solvent must also be considered. This leads to investigation of hydrogen bonding phenomena and of water hydration effects. NMR techniques may be used to study hydrogen bonding phenomena. In this area there has been a greater effort to quantify phenomena rather than merely to identify them. Analysis is difficult, however, because of the complexity of the interactions.

This work is clearly of interest in elucidating conformation and potential metal binding sites and may also relate to questions concerning transport properties and cationic regulation of enzymic processes. Competition between water and metal ions in sugar binding may also yield details of structures of macromolecules containing sugars in aqueous solution. Little interest has been shown, however, in sugar interactions with the non-metallic cation ammonium in aqueous solution. The potential reactivity of aldoses and ketoses with ammonia presents, at first, a discouraging impediment. This reactivity proceeds through hemiaminals, imines and, thence, to polymers. The anhydrosugars and the polyhydric alcohols, however, are free from this difficulty. The study of the interaction of anhydrosugars with ammonium ion may relate to questions of enzyme or proteins binding with substrates containing sugar subunits, since proteins contain, for example, the substituted ammonium residue, lysine. It is interesting to note the relatively high lysine content of ribonuclease and of ribosomal protein [8, 9]. The lysine residues appear to play an essential role in specific protein-RNA complex formation in the ribosomes [9]. Arginine has a subsituted guanidinium cation, and both arginine and lysine could serve as the counterion for the RNA phosphates. The high proportion of lysine suggests the possibility of a specific lysine interaction with the riboses through the substituted ammonium residue.

Water association in the control of biochemical reactions has also received considerable interest [17]. As the solvent medium of living systems, water merits in depth study and, indeed, of all solvents it is the one about which most is known.

Water is not merely an inert or static environment, nor is it merely a transport medium. It exercises many organizational activities and can form

particular structures in response to the presence of hydrophobic groups and may establish other types of association in the presence of ionic or polar groups. Furthermore, water can provide a supporting bridge for many biological conformations.

A water molecule possesses two binding potentials. It is a dipole with excess charge on the oxygen and, therefore, tends to associate with polar groups. It also possesses the capacity to act as an H-donor, by virtue of its labile hydrogens, and as an H-acceptor, by virtue of the two lone pairs of electrons on the oxygen. It should be noted that the H-bond of water retains its strength when it is linear or is within a maximum deviation of 30^{o} [18].

The vapour pressure of water may be considered to represent the activity of water itself. It reflects the tendency of individual water molecules to escape from the liquid water medium. In turn, it is a reflection of the number of free water molecules co-existing with the various self-association complexes of water and of their kinetic energy, 3/2 RT.

The substitution of D_2O for H_2O must be considered in light of the solvent isotope effect between light and heavy water [19] and of the solvent isotope effect for ionic hydration [20]. Table I, reproduced from reference [21], gives the ratio of vapour pressures, P_{H_2O}/P_{D_2O}, as a function of temperature. This is one representation of the solvent isotope effect. From the lower vapour pressure of D_2O, it may be concluded that D_2O in the liquid phase exists in a greater degree of order and with more self-association than H_2O, while this difference diminishes with temperature. Table II lists some of the intrinsic differences of thermodynamic values for H_2O and D_2O, as measured and as calculated by partitioning of contributions from translations, librations, and vibrations[19].

TABLE I

Variation of the ratio of vapour pressure of H_2O to that of D_2O as a function of temperature [21].

T, ^oC	P_{H_2O}/P_{D_2O}
0	1.255
10.0	1.182
20.0	1.154
30.0	1.137
40.0	1.122
50.0	1.107
60.0	1.094
70.0	1.081
80.0	1.071
90.0	1.061
100.0	1.052

Quantity	Vibrations	Librations	Translations	Calc. Value	Expl. Value
ΔH, cal mol^{-1}	-3303.1	-581.9	———	-3885	-3886 ± 23
ΔS, cal deg^{-1} mol^{-1}	0.034	1.0665	0.3164	1.417	1.439 ± 0.031
ΔG, cal mol^{-1}	-3313.2	-900.1	-94.3	-4308	-4295 ± 24
ΔC_p, cal deg^{-1} mol^{-1}	0.1550	1.166		1.32	1.70
ΔL cal mol^{-1}	———	———	———	336	307

TABLE II

Comparison of theoretical and experimental thermodynamic differences for H_2O and D_2O at 25°.

Differences are the quantity for D_2O minus the quantity for H_2O [19].

An interesting example of hydrogen bonding phenomena, as shown by ^{13}C, is revealed by the carbonyl chemical shifts for acetic acid in several solvents [22] (see Figure 2).

The interpretation of these results is not entirely clear but may be tentatively based [23] on the following equilibria (where S = solvent molecule):

$$
\begin{aligned}
& 2CH_3COOH \rightleftarrows (CH_3COOH)_2 \\
& aCH_3COOH + b(CH_3COOH)_2 \rightleftarrows (CH_3COOH)_a + 2b \\
& (CH_3COOH)_n + mS \rightleftarrows n(CH_3COOH)\cdots S_m \\
& a, b, m, n = 1, 2, 3, \ldots\ldots
\end{aligned}
\qquad (1)
$$

The equilibrium constant for the formation of the 1:1 complex of acetic acid and acetone has been estimated to be 0.23 liter/mole. The corresponding value with chloroform is estimated to be 0.02 liter/mole. The data for water is interpreted by means of a 1:2 complex.

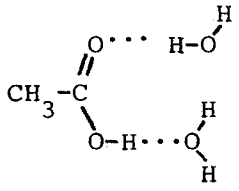

An example of PMR techniques applied to the study of hydrogen bonding is given by benzenethiol + dimethylformamide in CCl_4, which forms a simple 1:1 complex. If the proton acceptor is in excess, the chemical shift, ν, is given by the equation

$$
\frac{1}{(\nu - \nu_1)} = \frac{1}{(K\Delta_c C_B^o)} + \frac{1}{\Delta_c} \qquad (2)
$$

where $\Delta_c = \nu_2 - \nu_1$ and ν_1 is the chemical shift of the monomer proton donor and ν_2 that of the complex. Results for benzenethiol + dimethylformamide [23]

Figure 2. Plot of ^{13}C chemical shifts (relative to $^{13}CS_2$) of $CH_3{}^{13}COOH$ versus (volume fraction)$^{-1}$ in the solvents acetone, water, cyclohexane, and chloroform [22].

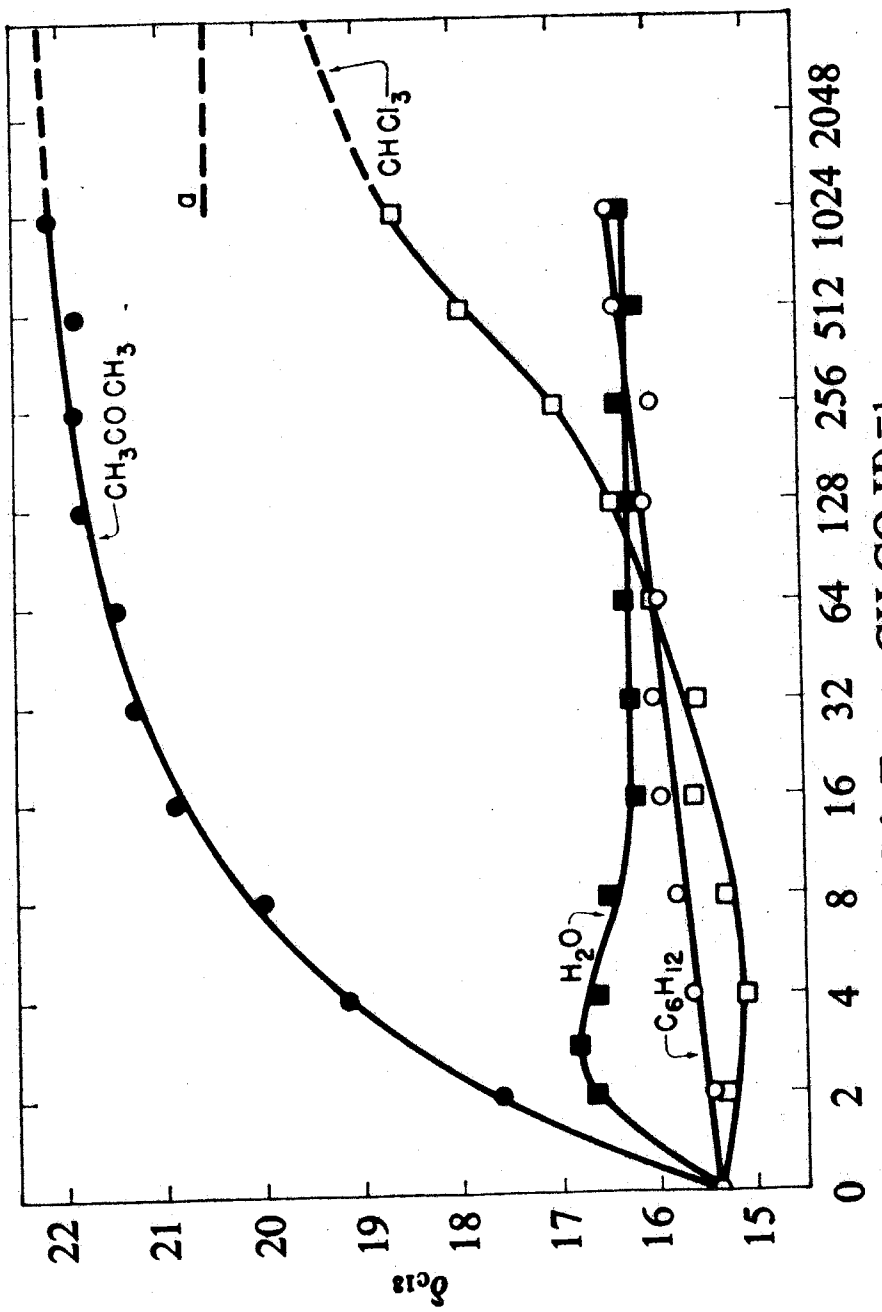
22
21
20
19
18
17
16
15
δ_{cis}
0
2
4
8
16
32
64
128
256
512
1024
2048
(Vol. Fract. $CH_3CO_2H)^{-1}$
CH_3COCH_3
a
$CHCl_3$
H_2O
C_6H_{12}

are shown in Figure 3.

The strength of hydrogen bonds may be determined by NMR or other techniques such as IR. Selected thermodynamic parameters for some intermolecularly hydrogen bonded systems [23] which relate to the present study are given in Table III.

The study of sugar ion complexation by ^{13}C NMR spectroscopy in aqueous D_2O solution may be advantageous for a number of reasons:

(1) In D_2O solution, the hydroxyl protons are replaced by deuterium. Although this does result in some simplification of the proton NMR spectrum, there are still CH proton-proton couplings, which makes spectral analysis of ^1H NMR more difficult than proton decoupled ^{13}C NMR spectra.

(2) The metal binding is to the hydroxyl which is directly bonded to carbon and, so, the electrostatic influence of bound metal is conducted through two bonds rather than three bonds, resulting in greater sensitivity.

(3) Aside from the proximity effects, ^{13}C chemical shifts extend over a greater range than proton shifts and are, thus, a more sensitive probe of molecular effects. This is due to the fact that, in the ^{13}C shielding, constant tensor, the paramagnetic term, dominates, giving a large dispersion of ^{13}C shifts, whereas, for ^1H, the diamagnetic term dominates because the hydrogen atom has large electronic excitation energies and no low-lying p orbitals [13, 14, 15].

(4) Double resonance may be used to decouple proton from carbon by rapidly stirring the proton spins [131,132] so as to give simple line spectra for carbon [15,16].

(5) D_2O is required for any aqueous proton resonance work. An aqueous solvent has advantages over non-aqueous solvents for studies of ionic interactions because a great deal is known about the thermodynamic properties

Figure 3. Plots of $1/(\nu - \nu_1)$ versus $1/C_B^o$ at several temperatures for benzenethiol + dimethylformamide in CCl_4 [24].

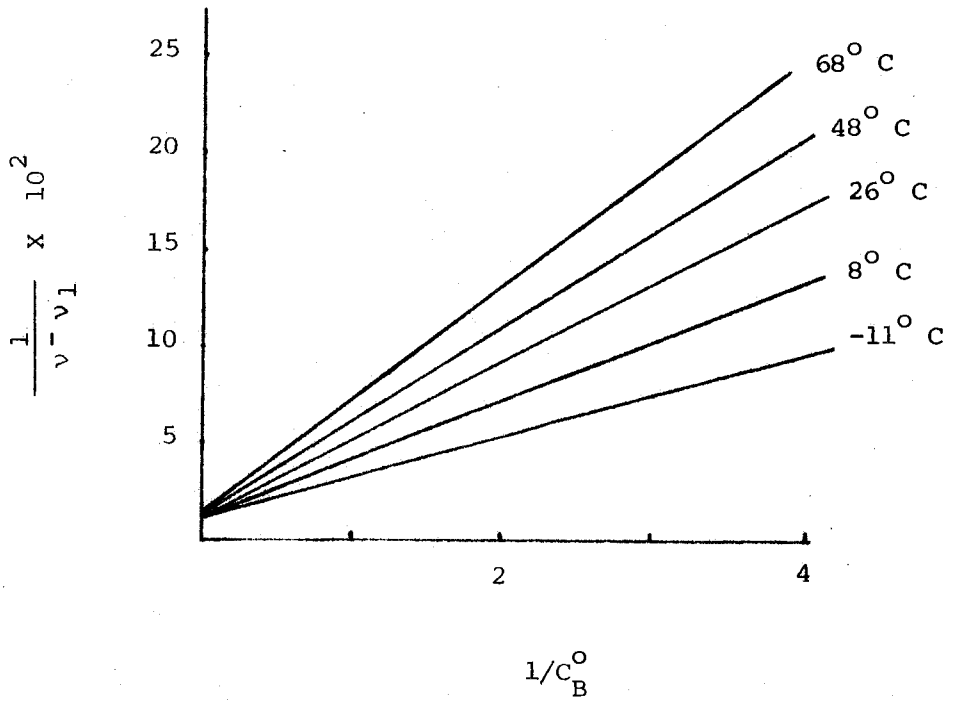
25
20
15
10
5
2
4
68° C
48° C
26° C
8° C
-11° C
$\frac{1}{\nu - \nu_1} \times 10^2$
$1/C_B^o$

System	Phase or Solvent	$-\Delta G^{\circ}$ (kcal/mole)	$-\Delta H^{\circ}$ (kcal/mole)	$-\Delta S^{\circ}$ (e.u.)
methanol-diethyl ether	vapour	———	4.7 ± 0.7	———
water-dioxane	CCl_4	———	3.3 to 3.7	———
phenol-dioxane	CCl_4	0.93 (20° C)	5.0 ± 0.2	13.9 ± 0.7
methanol-trimethylamine	vapour	———	5.85 ± 0.7	22.6 ± 3.0
aniline-tetrahydrofuran	C_6H_{12}	0.04	3.04	10.1
phenol-n-heptylfluoride	C_2Cl_4	———	2.1	———
d-phenol-n-heptylfluoride	C_2Cl_4	———	2.5	———

TABLE III

Selected thermodynamic parameters for some intermolecularly hydrogen bonded systems [23].

of aqueous, binary 1:1 salt solutions, whereas little is known about these properties for non-aqueous salt solutions.

(6) The ^{13}C atom does not undergo chemical exchange and, thus, the results obtained with this isotope are less ambiguous than those of PMR studies.

An accurate, consistent, quantitative analysis requires that complexation equilibria be expressed in terms of the activities of the participating species. Determination of activities of solutes comprises a significant portion of the present work.

In the analysis of solvent-solute interactions in equilibrium with a reporter species (in this work, a sugar), it is found that one has the complicated situation of a multi-component, competitive, multi-equilibrium. Previous methods of analysis have proven to be inadequate and special analytic techniques are required.

Interactions of the present type are comparatively weak and, at normal temperatures, are within the fast exchange limit on the NMR time scale. In the fast exchange limit, the observed chemical shift is the population-weighted average of the chemical shifts of the various species in the exchange process. A sensible analysis in this difficult situation requires experimental data obtained where all the important variables, temperature, and activities are varied independently. A model is then proposed which expresses the relationship of the observed dependent variables on the independent variables. This model is expressed in terms of a number of parameters and contains, implicitly, some assumptions about the stoichiometry of the competative multi-equilibrium.

The analytical technique used in the present study is non-linear regression in which the parameters which best reproduce the data for the given

model are found. With different stoichiometric assumptions, a new model can be tested in the same way. Comparison of the goodness of fit of these modified models allows the determination of the model which best fits the data. In this way the stoichiometry of the multi-equilibrium and the parameters of the best model are determined.

B. The N-oxide group has become increasingly more important as a biological functionality. Aliphatic N-oxides were recognized as early as 1945, when it was discovered that trimethylamine was oxidized to trimethylamine N-oxide and excreted in rats [25]. N-oxides were found to be biologically active when Neuberg [26] conducted his classic studies in vivo with trimethylamine N-oxide. Chemically, the N → O group is analogous to OH^+ and, hence, protonated N-oxides represent possible electrophilic reagents. Much more important, however, is their role as a biological oxygenating agent in microsomal enzyme systems. N-oxides have been depicted as the main moiety responsible for biological oxidative demethylation of N-methyl derivatives[27, 28]. Xanthine oxidase catalyzes the transfer of labeled oxygen from nicotinamide N-oxide to xanthine in the course of the formation of uric acid [29].

Many N-oxides have been found in nature. For instance, substituted quinoline N-oxides and quinoxalin N,N-dioxides have been found to be antiviral agents [30] and a large number of N-oxides have been shown to have antibacterial activity, including the antibiotics aspergillic acid, emimycin, iodinin, and myxin. The latter compounds are all formally related to diketopiperazines.

Finally, several pyrrolizidine alkaloids, such as senecionine N-oxide, have been demonstrated to be the tumor inhibitory principals of plant extracts [31]. It must be added, however, that purine N-oxides have proven to be potent oncogenic[1] agents.

---

[1] An agent which induces any form of neoplasm is oncogenic. The term carcinogenic should be reserved for agents inducing carcinomas.

In order to gather insight into the structures and electronic configurations of this class of biologically important compounds, we have determined the ^{13}C chemical shift parameters of a series of pyridines and their N-oxides.

Figure 4. Structures of aspergillic acid, enimycin, iodinin, and myxin.

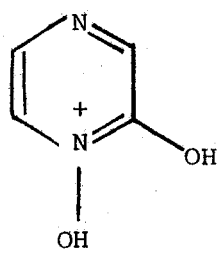

aspergillic acid

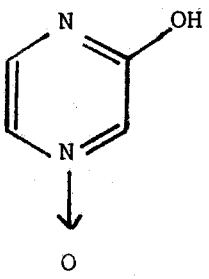

enimycin

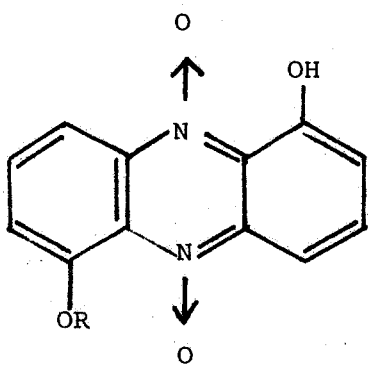

R=H; iodinin

$R=CH_3$; myxin

2.0
Dynamic NMR

The shielding, σ, of a nucleus dissolved in a liquid medium is expressed [32, 33] as

$$\sigma = \sigma_g + \sigma_b + \sigma_a + \sigma_w + \sigma_E + \sigma_c \quad (3)$$

where σ_g is the shielding in the gas phase, σ_b is due to the bulk diamagnetic susceptibility of the sample, σ_a is a term arising from the non-zero averaging of any anisotropy which may exist in the diamagnetic susceptibility of the solvent molecules, σ_w is the van der Waals term, σ_E is the reaction field term, and σ_c is the apparent complexation shielding which may arise out of some specific molecular association phenomenon involving the solute in rapid exchange between varying magnetic environments.

Formulations for the gas phase nuclear shielding tensor are numerous and somewhat intractible but may be generally divided into perturbation theories, which require consideration of excited states, and variational theories, which do not [34]. The problem of the bulk diamagnetic susceptibility may be eliminated with the use of an internal standard , and the proper choice of the internal standard will minimize the specific and non-specific medium effects on the standard. In suitable cases, the effect of the specific complexation shielding is greater than the non-specific medium effects and the latter can be ignored.

The theory of spectra observed in a system in which there is chemical exchange may be obtained by consideration of the Bloch equations, suitably modified for two site exchange.

Consider the case of a rapid reversible exchange of the magnetic nucleus

X between the two molecular environments A and B. It may be assumed that the transition state is sufficiently short-lived, so that magnetization changes during the transfer of X may be neglected. Denote the first order lifetimes of X in A and B, by τ_A and τ_B, respectively. The components of the X nuclear magnetization are denoted by u and v, which are the in phase and out of phase components, respectively, with the rotating radiofrequency field and M_z, which is the component in the direction of the main magnetic field. The magnetization can then be written as the sum of the contribution of the A and B systems.

(4)
$$u = u_A + u_B$$
$$v = v_A + v_B$$
$$M_z = M_z^A + M_z^B$$

The modified Bloch equations in the rotating system are [34,37]

(5)
$$\frac{du_A}{dt} - \Delta\omega_A v_A = \frac{-u_A}{\tau_{2A}} + \frac{u_B}{\tau_B}$$
$$\frac{du_B}{dt} - \Delta\omega_B v_B = \frac{-u_B}{\tau_{2B}} + \frac{u_A}{\tau_A}$$
$$\frac{dv_A}{dt} - \Delta\omega_A u_A = \frac{-v_A}{\tau_{2A}} + \frac{v_B}{\tau_B} - \omega_1 M_z^A$$
$$\frac{dv_B}{dt} - \Delta\omega_B u_B = \frac{-v_B}{\tau_{2B}} + \frac{v_A}{\tau_A} - \omega_1 M_z^B$$
$$\frac{dM_z^A}{dt} - \omega_1 v_A = \frac{M_o^A}{T_{1A}} - \frac{M_z^A}{\tau_{1A}} + \frac{M_z^B}{\tau_B}$$
$$\frac{dM_z^B}{dt} - \omega_1 v_B = \frac{M_o^B}{T_{1B}} - \frac{M_z^B}{\tau_{1B}} + \frac{M_z^A}{\tau_A}$$

where M_o^A and M_o^B are the equilibrium Z magnetizations of the X nuclei in sites A and B and where

(6)
$$\Delta\omega_A = \omega_A - \omega$$
$$\Delta\omega_B = \omega_B - \omega$$
$$\omega_1 = \gamma H_1 \quad , \quad \text{measured in radians sec}^{-1}$$

and

(7)
$$\tau_{1A}^{-1} = T_{1A}^{-1} + \tau_A^{-1}$$
$$\tau_{2A}^{-1} = T_{2A}^{-1} + \tau_A^{-1} \qquad \text{in sec}^{-1}.$$

The last two equations represent the modification of the spin-lattice (longitudinal) and spin-spin (transverse) relaxation times, T_{1A} and T_{2A}, of X in the A environment. Similar relations apply when X is at site B.

The modified Bloch equations can be solved in the steady state approximation. The lineshapes of the absorbtion and dispersion mode signals are given by the total complex moment [37], $G = G_A + G_B$

(8)
$$= u + iv$$
$$= \frac{-i\omega_1 M_o [(\tau_A + \tau_B) + \tau_A\tau_B(\alpha_A p_B + \alpha_B p_A)]}{(1 + \alpha_A\tau_A)(1 + \alpha_B\tau_B) - 1}$$

where

(9)
$$\alpha_A = T_{2A}^{-1} - i(\omega_A - \omega)$$
$$\alpha_B = T_{2B}^{-1} - i(\omega_B - \omega)$$

and where

(10)
$$p_A = \frac{\tau_A}{\tau_A + \tau_B} \qquad \text{and} \qquad p_B = \frac{\tau_B}{\tau_A + \tau_B}$$

are the fractional populations at the A and B sites. For conditions of rapid exchange, τ_A and $\tau_B \ll 1$ and, hence, terms containing $\tau_A\tau_B$ can be neglected and

G is approximated by

$$G = \frac{-i\omega_1 M_o (\tau_A + \tau_B)}{\alpha_A \tau_A + \alpha_B \tau_B} \quad . \tag{11}$$

The imaginary part v is given by

$$v = - \frac{\omega_1 M_o \tau_2}{1 + \tau_2^2 (p_A\omega_A + p_B\omega_B - \omega)^2} \tag{12}$$

where

$$\tau_2^{-1} = T_{2A}^{-1} p_A + T_{2B}^{-1} p_B \tag{13}$$

Hence, resonance absorption occurs when the radiofrequency ω has the value

$$\omega = p_A\omega_A + p_B\omega_B \tag{14}$$

This last relationship, given for rapid exchange, may be generalized directly for cases of exchange between three or more sites.

In the regime of the fast exchange limit, i.e. where the rate of exchange between species is appreciably faster than the reciprocal difference in angular precession frequencies of the resonating nuclei [38], the analysis of NMR shielding versus concentration may be used to obtain values of stability constants [39]. Simple systems yield readily to a straightforward analysis.

As a first example, consider the hypothetical ideal equilibrium behaviour of a 1:1 complex formed between a donor, D, and an acceptor species, A, [40].

(15)

$$D + A \rightleftarrows C$$

$$\frac{[C]}{[D]\ [A]} = K$$

The observed shielding, σ, is a concentration weighted average of its value in the free acceptor, σ_A, and in the complex, σ_C.

(16) $$\frac{(\sigma - \sigma_A)}{(\sigma_C - \sigma_A)} = \frac{\Delta}{\Delta_C} = \frac{[C]}{([C] + [A])}$$

This formula is often referred to as the Benesi-Hildebrand equation where it arises in the context of optical spectroscopy [41]. It may be combined with the equilibrium expression to give Scott's equation [42]

(17) $$\frac{[D]}{\Delta} = \frac{1}{K \Delta_C} + \frac{[D]}{\Delta_C}$$

A least-squares fit

(18) $$y = b_1 + b_2 x$$

where $y = [D]/\Delta$, and $x = [D]$, yields

(19) $$\Delta_C = 1/b_2$$

$$K = b_2/b_1$$

with standard deviations

(20) $$(\delta\Delta_C)^2 = (\delta b_2)^2/b_2^4$$

$$(\delta K)^2 = (\delta b_2)^2/b_1^2 + b_2^2 (\delta b_1)^2/b_1^4 \quad .$$

In practice, the free donor concentration, [D], is unknown; it differs from the total initial donor concentration by the complex concentration. When the acceptor concentration is kept small, the total initial donor concentration is a good first approximation to [D]. At each concentration, the derived

values of Δ_C and K may be used for a second Scott analysis, yielding better values of Δ_C and K, and so on to self-consistency.

Equilibrium systems more involved than a simple 1:1 association have been disentangled by an analysis of chemical shift data. For the system of n-mer formation represented as

(21) $$nA \rightleftarrows A_n \quad , \quad n = 1, 2, \ldots . n$$

$$K_n = \frac{C_n}{C_1^n}$$

where C is the concentration, the subscript indicating monomer, dimer, trimer, ... , n-mer. The shift frequency of one absorption peak, which is the weighted average of all contributors, is given [43] for ideal equilibrium behaviour as

(22) $$\nu = \frac{(\nu_1 C_1 + 2\nu_2 C_2 + 3\nu_3 C_3 + \ldots + n\nu_n C_n)}{(C_1 + 2C_2 + 3C_3 + \ldots + nC_n)}$$

$$= \frac{(\nu_1 C_1 + 2\nu_2 K_2 C_1^2 + \ldots . n\nu_n K_n C_1^n)}{(C_1 + 2K_2 C_1^2 + \ldots nK_n C_1^n)}$$

One approach to the disentanglement of such a system has been to make the assumption that all but one K_n can be neglected (i.e. only monomer and n-mer are present). Then

(23) $$\nu = \frac{(\nu_1 C_1 + n\nu_n K_n C_1^n)}{(C_1 + nK_n C_1^n)}$$

and since the stoichiometric (total) concentration

(24) $$C = C_1 + nK_n C_1^n \quad , \quad \text{then}$$

$$(25) \qquad \nu = \frac{(\nu_1 C_1 + n\nu_n K_n C_1^n)}{C}$$

A ν versus C curve is determined experimentally and then compared with trial-and-error computed curves until the best fit is found. This method is illustrated for O-cresol in Figure 5, taken from the work of Griffith and Socrates [44]. The fit for n = 3 indicates that the prominent H-bonded species present is the trimer.

Figure 5. Plot of hydroxyl proton resonance of O-cresol relative to TMS (in cycles per second) versus the log of concentration [44]. The curves were calculated assuming only dimer, trimer, and tetramer formation, respectively.

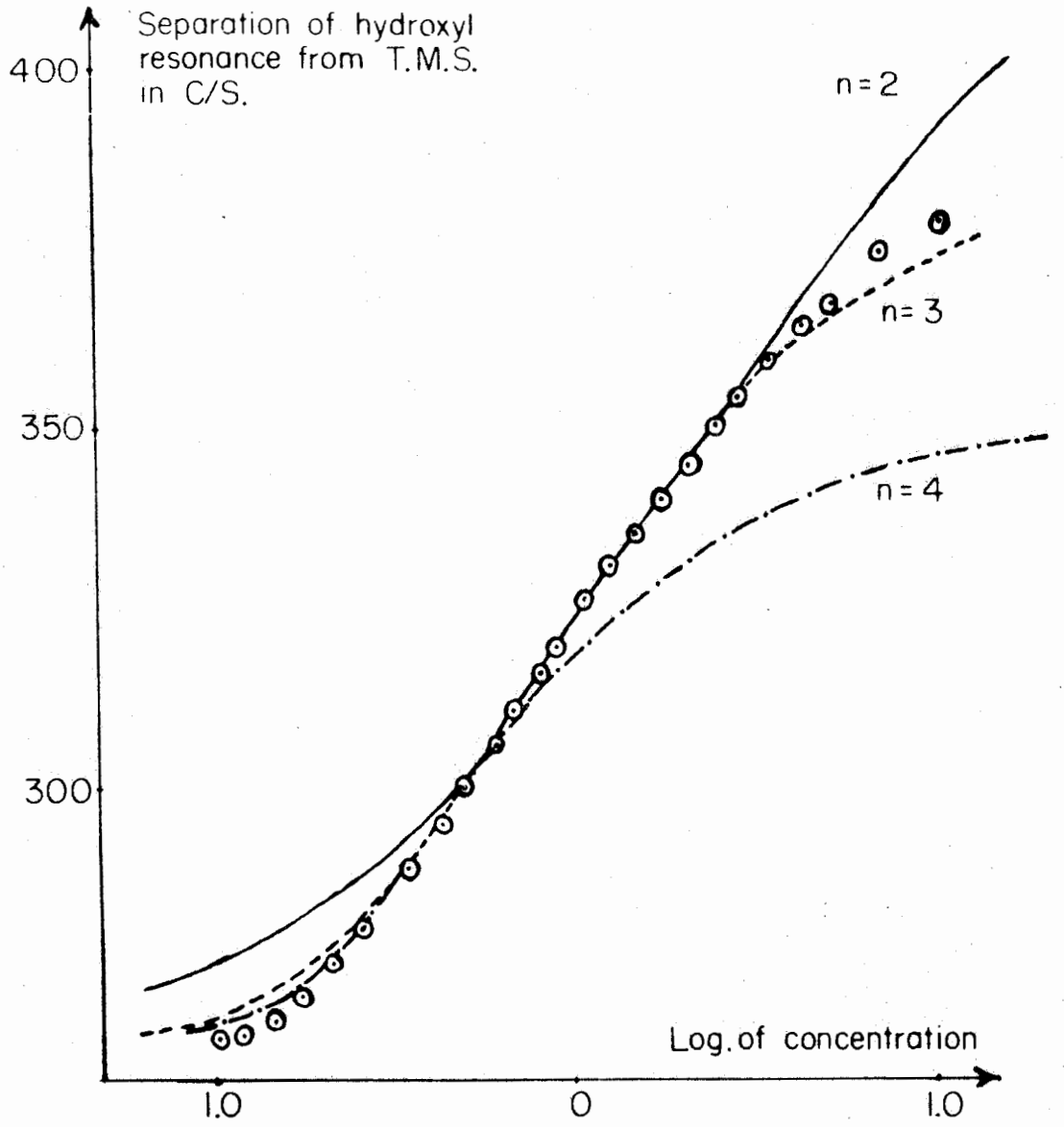
Separation of hydroxyl resonance from T.M.S. in C/S.
400
350
300
n=2
n=3
n=4
Log. of concentration
1.0
0
1.0

2.1

Derivation of Chemical Shift Expression for Species undergoing Competitive Multi-Equilibrium (Fast Exchange Limit)

Consider a molecule, E, with a number of ligand sites. Assume that a complex, E.nW.mA, of stoichiometry nm may be formed, where n molecules of solvent W and m molecules of solute A are engaged. In the fast exchange limit the chemical shift observed for nucleus i of E, δ^i_{obs}, is given as a population weighted sum,

(26) $$\delta^i_{obs} = \sum_{nm} p_{nm} \delta^i_{E.nW.mA}$$

The mole fraction, p_{nm}, of species E in the ligation state E.nW.mA is determined by the appropriate equilibrium expression, given in terms of activities,

(27) $$K^{nm} = \frac{a_{E.mW.mA}}{a_E (a_W)^n (a_A)^m} .$$

for $E + nW + mA \rightleftarrows E.nW.mA, \quad n, m = 1, 2, \ldots .$

or, given in terms of concentrations and activity coefficients,

(28) $$K^{nm} = \frac{C_{E.nW.mA}}{C_E (C_W)^n (C_A)^m} \cdot \frac{\gamma_{E.nW.mA}}{\gamma_E (\gamma_W)^n (\gamma_A)^m} .$$

Now, for C_E small,

(29) $$\gamma_{E.nW.mA}/\gamma_E \approx 1 \qquad [45]$$

(30) $$K^{nm} \approx \frac{C_{E.nW.mA}}{C_E (a_W)^n (a_A)^m}$$

$$(31) \qquad P_{n'm'} = \frac{C_{E.n'W.m'A}}{C_E^o}$$

$$= \frac{K^{n'm'} C_E (a_W)^{n'} (a_A)^{m'}}{C_E^o}$$

$$= \frac{K^{n'm'} C_E (a_W)^{n'} (a_A)^{m'}}{\sum_{nm} K^{nm} C_E (a_W)^{n} (a_A)^{m}}$$

Therefore, δ^i_{obs} is given by

$$(32) \qquad \delta^i_{obs} = \frac{\sum_{n'm'} \delta^i_{E.n'W.m'A} \cdot K^{n'm'} (a_W)^{n'} (a_A)^{m'}}{\sum_{nm} K^{nm} (a_W)^{n} (a_A)^{m}}$$

or, since $K^{oo} = 1$,

$$(33) \qquad \delta^i_{obs} = \frac{\delta^i_{E_0} + \sum_{n',m' \neq 0} \delta^i_{E.n'W.m'A} K^{n'm'} (a_W)^{n'} (a_A)^{m'}}{1 + \sum_{n,m \neq 0} K^{nm} (a_W)^{n} (a_A)^{m}}$$

The summation extends over all the species that enter into the inner ligation sphere of E.

The equation for δ^i_{obs} may also be derived from the grand partition function for an ensemble of multicomponent subsystems. The grand partition function for two components is [46]

$$(34) \qquad \Xi = \sum_{N_1, N_2} Q(N_1, N_2, V, T) \lambda_1^{N_1} \lambda_2^{N_2} \quad ,$$

where the Q are the canonical partition functions with occupation numbers N_1, N_2 of components 1 and 2, and where $\lambda_1 = e^{\mu 1/kT}$, $\lambda_2 = e^{\mu 2/kT}$ are the

absolute activities of 1 and 2. The probability that a subsystem has N_1, N_2 molecules of 1 and 2, respectively, is then

(35)
$$P(N_1,N_2,V,T,\mu_1,\mu_2)$$
$$= \frac{Q(N_1,N_2,V,T)\ \lambda_1^{N_1}\lambda_2^{N_2}}{\Xi}$$
$$= \frac{Q(N_1,N_2,V,T)\ \lambda_1^{N_1}\lambda_2^{N_2} \ / \ Q(0,0,V,T)}{\Xi/Q(0,0,V,T)}$$
$$= \frac{K(N_1,N_2,V,T)\ \lambda_1^{N_1}\lambda_2^{N_2}}{\sum_{N_1'N_2'} K(N_1',N_2',V,T)\ \lambda_1^{N_1'}\ \lambda_2^{N_2'}}$$

where $K(N_1,N_2,V,T)$ is the equilibrium constant for equilibria between zero molecules in the subsystem and N_1, N_2 molecules of components 1 and 2. The use of absolute activities presents no problem to the straightforward derivation of δ^i_{obs} from this point, since the relative activity, a, is obtained as the ratio of the absolute activity to the activity in some reference state [47]. The usual assumption of the independence of subsystems is equivalent to the assumption of ideality.

This insight, in terms of the grand partition function, is useful because it allows the generalization of the expression for the chemical shift to greater than two components in an obvious way.

3.0

Regression Theory [48 - 56]

One of the elementary aspects of regression analysis is the technique of curve fitting, wherein a function expressed in terms of some unknown parameters is used to approximate the dependence of some experimental measurements on some other independent variables in the experiment. The most well-known criterion for curve fitting is obtained when the parameters are solved for those values which minimize the sum of the squares of the differences between the observed and predicted values of the dependent variable, summed for all cases within the experiment. In order to consider the theory behind this technique, we must first consider the necessary and sufficient conditions for the existence of an unconstrained relative Minimum [48].

Necessary and Sufficient Conditions for Unconstrained Relative Minima

We wish to discover the minima of an objective function

(36) $$I\ (x_1, x_2, \ldots\ldots x_n) \quad .$$

Suppose that the point

(37) $$\bar{x}^* = \begin{bmatrix} x_1^* \\ x_2^* \\ \cdot \\ \cdot \\ \cdot \\ x_n^* \end{bmatrix}$$

is the minimum sought and there is another point, $\bar{x} = \bar{x}^* + \delta\bar{x}$, slightly

displaced from it. Since $\bar{x}^*$ is the relative minimum,

$$\delta I = I(\bar{x}^* + \delta\bar{x}) - I(\bar{x}^*) \geq 0 \tag{38}$$

for all displacements

$$\delta\bar{x} = \begin{bmatrix} \delta x_1 \\ \delta x_2 \\ \cdot \\ \cdot \\ \cdot \\ \delta x_n \end{bmatrix} \tag{39}$$

Expand the above in a Taylor series about the minimum to obtain

$$\delta I = \sum_{i=1}^{n} \left(\frac{\partial I}{\partial x_i}\right)_{\bar{x}^*} \delta x_i + \frac{1}{2} \sum_{j=1}^{n} \sum_{i=1}^{n} \delta x_j \left(\frac{\partial^2 I}{\partial x_i \partial x_j}\right) \delta x_i + O(\delta^3 x) \tag{40}$$

For very small displacements, the second-order terms are negligible and

$$\delta I = \sum_{i=1}^{n} \left(\frac{\partial I}{\partial x_i}\right)_{\bar{x}^*} \delta x_i + O(\delta\bar{x}^2) \tag{41}$$

The only way that $\delta I \geq 0$ can hold for all possible small values of $\delta\bar{x}$ is for

$$\left(\frac{\partial I}{\partial x_i}\right)_{\bar{x}^*} = 0 \quad , \quad i = 1, 2, \ldots . n. \tag{42}$$

On substituting, we obtain

$$\delta I = \frac{1}{2} \delta\bar{x}^T (\bar{\bar{H}})_{\bar{x}^*} \delta\bar{x} + O(\delta\bar{x}^3) \tag{43}$$

where $\bar{\bar{H}}$ is the symmetric matrix of second derivatives

$$(44) \qquad \bar{\bar{H}} = \begin{bmatrix} \frac{\partial I^2}{\partial x_1^2} & \frac{\partial I^2}{\partial x_1 \partial x_2} & \cdots & \frac{\partial^2 I}{\partial x_1 \partial x_n} \\ \frac{\partial^2 I}{\partial x_2 \partial x_1} & \frac{\partial^2 I}{\partial x_2^2} & & \vdots \\ \vdots & & \ddots & \vdots \\ \frac{\partial^2 I}{\partial x_n \partial x_1} & \cdots & \cdots & \frac{\partial^2 I}{\partial x_n^2} \end{bmatrix}$$

known as the Hessian matrix. The required conditions are then seen to be

$$(45) \qquad \left(\frac{\partial I}{\partial x_i}\right)_{\bar{x}^*} = 0 \quad , \quad i = 1, 2, \ldots n$$

$$(46) \qquad \delta\bar{x}^T \bar{\bar{H}} \delta\bar{x} \geq 0. \qquad H \text{ is positive-definite or semidefinite.}$$

A symmetric positive-definite matrix is characterized by having all positive eigenvalues. A positive semidefinite matrix has some zero eigenvalues.

Necessary and Sufficient Conditions for Minima having Equality Constraints

In the case where we have equality constraints, the problem of minimizing an objective function I may be written

$$(47) \qquad \underset{x_i}{\text{Min}} \quad I \ (x_1, x_2, \ldots x_n) \quad , \ i = 1, 2, \ldots n$$

where $$h_j \ (x_1, x_2, \ldots x_n) = 0, \ j = 1, 2, \ldots m$$

A convenient way of tackling these problems is through the use of the Lagrange multiplier.

Let us form the Lagrangian L by adjoining the equality conditions to the objective function through m·Langrange multipliers λ_j

$$L(\bar{x}, \bar{\lambda}) \equiv I(\bar{x}) - \sum_{j=1}^{m} \lambda_j h_j(\bar{x}) \quad . \tag{47}$$

For any small displacements from the optimum x*, λ*, on expanding the above in a Taylor series, we obtain

(48)

$$\delta L(\bar{x}^*, \bar{\lambda}^*) = \sum_{i=1}^{n}\left[\left(\frac{\partial I}{\partial x_i}\right)_{\bar{x}^*} - \sum_{j=1}^{m} \lambda_j^* \left(\frac{\partial h_j}{\partial x_i}\right)_{\bar{x}^*}\right]\delta x_i - \sum_{j=1}^{m} h_j(\bar{x}^*)\,\delta\lambda_j + O(\delta\bar{x}^2, \delta\bar{\lambda}^2)$$

$$= \sum_{i=1}^{n} \frac{\partial L(\bar{x}^*, \bar{\lambda}^*)}{\partial x_i}\,\delta x_i + \sum_{j=1}^{m} \frac{\partial L(\bar{x}^*, \bar{\lambda}^*)}{\partial \lambda_j}\,\delta\lambda_j + O(\delta\bar{x}^2, \delta\bar{\lambda}^2)$$

We may note that, for any small variation from the minimum $I(\bar{x}^*)$, we must have

$$\delta I(\bar{x}^*) \geq 0 \tag{49}$$

and, since the constraints must be satisfied, then $\delta h_j(\bar{x}^*) = 0$ must also hold. Thus, at the optimum, we must have

$$\delta L(\bar{x}^*, \bar{\lambda}^*) \geq 0 \tag{50}$$

But the only way this can be true for all small values of δx_i and $\delta\lambda_j$ is for

$$\frac{\partial L}{\partial x_i} = 0 \qquad i = 1, 2, \ldots n \tag{51}$$

(52) $$\frac{\partial L}{\partial \lambda_j} = 0 \qquad j = 1, 2, \ldots m \quad .$$

Then the problem of minimizing an objective function with equality constraints is seen to be equivalent to the problem of unconstrained minimization of the corresponding Lagrangian.

3.1
Unconstrained Nonlinear Optimization Techniques [48,49,53,57-60]

Unconstrained nonlinear optimization occurs in the context of regression analysis, wherein one postulates a model which predicts an observed variable mathematically in terms of some independent variables and some parameters plus observational or measurement error. It can be represented by

$$(53) \quad Y = f(x_1, x_2, \ldots, x_n, \theta_1, \theta_2, \ldots, \theta_m) + e$$

$$= f(\bar{x}, \bar{\theta}) + e \quad .$$

For many observations with different conditions, one would have

$$(54) \quad Y_j = f(\bar{x}_j, \bar{\theta}) + e_j, \quad j = 1, \ldots N$$

or $$\bar{Y} = \bar{f}(\bar{\bar{x}}, \bar{\theta}) + \bar{e}$$

where the vector of observations is expressed in terms of the data matrix, $\bar{\bar{x}}$, parameters $\bar{\theta}$, and error $\bar{e}$. It is assumed for statistical purposes that $\bar{e}$ comes from some distribution. It may be shown that, with conditions of normally distributed independent error, least squares is the correct method for parameter determination [49].

We then have an objective function $I(\bar{\theta})$ to minimize with respect to $\bar{\theta}$. For least squares

$$(55) \quad I = \bar{g}^T(\bar{\theta})\, \bar{g}\,(\bar{\theta})$$

$$= \sum_j (Y_j - f(\bar{x}_j, \bar{\theta}))^2 \quad .$$

Consider the following definitions:

(56) the gradient, $$\bar{q}_i \equiv \left(\frac{\partial I}{\partial \bar{\theta}}\right)_{\bar{\theta}=\bar{\theta}_i} ,$$

(57) the Hessian, $$\bar{\bar{H}}_i \equiv \left(\frac{\partial \bar{q}}{\partial \bar{\theta}}\right)_{\bar{\theta}=\bar{\theta}_i} ,$$

and (58) the Jacobian, $$\bar{\bar{J}}_i \equiv \left(\frac{\partial \bar{g}}{\partial \bar{\theta}}\right)_{\bar{\theta}=\bar{\theta}_i} .$$

All optimization techniques are iterative methods in which, given an estimate, $\bar{\theta}_i$, near the minimum, $\bar{\theta}^*$, a correction, $\bar{\sigma}_i = \Delta\bar{\theta}_i = \bar{\theta}_{i+1} - \bar{\theta}_i$, is determined, $\bar{\sigma}_i = \alpha_i \bar{p}_i$, for a stepsize, α_i, and search direction, $\bar{p}_i$. Let $\bar{n}_i = \Delta\bar{q}_i$. Without going into any detail then, the important methods may be enumerated according to the manner in which the search direction is determined. The stepsize is chosen according to some acceptability criteria for which $I(\theta_{i+1}) < I(\theta_i)$. The above definitions apply in common to the different methods below.

3.1.1
Steepest Descents

The steepest descents method is defined by

(59) $\bar{p}_i = -\bar{q}_i$, i.e. the search direction is

opposite the gradient. It has the advantage of simplicity, where only the elements of the gradient need be determined and convergence is relatively fast away from the minimum, $\bar{\theta}^*$, but convergence is ponderously slow near $\bar{\theta}^*$. It is seldom used.

3.1.2

Newton-Raphson: $\bar{p}_i = - [\bar{\bar{H}}_i]^{-1} \bar{q}_i$

(60)

The Newton-Raphson method is a powerful method in which the curvature is used to correct the gradient to give the search direction. If it works, rapid convergence is guaranteed. However, its disadvantages are that the matrix of second derivatives is required and, for estimates away from $\bar{\theta}^*$, $\bar{\bar{H}}_i$ may become singular.

3.1.3

Gauss-Newton: $p_i = - [\bar{\bar{J}}_i^T \bar{\bar{J}}_i]^{-1} \bar{\bar{J}}_i^T \bar{g}_i$

(61)

The Gauss-Newton method is essentially a linearized Newton-Raphson, where the term in brackets approximates the Hessian. It is used widely for least squares. Various modifications allow for an approximate inverse to be calculated, avoiding problems of singularities. It has the advantage of only requiring first derivatives. The disadvantage of this method, which was encountered in this study is that, where a good first approximation is unavailable, many iterations are required. From a statistical viewpoint, this method may be regarded as stepwise linear regression on the parameters. At each step $[\bar{\bar{J}}_i^T \bar{\bar{J}}_i]^{-1}$ is an estimate of the covariance matrix of the parameters.

The Gauss-Newton method has good convergence properties near the minimum. In this study, where it was used (see Chapters 5 and 6),a first approximation was obtained by "chemical intuition" or trial and error. Three programs were used: BMDX85 [59], BMDX85/NAUGLER, and BMDP3R [60]. BMDX85 is a general least squares program which incorporates the use of inequality constraints. BMDX85/NAUGLER is a double precision modification of BMDX85 written after double precision was discovered to be essential. BMDP3R is an up to date version, double precision, allows linear equality constraints, and gives residual analysis. The latter program, which is implemented under MTS, is recommended for the value of the output it produces.

3.1.4

Levenberg-Marquardt: $p_i = - [\bar{\bar{J}}_i^T \bar{\bar{J}}_i + \lambda_i^2 I]^{-1} \bar{\bar{J}}_i^T \bar{g}_i$

(62)

The Levenberg-Marquardt method overcomes the difficiencies of the Gauss-Newton method by choosing a λ_i so that the search direction lies somewhere between the steepest descents direction and the Gauss-Newton direction. Thus, the best of both techniques can be achieved. A large enough choice of λ_i will ensure that a non-singular matrix is obtained.

3.1.5

Davidon-Fletcher-Powell: $\bar{p}_i = -[\bar{\bar{A}}_i]^{-1} \bar{q}_i$,

(63)

where $$\Delta\bar{\bar{A}}_i = \frac{\bar{\sigma}_i \bar{\sigma}_i^T}{\vec{\sigma}_i^T \bar{\eta}_i} - \frac{\bar{\bar{A}}_i \bar{\eta}_i \bar{\eta}^T \bar{\bar{A}}_i}{\bar{\eta}_i^T \bar{\bar{A}}_i \bar{\eta}_i}$$

In the DFP method, a variable metric, $\bar{\bar{A}}_i$, is used to approximate the Hessian and it is constructed so that only gradient information is required, it is never singular, and the search directions are conjugate, i.e. orthogonal with respect to the Hessian and, so, interaction between these "conjugate gradients" is eliminated. This method is extremely robust and has been implemented to optimize the calculated electronic energy in MINDO/3 molecular orbital calculations [61, 62] . Modifications of this procedure use differences to approximate the first derivatives.

In all the matrix methods described, various inversion or spectral decomposition techniques may be applied. In BMDX85, BMDP3R [59,60] Gauss-Jordon elimination [49] is applied with pivoting done in a stepwise manner until further improvements in the matrix-inverse are less than rounding error and so that boundary conditions of the parameters are not violated.

4.0
1,4-Anhydroerythritol and 1,4-Anhydrothreitol Synthesis and Characterization

Nearly quantitative yields of 1,4-anhydroerythritol* can be obtained simply by heating erythritol in a distillation flask containing a strong acid cation exchange resin, followed by vacuum distillation [63].

We have found that it is important that the product be distilled from the reaction mixture as it is formed to avoid side reactions. In a typical synthesis, 1 gm of erythritol (Sigma) and 0.1 gm of Fisher Rexyn 101(H^+) ion exchange resin was placed in a micro distillation flask in an oil bath which had been preheated to 140° C. The bath temperature was allowed to rise to 190° C, at which time product distilled out of the flask at 0.7 mm Hg. Product purity was achieved by the third redistillation, when the product distilled at 89° C (0.3 mm Hg).

Synthesis of 1,4-anhydrothreitol† was achieved in a similar manner from threitol. A recent report [64] has given the synthesis of 1,4-anhydrothreitol by epimerization of 1,4-anhydroerythritol *via* the monotosylate. One gm of d,ℓ-threitol (Sigma) was cyclized with 0.1 gm of Fisher Rexyn 101(H^+) ion exchange resin. A second distillation gave a boiling point at 130° C and 0.3 mm Hg. The reaction went smoother and faster than the cyclization of erythritol, as would be expected for the *trans* configuration of hydroxyls. The higher boiling point is consistent with the absence of intramolecular hydrogen bonding and with greater intermolecular hydrogen bonding for *trans* diols compared to *cis* diols.

The ^1H spectrum of 1,4-anhydroerythritol-d_2, which was obtained by lyophilization from D_2O, was recorded at 100 MHz in $HFCCl_2$ at room

---

*Cis-3,4-dihydroxy tetrahydrofuran

†Trans-3,4-dihydroxy tetrahydrofuran

Figure 6. (a) The ^{1}H NMR spectrum of 1,4-anhydroerythritol-d_2, in $HFCCl_2$ with internal hexamethyl disiloxane reference; external ^{19}F field frequency lock. Sweep offset 84823 Hz, sweep width 100 Hz.

(b) The ^{1}H NMR spectrum of 1,4-anhydrothreitol in D_2O with internal reference TMS; external ^{19}F lock. Sweep offset 85315 Hz, sweep width 100 Hz.

Spectrometer frequency 100 MHz.

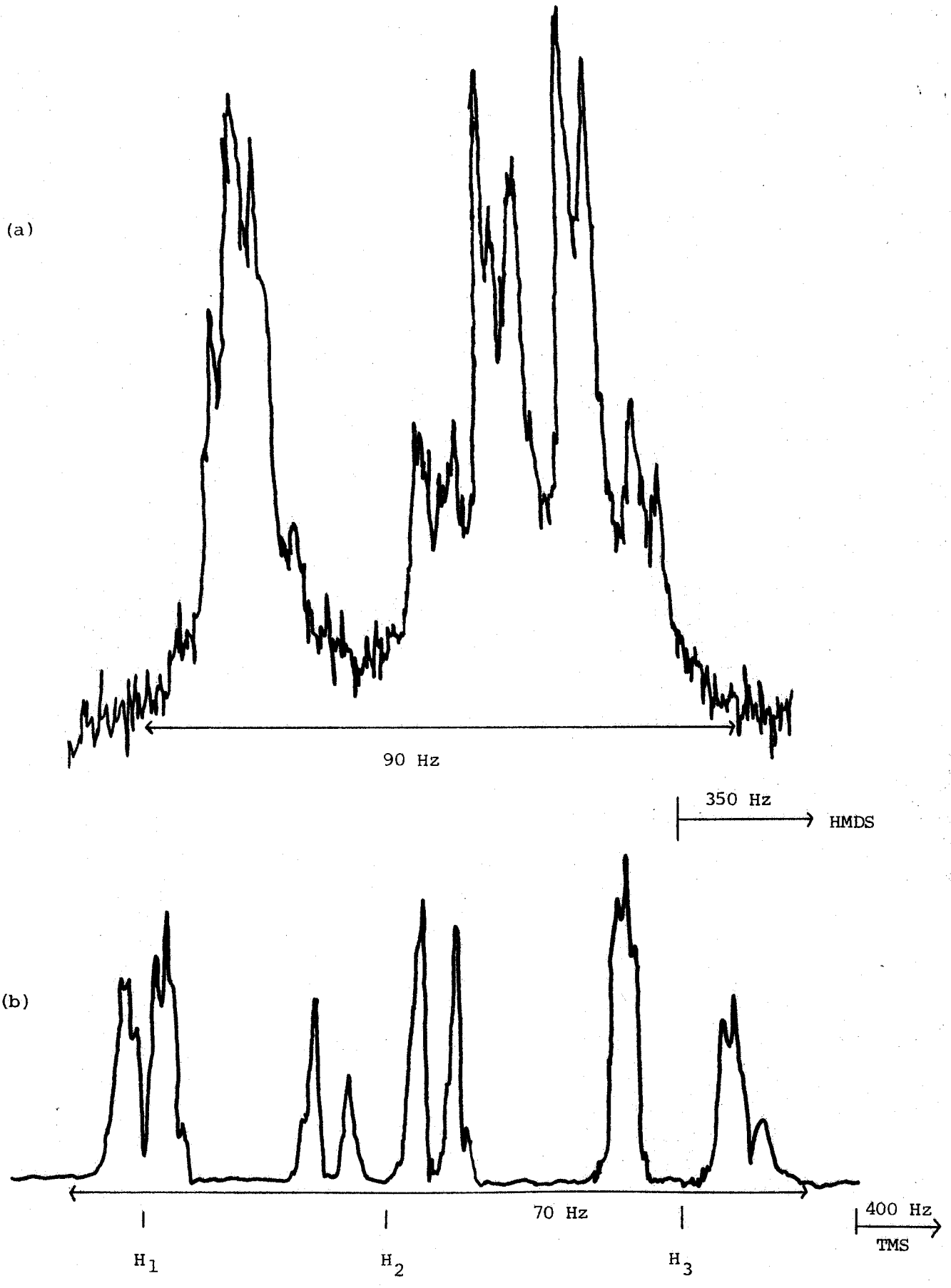
(a)
90 Hz
350 Hz
HMDS
(b)
70 Hz
400 Hz
TMS
H1
H2
H3

temperature in a sealed tube using an external fluorine lock. A deceptively simple spectrum, consistent with an AA'BB'CC'system, yielded a doublet of doublet of doublets, with relative intensities 1:3:3:1, in that region which gave 2/3 of the total proton intensity.

The $^{13}C\{^{1}H\}$ spectrum (proton irradiation off during acquisition) of 1,4-anhydrothreitol was recorded at 25.2 MHz in D_2O with internal deuterium lock at room temperature. Splittings due to one and two directly bonded hydrogens were evident. The assignments and chemical shifts calculated relative to TMS were in agreement with literature values [65].

The $^{13}C\{^{1}H\}$ spectrum (proton irradiation off during acquisition) of 1,4-anhydroerythritol was recorded at 25.2 MHz and 15.08 MHz in D_2O with internal deuterium lock at room temperature. Splittings characteristic of one directly bonded hydrogen on one carbon and two directly bonded hydrogens on the other carbon were seen. The assignments and chemical shifts calculated relative to TMS were consistent with values given in the literature [65,66].

The ^{1}H spectrum of 1,4-anhydrothreitol in D_2O was recorded at 100 MHz using an external flourine lock at room temperature. The spectrum was consistent with that of an AA'BB'CC' system in which J_{AC} and $J_{AC'}$ are negligible. The proton of intermediate chemical shift appeared as a doublet of doublets, being coupled to the other two protons, which appeared as doublets, to first order.

Gas chromatography-mass spectral analysis of 1,4-anhydroerythritol and 1,4-anhydrothreitol showed these materials to be relatively pure, as shown by the g.c. trace (due to the total ion current). The parent peak for both compounds had a value of 105 mass units. The molecular weight of each is 104. This discrepency can be rationalized as being due to an ion-

Figure 7. G.C. trace due to total ion current of 1,4-anhydroerythritol. Instrumental system consisted of a Varian Aerograph series 1400 gas chromatograph, a Hitachi-Perkin-Elmer RMU-6E Mass Spectrometer, and a System Industries, Sytem 150 data system. 100% represents the digitization value.

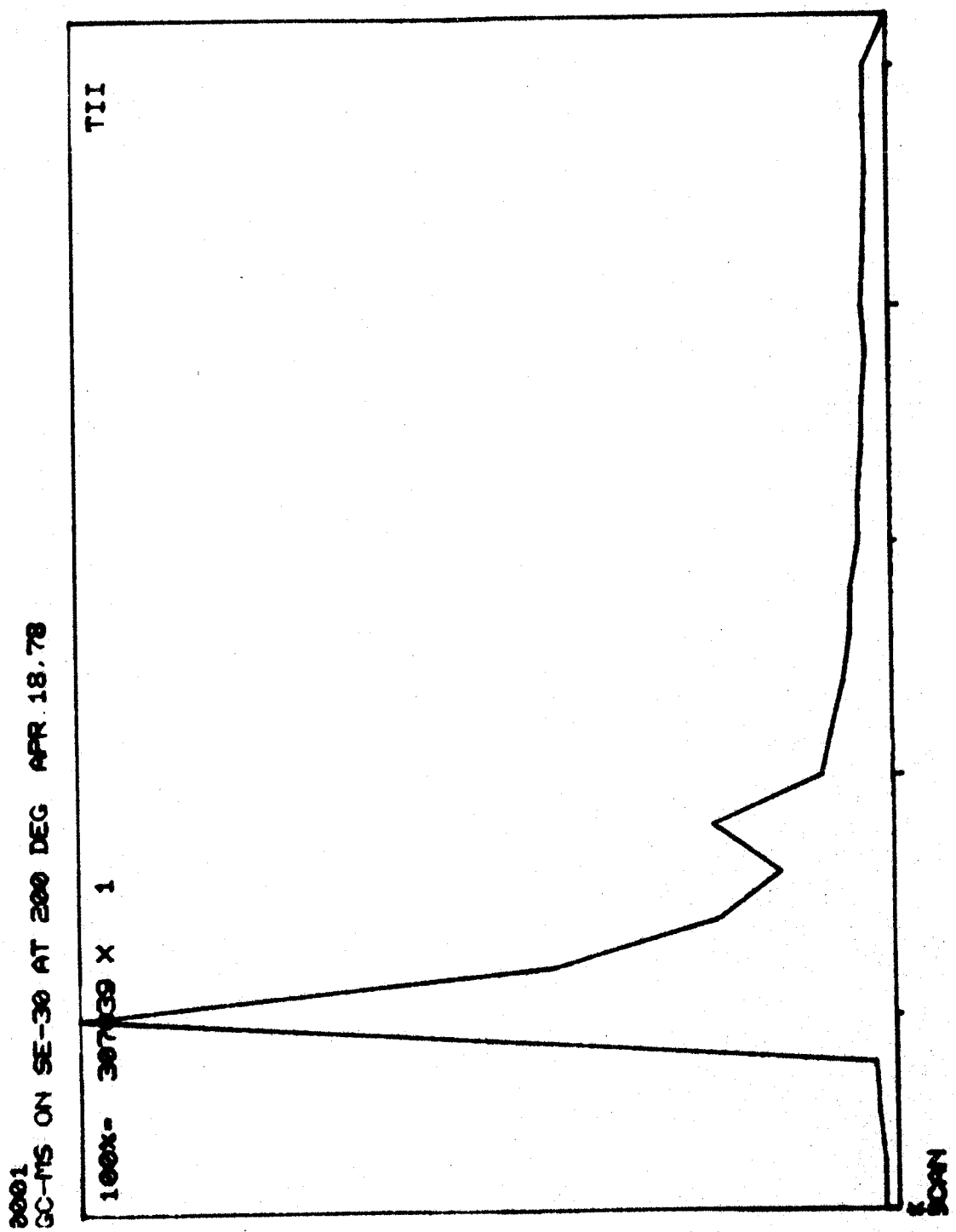
2001
GC-MS ON SE-30 AT 200 DEG APR 18.78
TII
100%- 307/39 X 1
SCAN

Figure 8. M.S. fragmentation pattern of 1,4-anhydroerythritol. Retention time = 36 seconds.

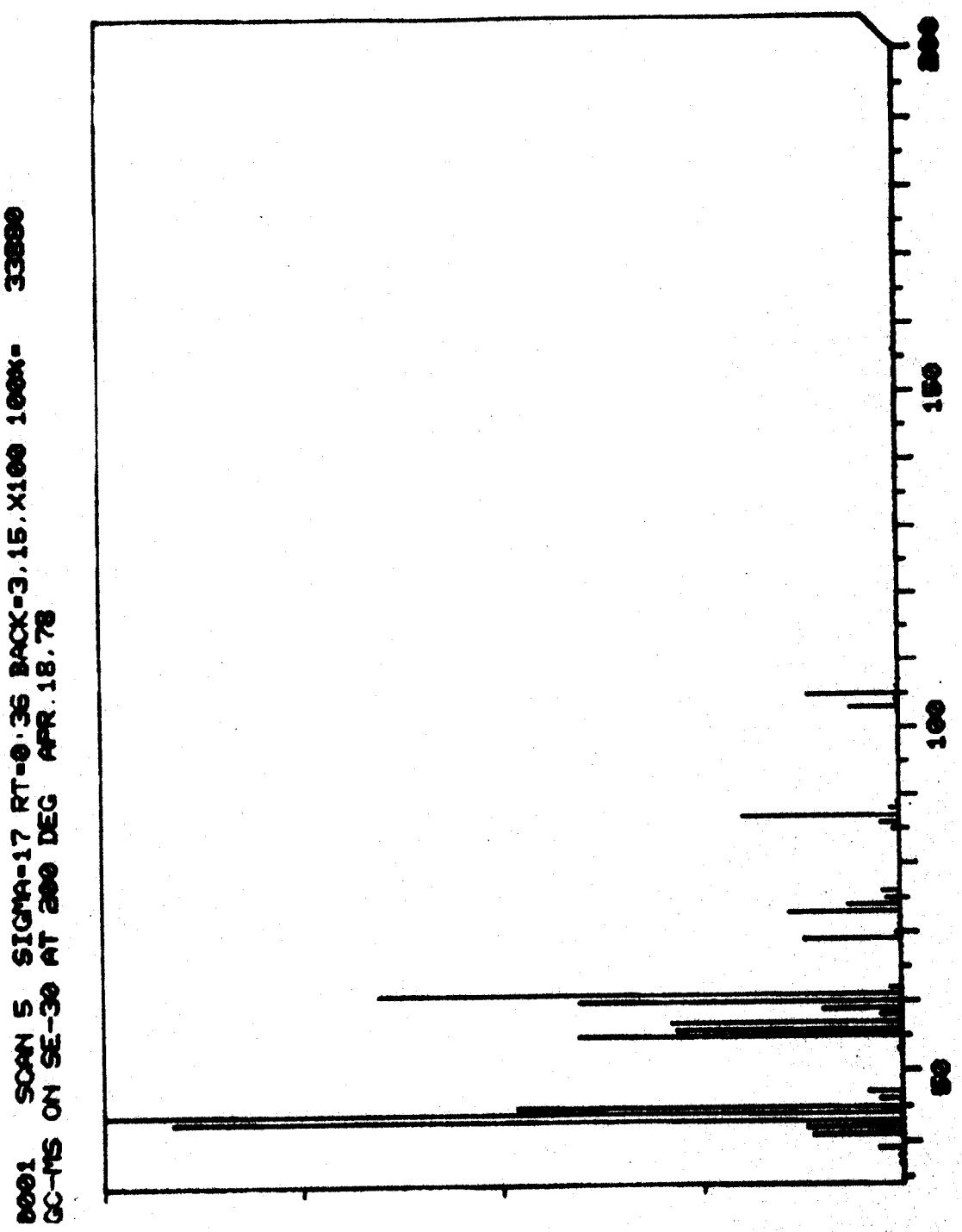
0001 SCAN 5 SIGMA-17 RT-0:35 BACK-3,15 X100 100%- 33000
GC-MS ON SE-30 AT 200 DEG APR.18,78
200
150
100
50

Figure 9. M.S. fragmentation pattern of 1,4-anhydrothreitol.

Retention time = 36 seconds.

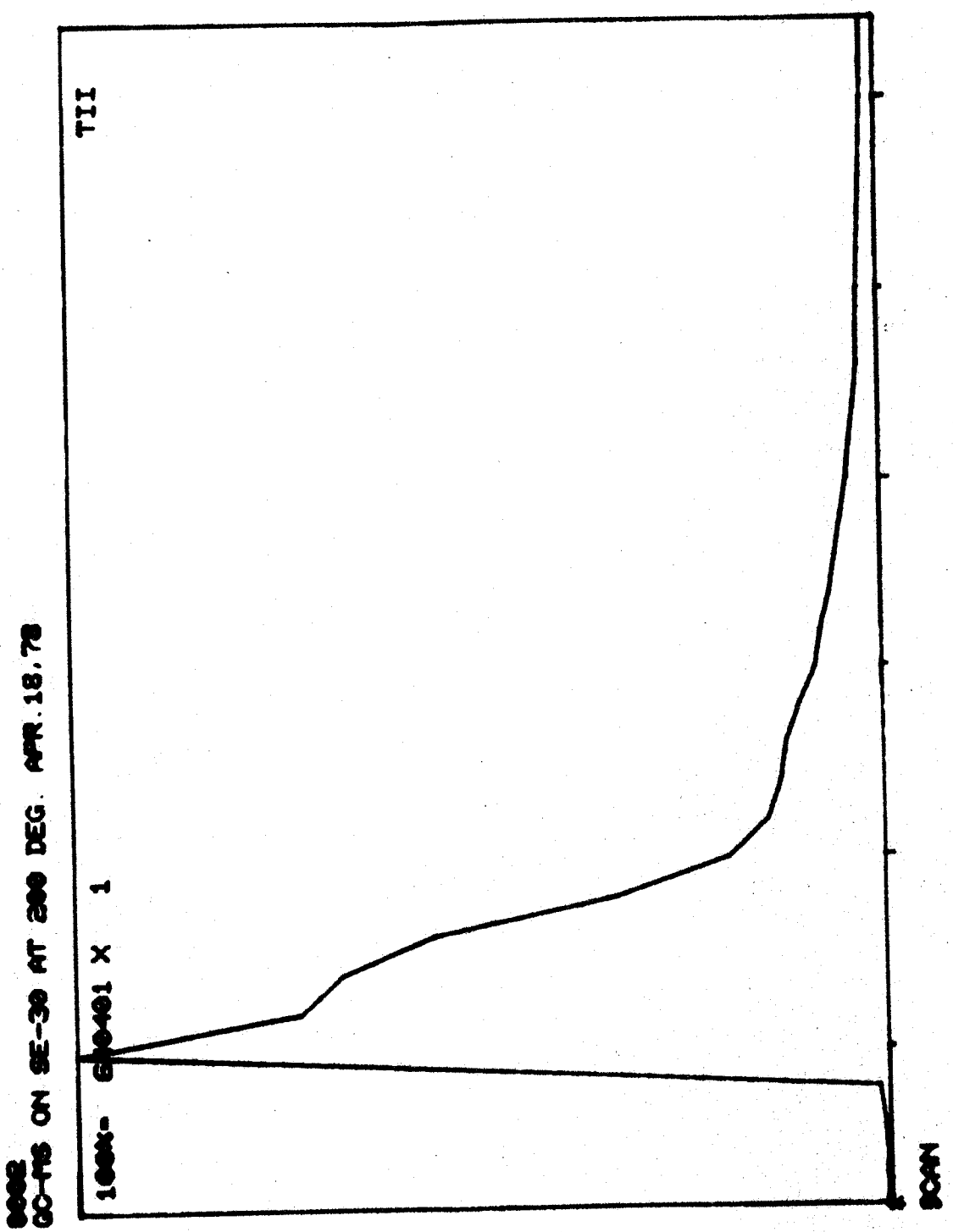
TII
SCAN

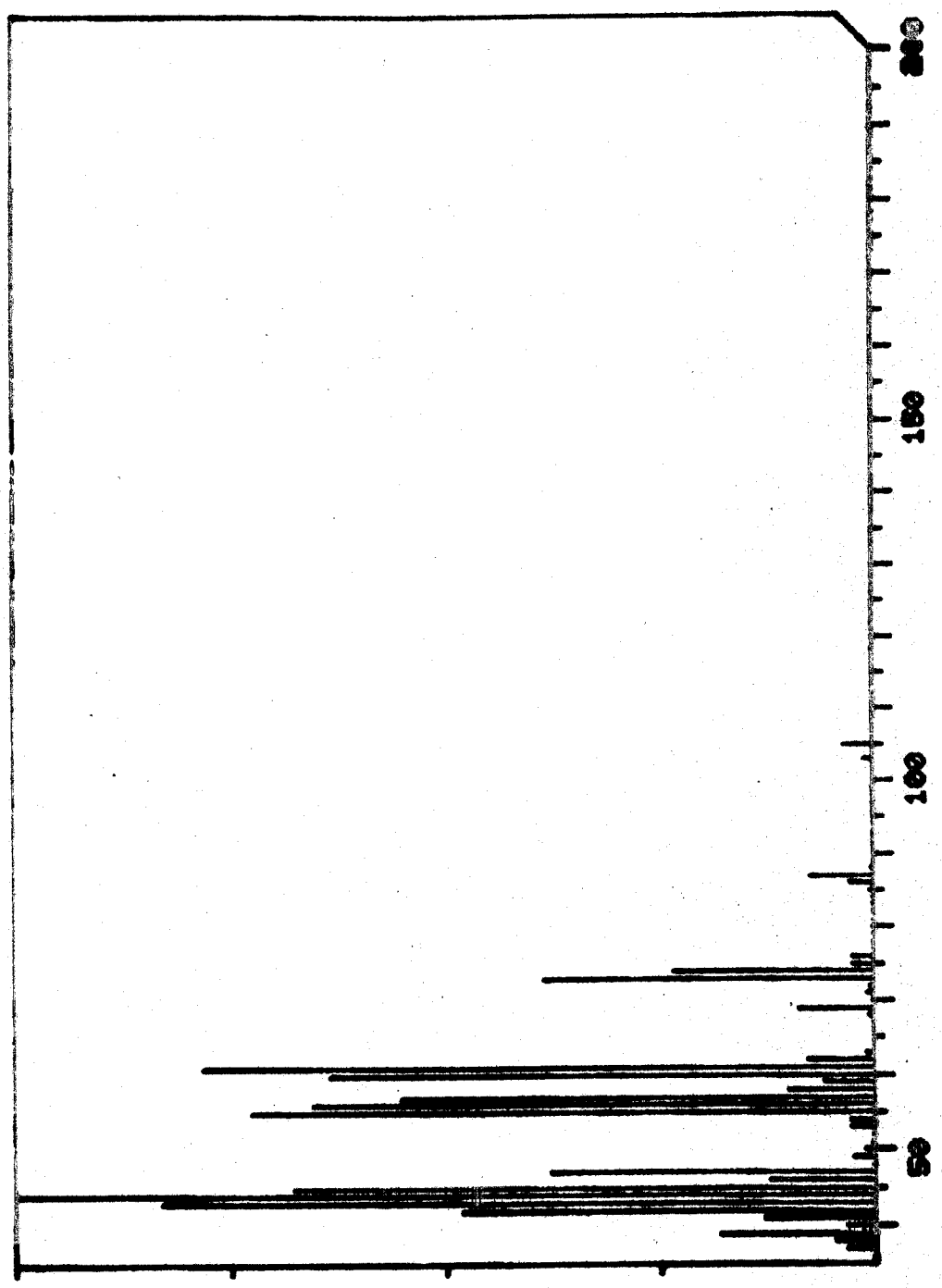
SCAN 5 SIGMA-11 RT-0.35 BACK-3,30 X100 100%
QC-FS ON SE-30 AT 200 DEG. APR.18,78
50
100
150

Figure 10. G.C. trace due to total ion current of 1,4-anhydrothreitol.

molecule reaction involving hydrogen atom transfer [67]. Many types of compounds, including alcohols which give molecular ions of low abundance, have a high cross section for such an ion-molecule reaction.

1,4-Anhydroerythritol gave a specific gravity of 1.33 and 1,4-anhydrothreitol gave a refractive index of 1.469 at room temperature.

In conclusion, the characterization studies of the two products provides no evidence that would suggest that they are not the expected products. Cyclization of polyhydric alcohols by the catalysis of strong acid ion exchange resin proved to be much more convenient than other methods [68,69] discussed in the literature. The anomeric specificity of the enzyme 6-phosphofructokinase has been established using structurally locked, isosteric analogues of D-fructose-1-phosphate [68]. 2,5-Anhydro-D-mannitol-1-phosphate is an alternate substrate of 6-phosphofructokinase, while 2,5-anhydro-D-glucitol-1-phosphate is a competitive inhibitor. With the intention of possibly elucidating the mechanism for these contrasting properties, the cyclization of D-mannitol and D-glucitol, to give the 2,5-anhydro products, was attempted. The volatile trimethyl silyl derivatives of the product mixtures were analyzed by g.c.-m.s., however, and proved to represent all possible furan, pyran and bicyclic structures. Potentially, separation of the products might yield useful materials.

4.1

^{13}C NMR Spectra

Typical experimental conditions for the determination of ^{13}C NMR spectra are represented by those for 1,4-anhydroerythritol. 25 µℓ of 1,4-anhydroerythritol, 0.1 molal, 10 µℓ dioxane, 0.04 molal, in 3.0 ml D_2O with the addition of a weighed portion of NH_4Cl were placed in a 12 mm sample tube and were deoxygenated with a stream of N_2 gas. NH_4Cl was recrystallized from water, vacuum dried, and weighed by analytical balance. The sample tube was spun in the probe at a rate of 25 rps. The temperature was thermostated with a temperature controller with a flow of cooling N_2 gas at 35 SCFH. The temperature reached upon equilibration was recorded using a double junction copper-constantan thermocouple and a Leeds and Northrop potentiometer[72] The junctions were encased in glass capillaries and the reference junction was placed in an ice water mixture and the other in the sample. A calibration curve for the double junction copper-constantan thermocouple was prepared with a variable temperature bath and comparison with the calibration table given in reference [70] showed that the latter calibration table was accurate to ± 0.1° C. Proton noise decoupled pulse FT NMR spectra were obtained at 25.2 MHz with an observe offset of 32001 Hz, using a 90° pulse of 22 µsec duration and a delay of 100 µsec before the start of digitization. Internal ^2H was used as a field-frequency lock. A 100.1 MHz proton decoupling RF field with an internal offset of 45040 Hz was applied with a 2 kHz noise bandwidth and 20 W power. A four pole Butterworth filter with cutoff frequency set to 1000 Hz was used to filter the observed signal and the ADC was set with 12 bits resolution for a signal of ± 1V. Of the order of 400 FID's were acquired at

a digitization rate of 2 kHz in a 16 K data set. A line broadening of 1 Hz was used before FT of the accumulated FID. Peak positions were determined by three point parabolic interpolation. The resolution limited by digitization is determined to be 0.125 Hz and the resolution limited by field inhomogeneity was measured to be of the order of 0.5 Hz at best. A Radiometer PHM 64 Research pH Meter was used for all pH measurements. For D_2O solutions, the correction pD = pH meter reading + 0.40, due to the glass electrode [71], was applied.

Dioxane was chosen as an internal chemical shift reference because it does not enter into any association complex reactions in the systems studied. Sodium 2,2-dimethyl,2-silapentane sulfonate, DSS, a common reference in aqueous solution, was rejected on this account and also because it does not give sufficient signal intensity in dilute solute where its detergency is minimized. In work with lysine (page 73) it was found that dioxane was stationary with respect to the resonances of the central carbons of lysine. A recent study by MacDonald [133] of amino acids used dioxane, 0.5% in D_2O, as an internal ^{13}C δ reference. Dioxane was assigned a chemical shift of 67.73 ppm.

RESULTS AND DISCUSSION

5.
Proton NMR Studies

A.H. Haines et al. [4] have studied the interaction of 1,4-anhydro-erythritol with sodium ions in acetone solution. The induced chemical shifts of proton resonances of the three proton positions are shown in Figure 11. They performed a Scott-Benesi-Hildebrand analysis of the equilibrium shift data assuming the formation of a 1:1 complex. The values of the equilibrium constant obtained from the chemical shift data for H(1), H(2), and H(3) are shown in Table IV. It is worthwhile at this point to compare the results of a non-linear regression analysis of the same data with a model in which the same assumptions implicit in the Scott-Benesi-Hildebrand technique [40,41] are nascent.

For the donor-salt complex, let the equilibrium expression be

$$K = \frac{[C]}{[D]\ [S]} \quad , \tag{64}$$

where [C] is concentration of complex and [D] and [S] are that of free donor and free salt, respectively.

Then, since

$$[C] + [D] = D_o \tag{65}$$

and

$$[C] + [S] = S_o, \quad \text{the initial concentrations,}$$

$$K = \frac{S_o - [S]}{(D_o - S_o + [S])\ [S]} \quad . \tag{66}$$

Since $[S] \geq 0$, we may solve for [S],

Figure 11. Induced chemical shifts ($\Delta\delta$),Hz of proton resonances of 1,4-anhydroerythritol, 0.136 M in acetone-d_6 solution, on addition of sodium iodide. H(1) ($-\odot-$), H(2) ($-X-$), H(3) ($-\boxdot-$); H(1) (+) with NBu_4I replacing NaI. Taken from reference [4]. See Figure 1.

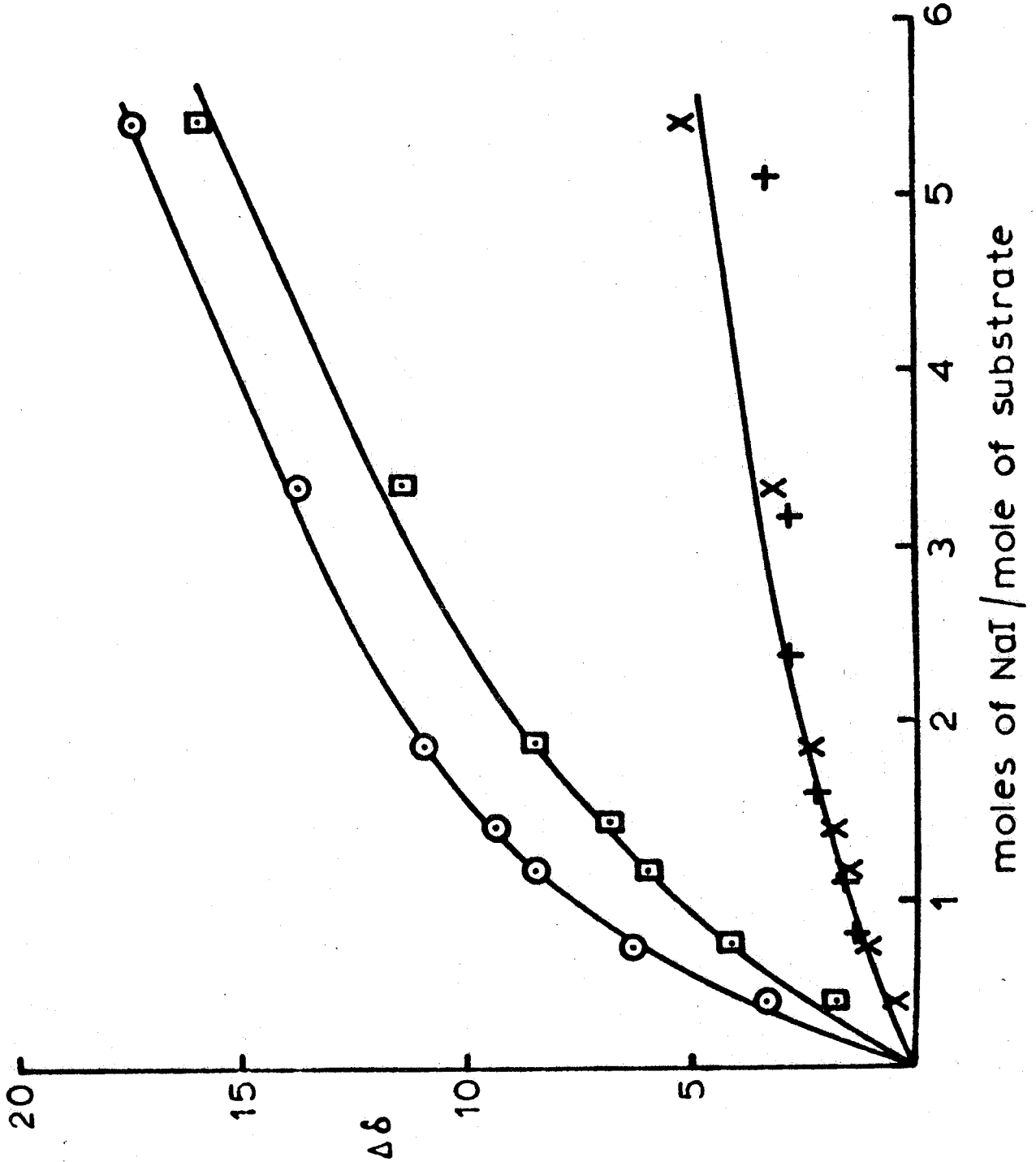
20
15
10
5
Δδ
1
2
3
4
5
6
moles of NaI/mole of substrate

TABLE IV

Measured and Predicted values of Δδ for various NaI molarities, Comparison of Scott-Benesi-Hildebrand with regression Model.

Molarity NaI	Δδ, Hz						Moles NaI/mole substrate
	H_1 measured,	predicted	H_2 measured,	predicted	H_3 measured,	predicted	
0.0	0.0	0.36	0.0	——	0.0	0.12	0.0
0.050	3.31	3.58	0.47	——	1.76	2.20	0.37
0.092	6.35	5.61	1.08	——	4.12	3.76	0.68
0.152	8.58	8.05	1.55	——	6.08	5.71	1.12
0.186	9.46	8.99	1.89	——	6.89	6.69	1.37
0.252	11.01	10.88	2.37	——	8.51	8.39	1.85
0.451	13.78	14.34	3.11	——	11.42	12.23	3.32
0.733	17.43	16.71	5.14	——	15.95	15.63	5.39
K, M^{-1} Scott-Benesi-Hildebrand	6 ± 0.6		1 ± 0.2		2.5 ±0.3		
K, M^{-1} Regression model	5.28 ± 0.7		——		2.18 ±0.6		

$$(67) \qquad [S] = \frac{K(S_o - D_o) - 1 + \sqrt{(K(D_o - S_o) + 1)^2 + 4K \cdot S_o}}{2K}$$

Given, $\delta_{obs} = n_D \delta_C + n_C \delta_C$, where n_D, n_C are the mole fractions of free donor and complex, and δ_D, δ_C are the chemical shifts of free donor and complex, respectively, we obtain $\delta_{obs} = \frac{\delta_D + \delta_C K [S]}{1 + K [S]}$

$$(68) \qquad \delta_{obs} = \frac{\delta_D + \delta_C/2[K(S_o - D_o) - 1 + \sqrt{[K(D_o - S_o) + 1]^2 + 4K \cdot S_o}}{\frac{1}{2}\left[K(S_o - D_o) + 1 + \sqrt{[K(D_o - S_o) + 1]^2 + 4K \cdot S_o}\right]}$$

This model equation is suitable for regression analysis of the given data in order to obtain the three unknown parameters, δ_D, δ_C, and K. The Regression program BMDX85 [59] was used, the FORTRAN coding of this model, with the necessary partial derivatives, is shown in subprogram form:

```
      SUBROUTINE FUN(F,D,P,X)
      DIMENSION D(1),P(1),X(1)
      DO=.136
      DX=DO-X(1)
      DKS=P(3)*DX
      SQDS=SQRT((DKS+1.)**2+4.*P(3)*X(1))
      F=(P(1)+.5*P(2)*(-DKS-1.+SQDS))/(.5*(-DKS+1.+SQDS))
      D(1)=2./(-DKS+1.+SQDS)
      D(2)=(-DKS-1.+SQDS)/(-DKS+1.+SQDS)
      D(3)=(P(2)-P(1))*(-.5*DX+((DKS+1.)*DX+2.*X(1))
     . /SQDS)/(.25*(-DKS+1.+SQDS)**2)
      RETURN
      END
```

where the identifications

$F \equiv \delta_{obs}$, $S_o \equiv X(1)$, $D_o \equiv DO$

$D(1) \equiv \partial \delta_{obs} / \partial \delta_D$,

$D(2) \equiv \partial \delta_{obs} / \partial \delta_C$,

$D(3) \equiv \partial \delta_{obs} / \partial K$, are made.

Table IV shows the comparison between the measured and the predicted values of $\Delta\delta$ for various values of the molarity of NaI and a comparison of the K values determined by the Scott-Benesi-Hildebrand technique and those determined by the regression model. The predicted values of $\Delta\delta$ given in Table IV are determined after the regression parameters have been obtained. The predicted values of $\Delta\delta$ for H(2) are not reproduced because the regression program BMDX85 [59] failed to converge after 100 iterations. This may be because of the poor quality of the data. The error ranges, based on standard deviations in computed line-positions for H(1), H(2), and H(3), are approximately 0.13, 0.05, and 0.05 Hz, respectively [4]. Additional error will accrue from the volumetric preparation of the various concentrations of NaI solution.

The comparison of the results of the Scott-Benesi-Hildebrand analysis and those of the regression model shows that essentially the same values of K are determined for each proton. The regression model is capable of adequately reproducing the data. The deficienceis of these two techniques, as applied to this data, are the same since they rely on the same assumptions. The assumptions of these analyses, some or all of which must be incorrect, are: (1) the equilibrium expression is given in terms of concentrations rather than activities, ideal equilibrium behaviour is assumed; (2) a 1:1 complex only is assumed; and (3) no interaction between substrate and solvent may be assumed.

Figure 11 also shows the induced chemical shift for H(1) with the addition of tetrabutylamonium iodide (NBu_4I). This data cannot be reconciled completely with the simple assumption of a Na-substrate interaction only in acetone solution. It is reasonable to suppose that NBu_4^+ is too

bulky, and less polar due to the aliphatic chains, to interact strongly with 1,4-anhydroerythritol. Although iodide is the least basic of all the halides [73], it may interact by hydrogen bonding with the hydroxyl protons or electrostatically by monopole-dipole interaction when it is at the opposite side of the molecule. An additional possibility is that the solvent, acetone, interacts with the substrate molecule and the addition of electrolytes alters the solvent structure so as to change the extent of the solvent-substrate interaction. For the system studied by A.H. Haines et al., there is not sufficient data to resolve the problem. But, clearly, if a given equilibrium can be isolated analytically, the values of the equilibrium constant, as determined from the chemical shifts of each nucleus, should be the same.

Figure 12. ^{1}H-noise decoupled ^{13}C NMR spectrum, at 25.2 MHz, of 1,4-anhydroerythritol, 1.4 M, in D_2O. Line separation 12.3 Hz, at room temperature.

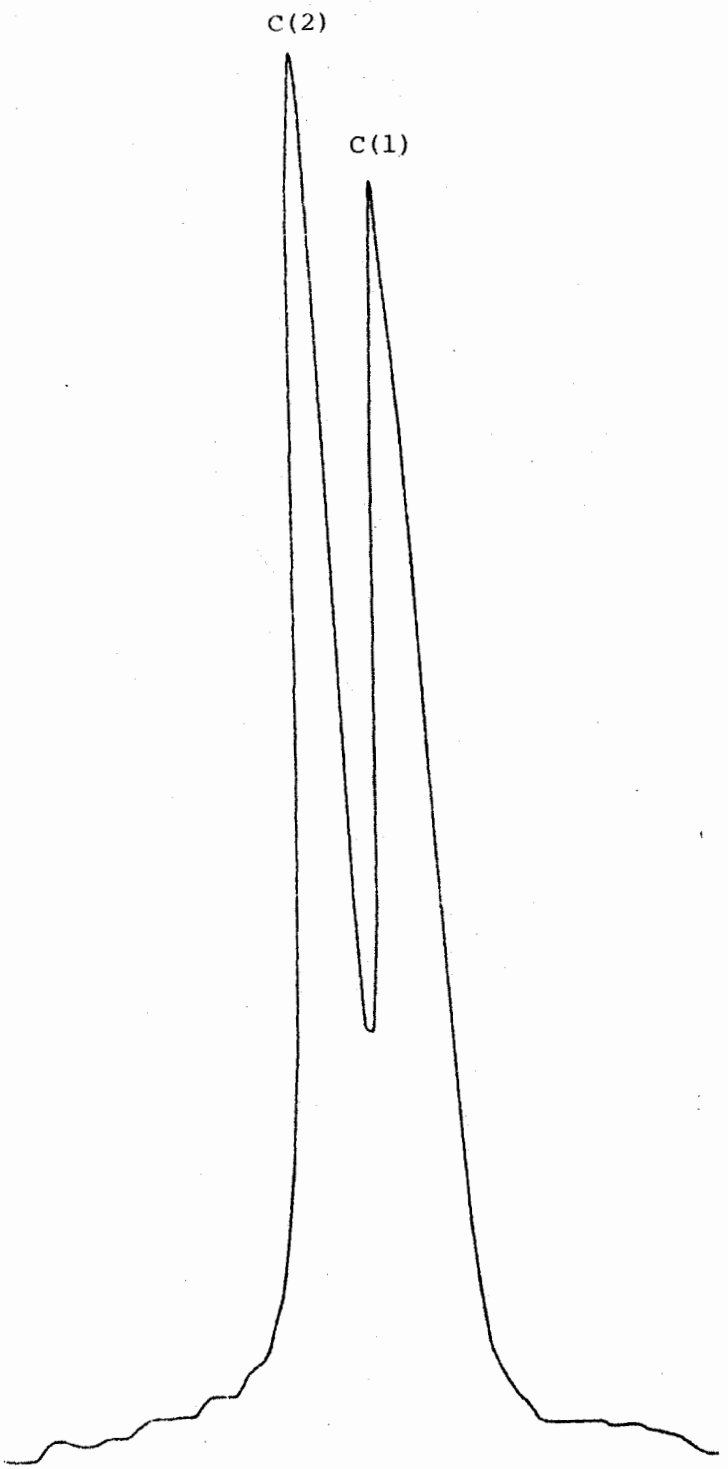
C(2)
C(1)

Figure 13. ^{1}H-noise decoupled ^{13}C NMR spectrum, at 25.2 MHz, of 1,4-anhydroerythritol, 1.4 M, and NH_4Cl, 6.65 M, in D_2O. Line separation 19.9 Hz, at room temperature.

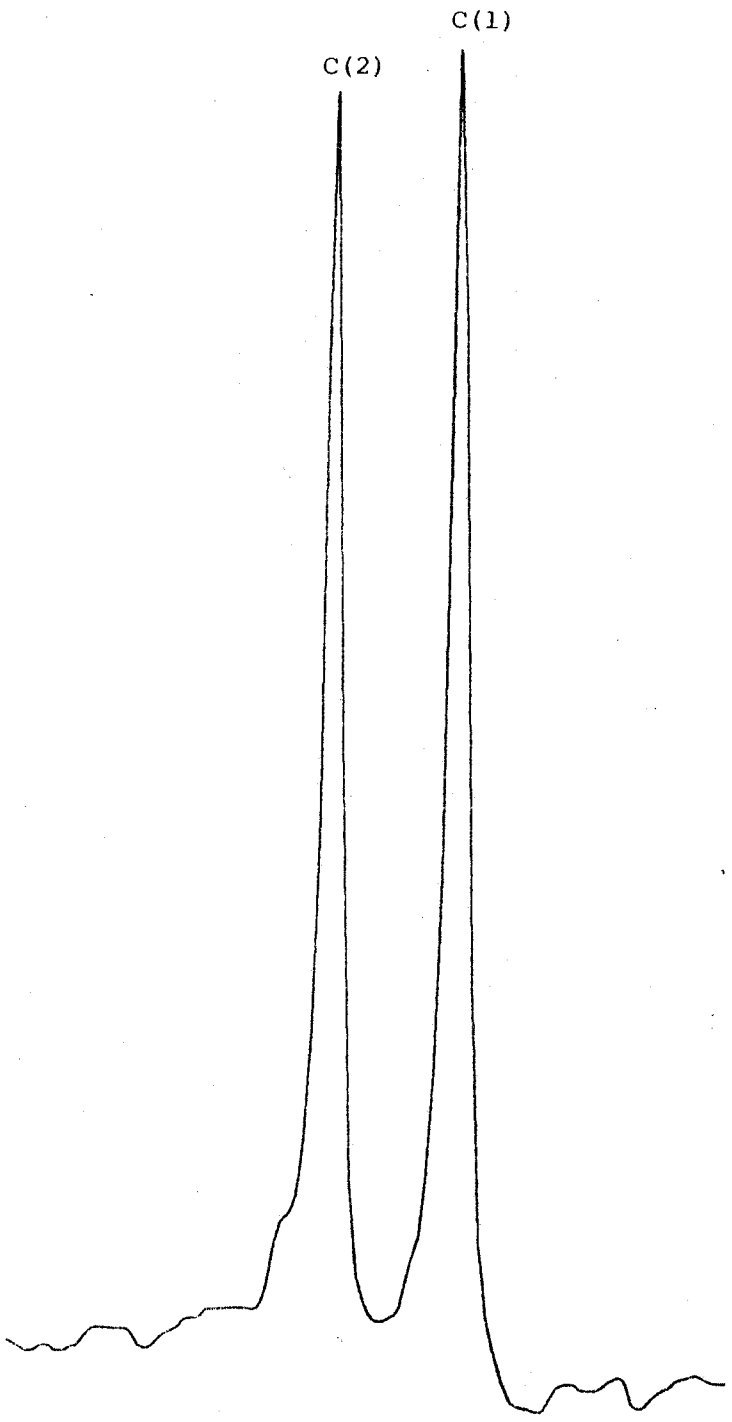
C(2)
C(1)

^{13}C NMR Studies

6.0

A. (Cyclytols and Ligands)

At 0° C and in the absence of salts, 1,4-anhydroerythritol in D_2O solution has a measured $\Delta\delta_{1,2}$= 0.42 ppm*. The maximum value of $\Delta\delta_{1,2}$ seen at 100° and saturated NH_4Cl is .965 ppm (24.3 Hz). Figure 14 shows that saturation (7.48 molal) of an aqueous solution of 1,4-anhydroerythritol, with NH_4Cl at room temperature, increased the $\Delta\delta_{1,2}$ to a value of 0.81 ppm. Further addition of the chloride salt, tetramethylammonium chloride, tends to cause the $\Delta\delta_{1,2}$ value to decrease towards its original value.

Figure 15 shows that the addition of tetrabutylammonium chloride to a solution of 1,4-anhydroerythritol, saturated in ammonium chloride and containing 1.23 molal tetramethylammonium chloride, may tend to increase $\Delta\delta_{1,2}$ somewhat.

These trends may be interpreted as follows. Ammonium chloride interacts specifically either through the ammonium ion or through the chloride ion to form a complex in equilibrium with other forms of 1,4-anhydroerythritol in solution, which has an increased value of $\Delta\delta_{1,2}$. The addition of tetramethylammonium chloride and tetrabutylammonium chloride alters the position of the equilibrium and decreases the observed $\Delta\delta_{1,2}$, which is an average for all species present in solution. If, for instance, 1,4-anhydroerythritol forms a specific complex with the chloride ion, then the equilibrium of that complex would be controlled by the activity of the chloride ion in solution. One would expect that, with increasing chloride ion concentration, the activity of the chloride ion would increase monotonically in spite of non-ideality due to interionic effects. Thus, one would

---

*$\Delta\delta$ is the difference in chemical shifts of the two carbons, C(1) and C(2), and serves as a useful indicator of chemical shift changes in the absence of an internal reference. In essence, one line serves as an intra-molecular reference for the other.

Figure 14. Plot of $\Delta\delta_{1,2}$ of 1,4-anhydroerythritol, 1.6 molal, in 2.0 mℓ D_2O with NH_4Cl, 7.48 molal upon addition of $(CH_3)_4NCl$. Spectra taken at room temperature on TT 14.

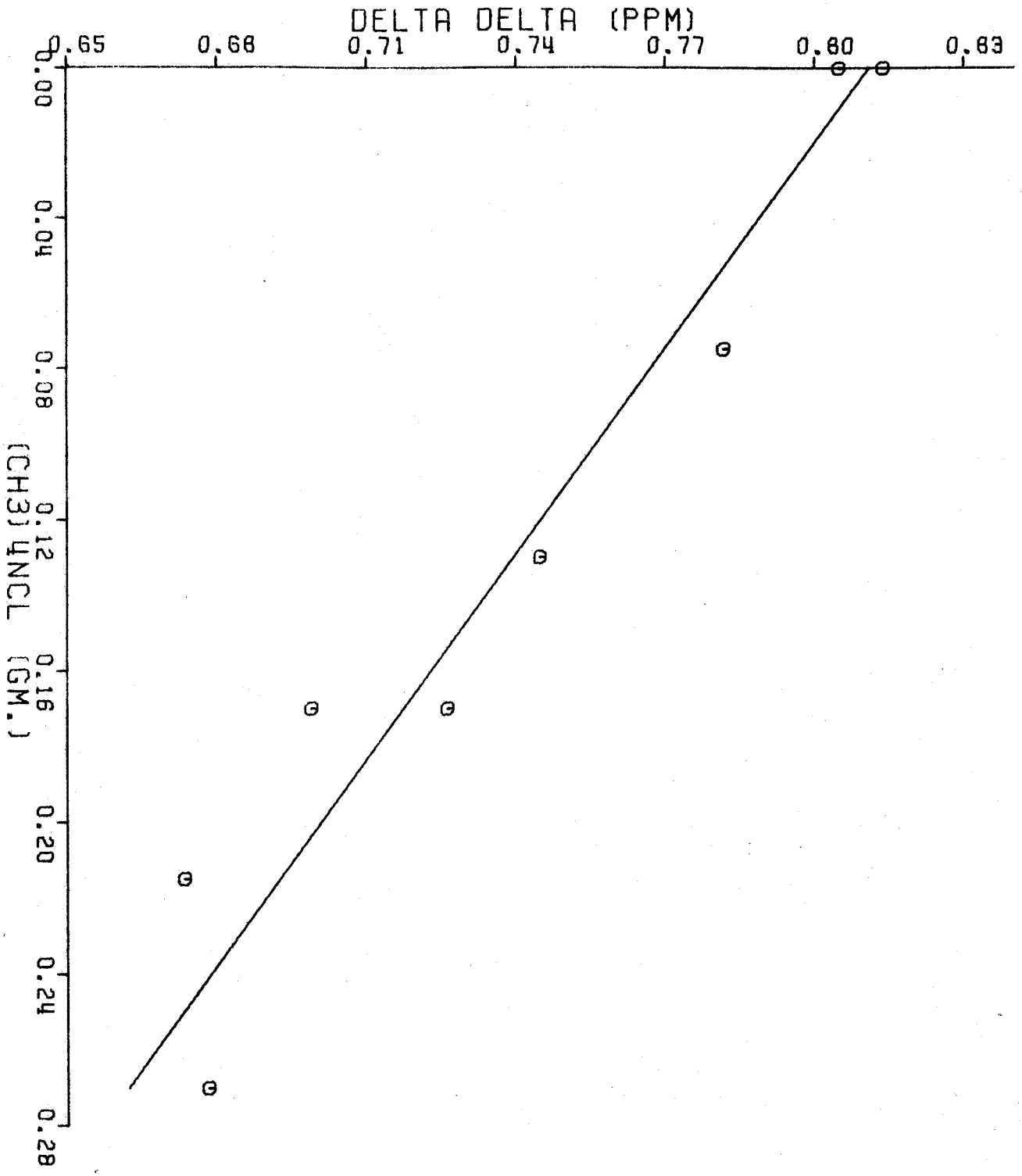

DELTA DELTA VERSUS ADDED TETRAMETHYLAMMONIUM CHLORIDE

Figure 15. Plot of $\Delta\delta_{1,2}$ of 1,4-anhydroerythritol, 1.6 molal, in 2.0 mℓ D_2O with NH_4Cl, 7.48 molal, and $(CH_3)_4NCl$, 1.23 molal, upon addition of $(C_4H_9)_3NCl$. Spectra taken at room temperature on TT 14.

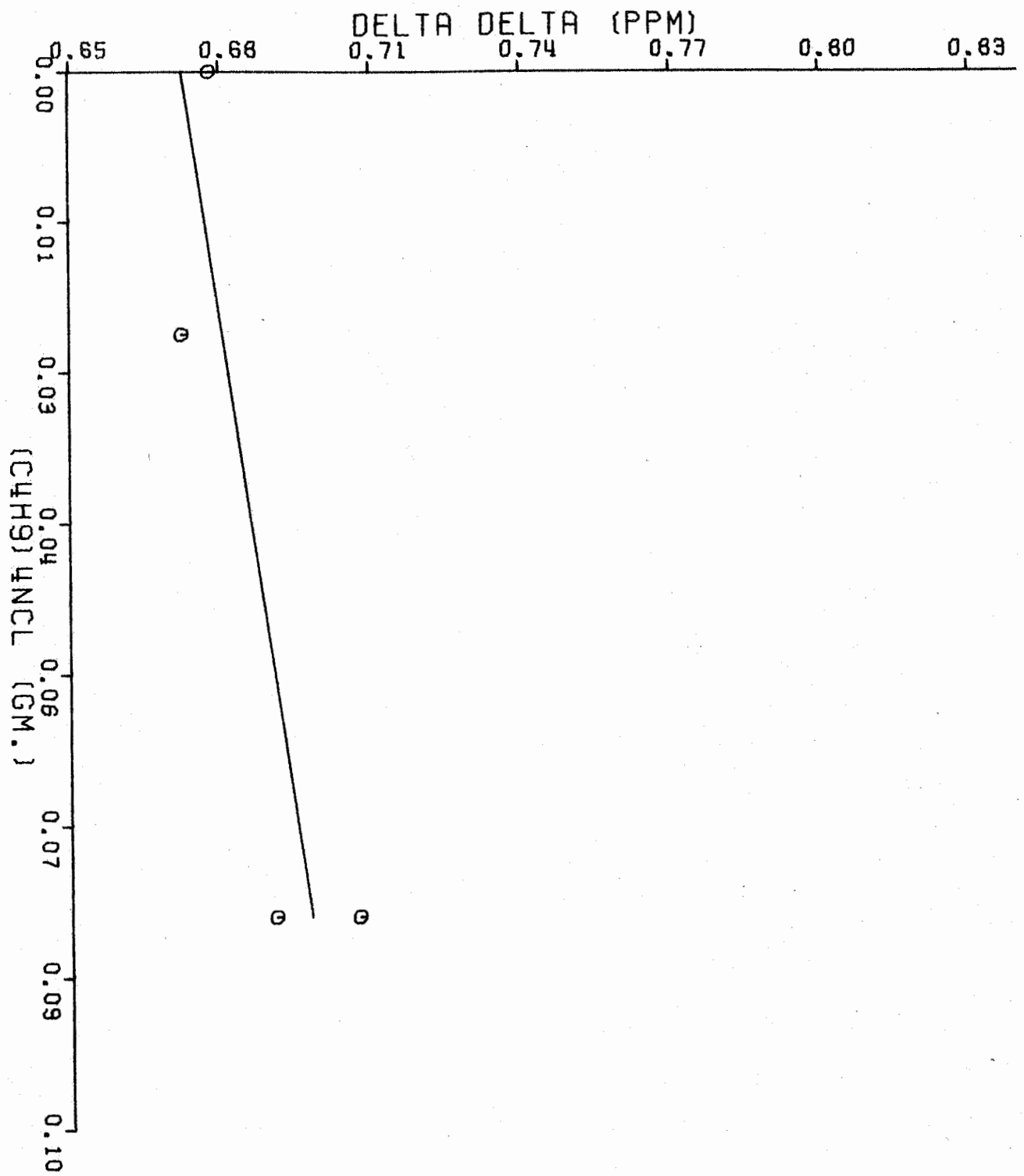

DELTA DELTA VERSUS ADDED TETRABUTYLAMMONIUM CHLORIDE

expect a uniform increase in the value of $\Delta\delta_{1,2}$ with added chloride. It is contradictory, then, when one concludes that the chloride does partici-pate in a specific complex with 1,4-anhydroerythritol. On the other hand, mixed electrolyte solutions can give rise to interionic effects whereby one ion can cause a decrease in the activity of another ion [74]. It is thus consistent with the data presented in Figures and to assume that spe-cific complexation between ammonium and 1,4-anhydroerythritol is responsible for the large change in $\Delta\delta_{1,2}$ and that the position of the equilibrium is controlled by the activity of the ammonium ion, which may vary due to inter-ionic effects.

Figure 16 shows the effect upon $\Delta\delta_{1,2}$ for 1,4-anhydrothreitol, 0.27 molal, of added ammonium chloride. The effect is much smaller than would be expected for complexation with ammonium ion. We explain this by the fact that 1,4-anhydrothreitol has its hydroxyls in the trans configuration, where they are not favorably disposed towards complexation.

In order to eliminate the possibility that H^+ or NH_3 were responsible for the observed large values of $\Delta\delta_{1,2}$, experiments were performed with the addition of aqueous HCl and aqueous ammonia. At a measured pD of 0.5, there was no change in the $\Delta\delta_{1,2}$ for 1,4-anhydroerythritol and 1,4-anhydro-threitol up to the limit of resolution , 0.5 Hz. In 2.47 molar NH_3, pD = 11.6, there was no change in $\Delta\delta_{1,2}$ up to the limit of resolution. In 2.47 molar NH_3, the concentration of ammonium ion is negligible.

Figure 16. Plot of $\Delta\delta_{1,2}$ of 1,4-anhydrothreitol, 0.27 molal, in D_2O upon addition of NH_4Cl. Spectra taken at room temperature on TT 14.

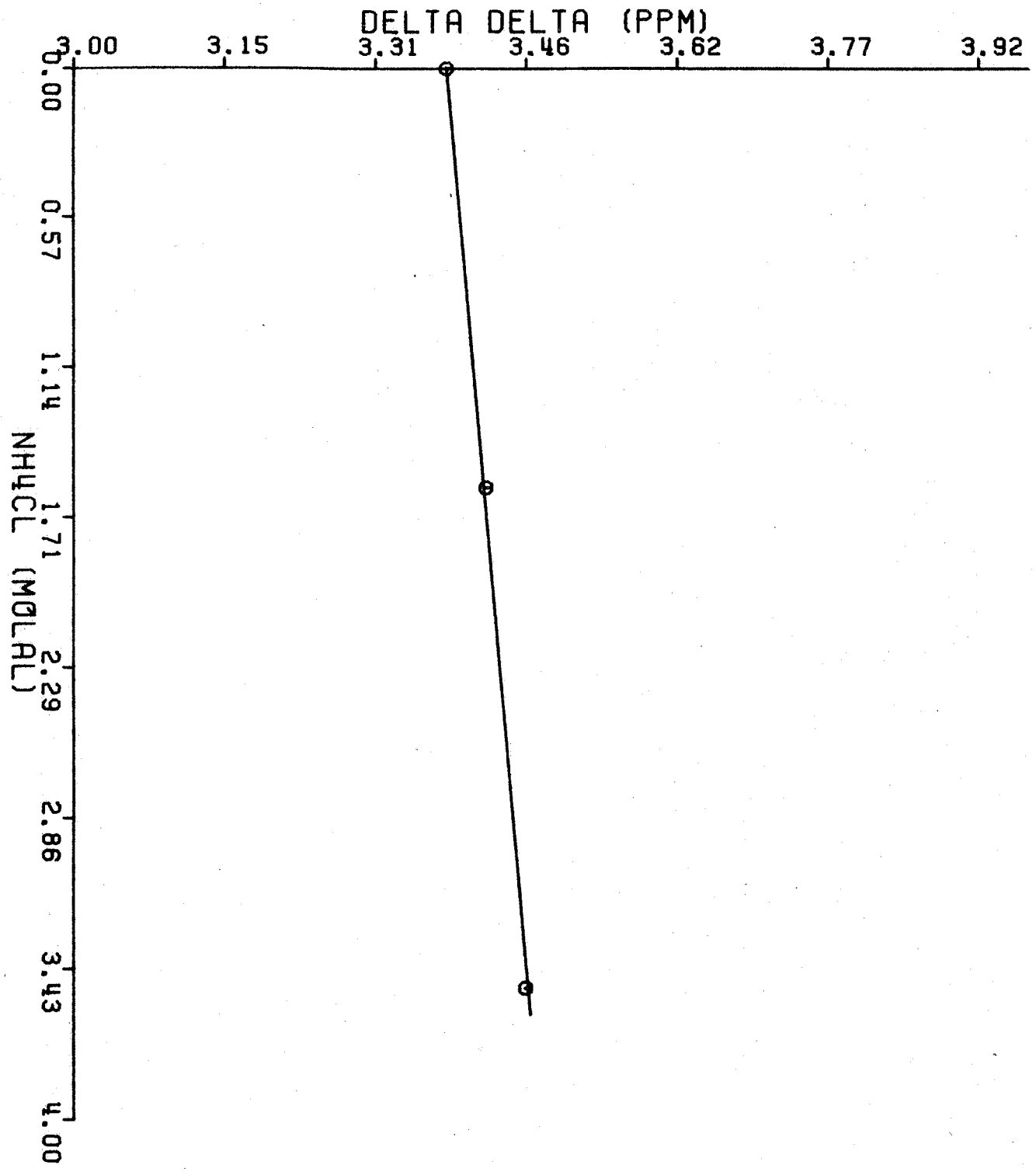

DELTA DELTA VERSUS ADDED AMMONIUM CHLORIDE

The effect of the variation of temperature may be studied in any investigation of equilibrium phenomenon. Figure 17 shows the change in the chemical shift of C(1) (with respect to reference dioxane) of 1,4-anhydroerythritol in D_2O with changing temperature. The solid line represents the best fit parabola, which is meant to indicate the trend only. The trend clearly shows an initial shift upfield towards dioxane with increasing temperature, the chemical shift reaching a minimum at about 55^{o} C, and a downfield shift with further increase in temperature. Figure 18 shows the corresponding trend for C(2). The best fit straight line again simply indicates the trend.

Figure 19 shows the plots of the C(1) and C(2) chemical shifts of 1,4-anhydroerythritol, 0.2 molal, in $CDCl_3$ at various temperatures. In contrast to the previous two plots, monotonic behaviour of the shifts is evident and the least squares fit parameters are shown on the Figure. Figure 20 shows similar plots for 1,4-anhydrothreitol, 0.1 molal, in D_2O as a function of temperature. Again, monotonic behaviour is evident.

1,4-Anhydroerythritol in aqueous solution clearly undergoes a unique interaction with the solvent. The conclusions one would make from the data presented in Figures 17 - 20 are that, because of its geometric features, 1,4-anhydroerythritol is capable of a specific interaction with water and ammonium ion to an extent that 1,4-anhydrothreitol is not. The equilibrium of this interaction is controlled by the activity of the water, which is temperature dependent since at higher temperatures kT allows the disruption of water clusters to form ultimately more water monomers. Chloroform is relatively inert to these two compounds due to its more nonpolar character compared to water. In order to test these assertions and couterproposals, it is necessary to establish a model which adequately reproduces the data.

Figure 17. Plot of C(1) chemical shift relative to reference dioxane versus temperature of 1,4-anhydroerythritol at 0.1 molal in D_2O. Spectrum from XL 100.

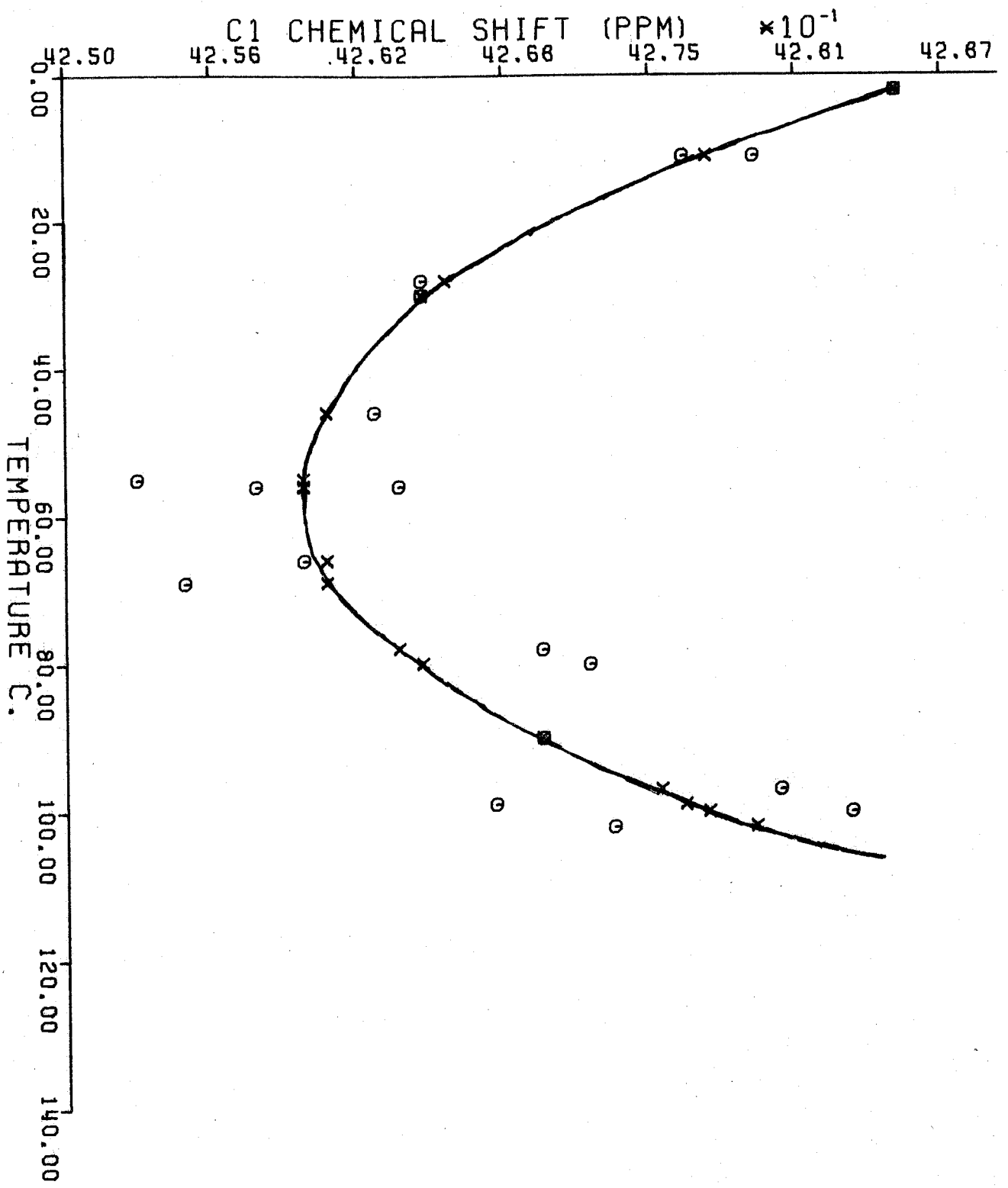

CHEMICAL SHIFT OF C1 VERSUS TEMPERATURE, REFERENCE DIOXANE

Figure 18. Plot of C(2) chemical shift relative to reference dioxane versus temperature of 1,4-anhydroerythritol at 0.1 molal in D_2O. Spectrum from XL 100.

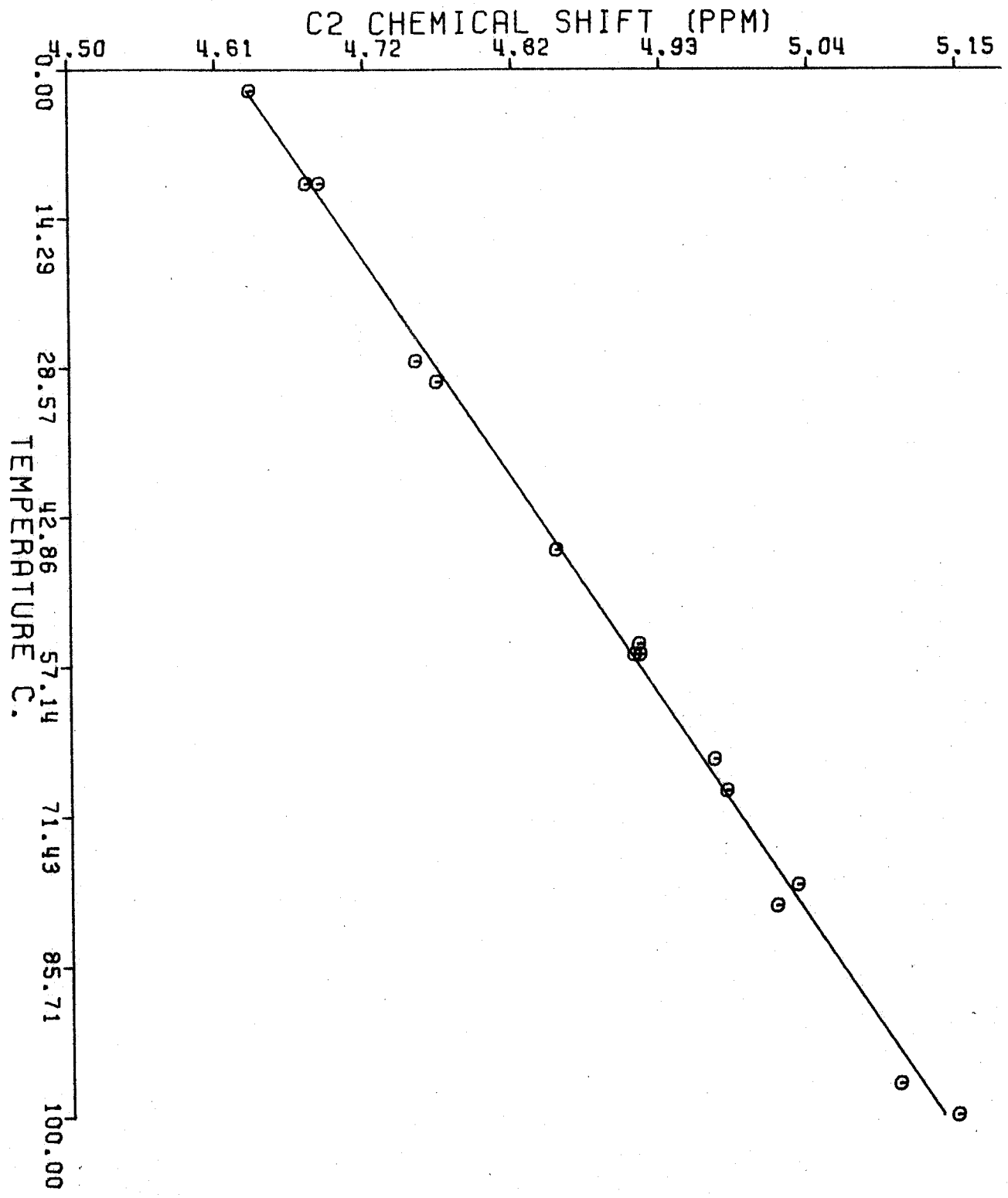

CHEMICAL SHIFT OF C2 VERSUS TEMPERATURE, REFERENCE DIOXANE

Figure 19. Plots of C(1) and C(2) chemical shifts of 1,4-anhydroerythritol, reference dioxane, 0.2 molal in $CDCl_3$ versus temperature. Spectrum from XL 100.

⊙ - C(1)

⊡ - C(2)

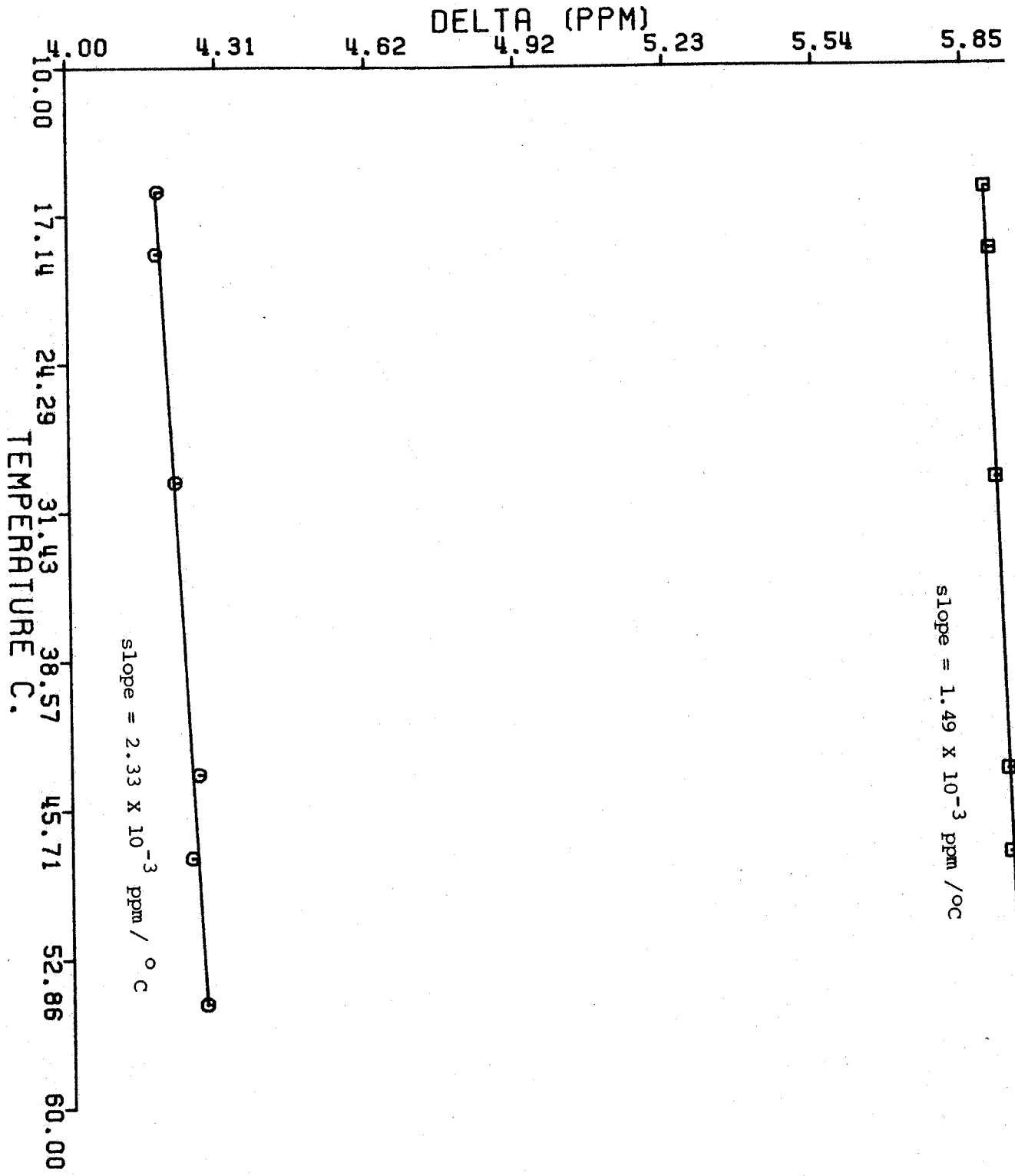

CHEMICAL SHIFT OF C1 C2 VERSUS TEMPERATURE

Figure 20. Plots of C(1) and C(2) chemical shifts of 1,4-anhydrothreitol, 0.1 molal in D_2O, versus temperature. Spectrum from XL 100.

⊙ - C(1)

⊡ - C(2)

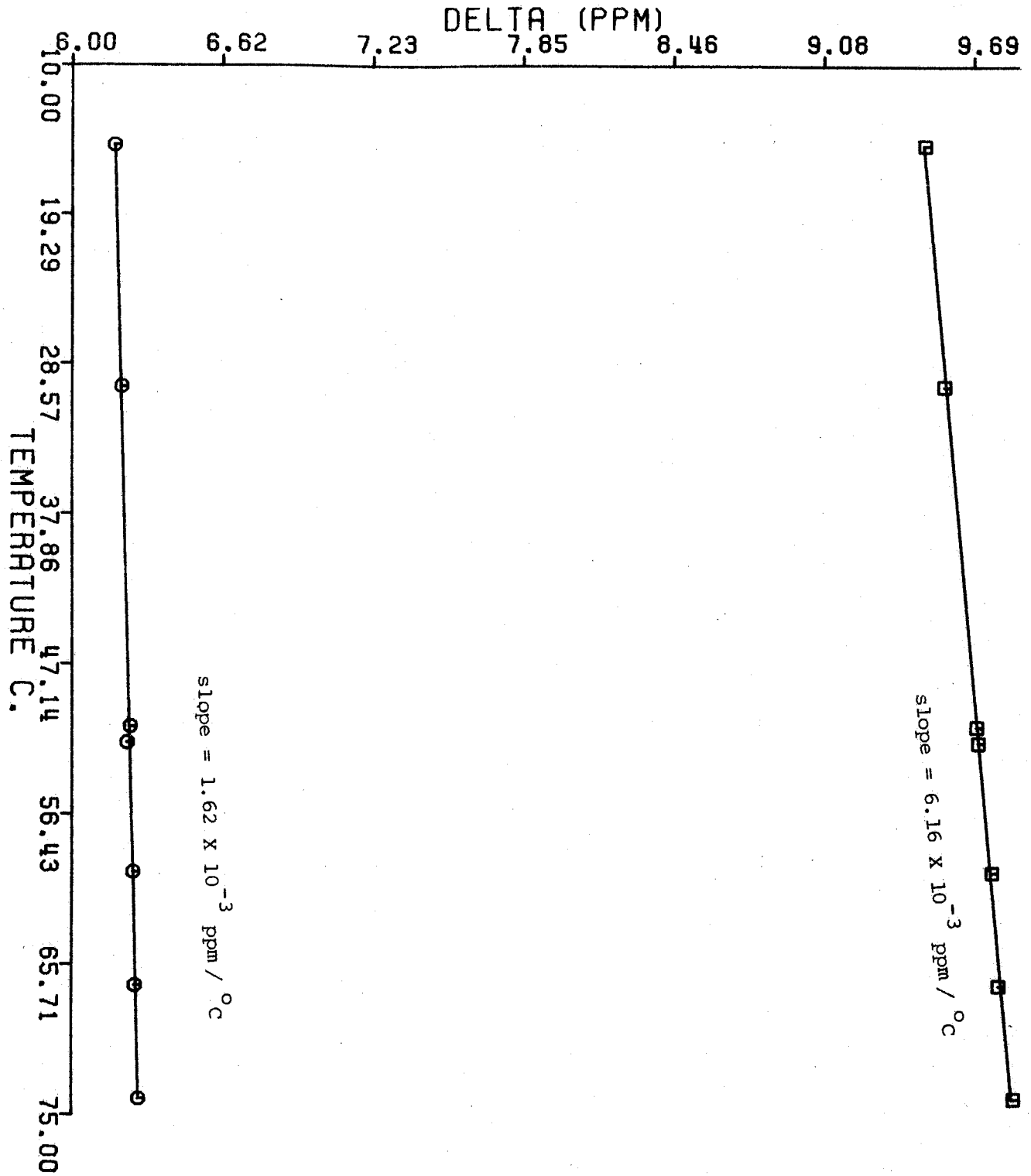

CHEMICAL SHIFT OF C1 C2 VERSUS TEMPERATURE

Table V shows the induced ^{13}C chemical shift in 1,4-anhydroerythritol, 0.13 molal, in D_2O with the addition of NH_4Cl. Dioxane was used as the reference. Spectra were obtained on the TT 14, at 16.08 MHz at room temperature. Temperature of the sample is not known due to dielectric heating of strong electrolyte solutions by intense RF fields. In spite of this limitation, regular trends in the chemical shifts can be seen.

The activity values at various concentrations of NH_4Cl shown in Table V were obtained from Figure 21, produced from data in reference [75], which gives the dependence of activity on concentration at 25°C. Activities must be used since solutions of NH_4Cl are known to depart significantly from ideality.

If one assumes a model in which equilibrium with a 1:1 complex is achieved and in which, because of a small equilibrium constant and small concentration of the donor species, corrections to the free salt concentration need not be made, then the observed ^{13}C chemical shift is

$$\delta^i_{obs} = \frac{\delta^i_D + \delta^i_C K [S]}{1 + K [S]} \quad , \tag{69}$$

(see eqn. # 68, page 54), where δ^i_D, δ^i_C are the chemical shift values of a given nucleus in the free donor and in the molecule complex, respectively, and K and [S] are the equilibrium constant and the total salt concentration respectively. Since we have shown activities must be used instead of concentration, equ. (69) becomes

$$\delta^i_{obs} = \frac{\delta^i_D + \delta^i_C K a_S}{1 + K a_S} \tag{70}$$

TABLE V

Measured and Predicted ^{13}C Chemical Shifts, $\delta\ ^{13}C$, of 1,4-Anhydroerythritol with Addition of NH_4Cl.

Concentration NH_4Cl, molal	Activity, NH_4Cl	Measured $\delta_{C(1)}$, (ppm) reference Dioxane	Predicted $\delta_{C(1)}$, (ppm)	Measured $\delta_{C(2)}$, (ppm) reference Dioxane	Predicted $\delta_{C(2)}$, (ppm)	Measured $\Delta\delta_{1,2}$, (ppm)	Predicted $\Delta\delta_{1,2}$, (ppm)
0.0	0.0	4.27300	4.27329	4.78400	4.78419	0.51100	0.51097
0.0	0.0	4.27600	4.27329	4.79100	4.78419	0.51500	0.51097
0.0	0.0	4.27600	4.27329	4.78200	4.78419	0.50600	0.51097
0.0	0.0	4.27600	4.27329	4.78800	4.78419	0.51200	0.51097
0.00370	0.00370	4.27500	4.27325	4.79000	4.78439	0.51500	0.51121
0.01230	0.01230	4.27400	4.27314	4.79200	4.78485	0.51800	0.51178
0.02160	0.01940	4.26900	4.27305	4.78500	4.78523	0.51600	0.51225
0.08560	0.06850	4.27400	4.27242	4.78600	4.78786	0.51200	0.51550
0.15550	0.11580	4.27500	4.27182	4.78300	4.79039	0.50800	0.51863
0.25570	0.18000	4.26900	4.27100	4.78400	4.79382	0.51500	0.52288
0.39670	0.26460	4.27500	4.26993	4.80100	4.79835	0.52600	0.52848
0.4662	0.30540	4.26500	4.26941	4.79200	4.80053	0.52700	0.53118
0.58440	0.37340	4.25800	4.26854	4.79300	4.80416	0.53600	0.53568
0.72380	0.45090	4.26200	4.26756	4.81900	4.80831	0.55700	0.54080
0.81950	0.50480	4.26400	4.26687	4.82000	4.81119	0.55600	0.54437
0.94290	0.57230	4.26100	4.26602	4.81600	4.81479	0.55500	0.54883
1.11600	0.68080	4.26000	4.26464	4.82300	4.82059	0.56300	0.55600
3.5600	1.99540	4.26700	4.24799	4.92600	4.89061	0.65900	0.64264
4.64700	2.60230	4.23800	4.24033	4.92900	4.92282	0.69100	0.68250
5.51000	3.08560	4.23600	4.23425	4.90300	4.94842	0.66700	0.71419
6.35100	3.55660	4.24400	4.22832	4.95200	4.97333	0.70800	0.74501
7.07700	3.96310	4.23700	4.22322	4.95100	4.99479	0.71400	0.77157
7.49300	4.19610	4.22100	4.22030	5.02300	5.00709	0.80200	0.78678
8.38200	4.69390	4.18000	4.21406	5.04300	5.03331	0.86300	0.81922
9.43600	5.28420	4.21100	4.20668	5.10000	5.06434	0.88900	0.85762

Predicted K, M^{-1}	$1.7996 \times 10^{-3} \pm .00007$	$1.7997 \times 10^{-3} \pm .00007$	$1.7995 \times 10^{-3} \pm .00007$
Predicted δ_{free} (ppm)	$4.2733 \pm .003$	$4.784 \pm .005$	$.0511 \pm .006$
Predicted δ_{Bound} (ppm) ($\Delta\delta$ Bound)	-2.798 ± 0.5	34.522 ± 0.6	37.313 ± 1.4

Figure 21. Smoothed curve representing the mean ionic activity coefficient, $\gamma_{\pm}$, of aqueous ammonium chloride at 25° C as a function of molality, m [75].

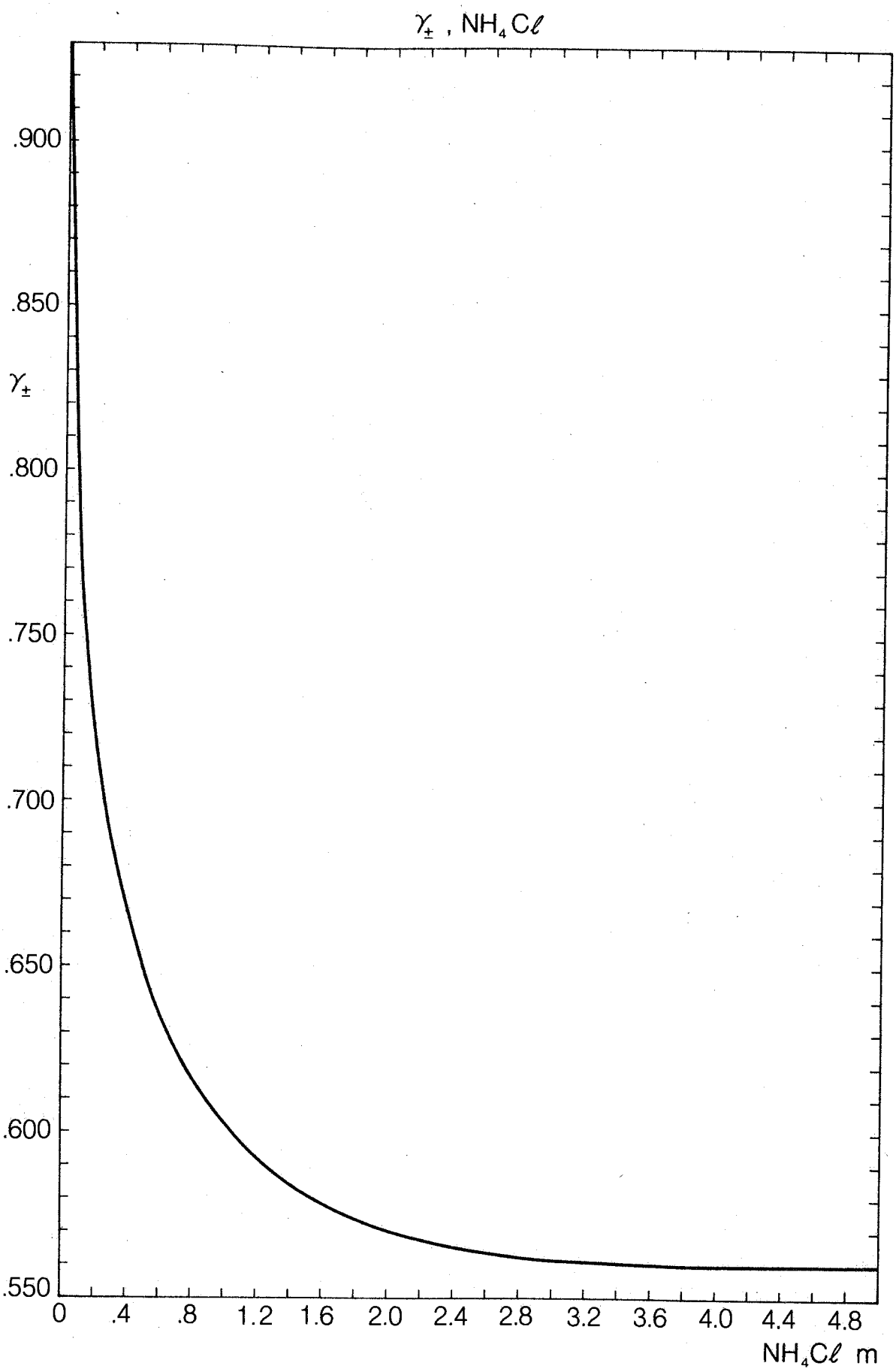
$\gamma_{\pm}$, $NH_4C\ell$
.900
.850
$\gamma_{\pm}$
.800
.750
.700
.650
.600
.550
0
.4
.8
1.2
1.6
2.0
2.4
2.8
3.2
3.6
4.0
4.4
4.8
$NH_4C\ell$ m

where a_S is the mean ionic activity of the salt and now K is defined as

(71) $K = \frac{a_C}{a_D a_S}$, in terms of activities of donor, a_D, salt, a_S, and of complex a_C.

In order to analyze the data presented in Table V, the model above was coded in FORTRAN subprogram form, with appropriate derivatives as shown,

```
SUBROUTINE FUN(F,D,P,X)
DIMENSION D(1),P(1),X(1)
F=(P(1)+P(2)*P(3)*X(1))/(1.+P(3)*X(1))
D(1)=1./(1.+P(3)*X(1))
D(2)=P(3)*X(1)/(1.+P(3)*X(1))
D(3)=(P(2)-P(1))*X(1)/(1.+P(3)*X(1))**2
RETURN
END
```

Non-linear regression analysis gave the parameters shown also in Table V (K, δ_{free}, δ_{Bound}, $\Delta\delta_{Bound}$). Note that the K values predicted by C(1), C(2), and $\Delta\delta_{1,2}$ are the same and that there is consistency amongst the δ^1_{free}, δ^2_{free}, δ^1_{bound}, δ^2_{bound}, and $\Delta\delta_{1,2\ free}$ and $\Delta\delta_{1,2\ bound}$ values. The predicted chemical shifts are calculated from the parameters determined in the regression analysis and they reproduce the measured values adequately.

A word of caution is necessary in interpreting the value of this analysis. We have seen that the ^{13}C chemical shifts of 1,4-anhydroerythritol are temperature dependent and no critical examination of this phenomenum has been offered as yet. The shifts given in Table V were measured without temperature control. Temperature was not part of the model. Furthermore, the assumption of only a 1:1 complex in a simple equilibrium is an assumption of this analysis that has not been given critical consideration.

Before going on to the temperature problem, it may be remarked that the roles of the donor and the acceptor may be reversed. In an attempt to observe an interaction between 1,4-anhydroerythritol and lysine ($^{+}NH_3(CH_2)_4CH(N^{+}H_3)COO^{-}$) in neutral solution, the ^{13}C spectrum of lysine, 0.13 M, was observed while the concentration of 1,4-anhydroerythritol was varied. Due to the low solubility, measurements were taken only up to 0.89 Molar in 1,4-anhydroerythritol. At this concentration, upfield shifts relative to the γ carbon of lysine were observed for the α methine carbon (+1.5 Hz) and the ε carbon (0.6 Hz). Both the α and ε carbons are bonded to amino functions and the $\Delta\delta_{1,2}$ of 1,4-anhydroerythritol showed an increase of 0.35 Hz. This indicates an interaction of 1,4-anhydroerythritol with the amino functions of lysine, with a concomitant shielding of the directly bonded carbons.

There are many conceivable approaches to the rationalization of the anomalous temperature behaviour of carbon C(1) of 1,4-anhydroerythritol in D_2O solution, as depicted in Figure 17 , as presented before. A conformational equilibrium of this non-rigid molecule is a possibility which might entail interconversion between an envelope and a half chair conformation during the making and breaking of an intramolecular hydrogen bond between adjacent cis hydroxyls [76]. There must be some participation of the solvent for this to be the case, however, because the temperature dependence of C(1) of 1,4-anhydroerythritol in $CDCl_3$, Figure 19 , shows an entirely different trend. The way in which a conformational equilibrium, or any equilibrium in which there is no stoichiometric change, may produce a temperature trend in the chemical shift,as is shown in 1,4-anhydroerythritol

is depicted in Figure 17, where the shifts of C(1) change sign after a certain temperature is reached. The explanation is that there must be equilibria with at least three states, i.e.

$$A \rightleftarrows B \rightleftarrows C \quad , \text{ with free energies of}$$

such states of order as

ΔG ,

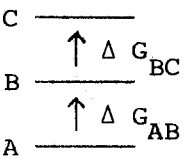

and chemical shifts out

of order, say,

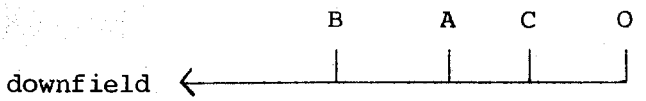

The expression for the observed shift is

$$(73) \qquad \delta_{obs} = \frac{\delta_A + \delta_B e^{-\Delta G_{AB}/RT} + \delta_C e^{-\Delta G_{AC}/RT}}{1 + e^{-\Delta G_{AB}/RT} + e^{-\Delta G_{AC}/RT}} \quad .$$

Then, as the temperature increases, the ratio of the populations of B to A will rise, driving the shift first downfield, then, with further increases in T, the relative population of C will become large enough to force the average observed shift upfield again. Since conformational changes result in little entropy changes unless there is a change in the symmetry, most of the free energy differences between such states is accounted for by the

enthalpy of the states.

The five parameter model given above was used for a regression analysis of the data, shown in Figure 17,18. After many initial parameter value estimates, no initial values iterated to a minimum solution which reproduced the main features of the data. Two possibilities are suggested: (1) the data does not have the functional form of the model, in spite of the observed minimum, or (2) there is a paucity of data and it is of too poor a quality to allow a five-parameter fit. The evidence of Figure 19 , the temperature trend in $CDCl_3$, would tend to support possibility (1).

Further ^{13}C data were collected. This was collected with temperature control and the recording of the various temperatures, and also with the addition of measured amounts of NH_4Cl in D_2O. The reasoning for this was that a large enough data set could explain the complexity of the observed phenomena. This data is shown in columns 4 - 7 in TABLE VII. Water was assumed to act as a ligand species, along with NH_4^+, and the activities of water and NH_4^+ at different temperatures and concentrations of NH_4Cl were determined as explained in the thermodynamic section. The calculated activities of water and NH_4^+ are shown in Table VII.

A general model, with undetermined stoichiometry, may be constructed for the dependence of the ^{13}C NMR chemical shifts upon the temperature and upon the activities of the two ligand species. Ignoring reactions with no stoichiometric change, this expression for δ^K_{obs} is

(74)

$$\delta^K_{obs} = \frac{\delta^K_o + \sum_{ij} \delta^K_{ij} e^{-g_{ij}/RT} (a_W)^i (a_A)^j}{1 + \sum_{ij} e^{-g_{ij}/RT} (a_W)^i (a_A)^j} ,$$

Figure 22. FORTRAN Subprogram encoded to represent conformational equilibrium model as given by equation (73).

```
 SUBROUTINE FUN(F,D,P,X)
 DIMENSION D(1),P(1),X(1)
R=1.98717
T=X(1)+273.
X1=EXP(-P(4)/(R*T))
X2=EXP(-P(5)/(R*T))
DEN=1.+X1+X2
NUM=1.+P(2)*X1+P(3)*X2
F=P(1)*NUM/DEN
D(1)=NUM/DEN
D(2)=P(1)*X1/DEN
D(3)=P(1)*X2/DEN
D(4)=P(1)*(-DEN*P(2)/(R*T)*X1+NUM/(R*T)*X1)/DEN**2
D(5)=P(1)*(-DEN*P(3)/(R*T)*X2+NUM/(R*T)*X2)/DEN**2
 RETURN
 END
```

where $g_{ij} = \Delta G_{ij} = \Delta H_{ij} - T\Delta S_{ij}$, (75)

which corresponds to the free energy of the reaction

$$E \rightleftarrows E \cdot iW \cdot jA \quad , \quad i = 1,2,\ldots, \quad j = 1,2,\ldots \quad ,$$

where E is the substrate, W is water, and A is ammonium. The expression for δ^K_{obs} accounts for the population averaging of all reactions within the allowable bounds of i and j, the number of each ligand. δ^K_o is the shift of nucleus K in the free substrate and δ^K_{ij} that of the ligated substrate. This functional model, with its necessary partial derivatives, was coded in subprogram form (shown in Appendix II) for non-linear parameter estimation using various available and modified programs. Specification of the stoichiometry in the model using decision table logic, an efficient programming technique, allowed the comparison of models with different stoichiometries. The imposition of linear equality constraints upon the thermodynamic parameters gave free energy values at 300^o K.

To give an example, by way of explanation, the stoichiometry implied by the reactions

$$E \rightleftarrows E \cdot W \rightleftarrows E \cdot A$$ gives rise to

(76)

$$\delta^K_{obs} = \frac{\delta_o + \delta_W \cdot e^{-g_W/RT} \cdot a_W + \delta_A \cdot e^{-g_A/RT} \cdot a_A}{1 + e^{-g_W/RT} \cdot a_W + e^{-g_A/RT} \cdot a_A}$$

with $g_W = \Delta H_W - T\Delta S_W$,

$g_A = \Delta H_A - T\Delta S_A$,

(77) $\Delta G_W\ (300^{\circ}\ K) = \Delta H_W - 300\ \Delta S_W$, and

$\Delta G_A\ (300^{\circ} K) = \Delta H_A - 300\ \Delta S_A$.

The number of parameters appearing either explicitly or implicitly in the regression model depends upon the stoichiometry chosen.

Table VI A.-G. shows the results of the parameter estimates and the residual mean square values for six models chosen in an attempt to explain the observed data. Model E. differs slightly from the rest in that it includes a term for a non-stoichiometric change, i.e. a conformational equilibrium. A. and B. give the results for the same model but, in the case of A., it is calculated using a double precision modification of BMDX85 [59] while, in B., additional parameters and linear equality constraints, to give ΔG values at 300° K, are included in a calculation using BMDP3R [60]. The results are very similar and the model used in calculations A. and B. gives the smallest value of the residual mean square, indicating that, of the six models, it is the best for the given data. The standard deviation estimates for the thermodynamic parameters ($\Delta H_{10} \equiv$ E10,..., $\Delta S_{10} \equiv$ S10,...) appear large and the standard deviations estimates for B120 $\equiv \delta^1_{20}$ and B220 $\equiv \delta^2_{20}$ also appear large, as does that for G20 = ΔG_{20}. It must be noted, however, that the relatively small temperature range employed does not allow the determination of the temperature effect upon ΔG unequivocally. The relatively small standard deviations estimated for G10, G01, and G11 are good as far as other calorimetric techniques are concerned. The standard deviation estimates of B120 and B220 are indeed not reliable estimates because, if B120 were to assume its lowest range, then the anomalous minimum in $\delta^1_{obs}(T)$ would not be reproduced for values of B120 < B110.

TABLE VI a

Parameter Estimates for Non-linear Models

Model: $E \rightleftarrows E\cdot H_2O \rightleftarrows E\cdot NH_4^+ \rightleftarrows E\cdot NH_4^+\cdot H_2O \rightleftarrows E\cdot 2H_2O$

	A. BMDX85/NAUGLER			B. BMDP3R		
Residual Mean Square	.000056886			.0000568878		
	Estimate	± S.D.		Estimate	± S.D.	
B10	4.289	.011	ppm	4.289	.011	ppm
B110	4.231	.035	"	4.231	.035	"
B101	4.118	.069	"	4.118	.069	"
B111	4.171	.098	"	4.171	.098	"
B120	4.84	8.58	"	4.85	9.14	"
E10	-1300.	2800	cal/m	-1300.	2900	cal/m
E01	3100.	1800	"	3100	1900	"
E11	7600	8200	"	7600	8000	"
E20	-3700	13000	"	-3700	15000	"
S10	-5.4	9.7	e.u.	-5.5	9.6	e.u.
S01	6.0	7.0	"	6.0	6.7	"
S11	14.3	25.5	"	14.3	26.1	"
S20	-23.4	65.4	"	-23.6	59.0	"
B20	4.58	.04	ppm	4.58	.04	ppm
B210	5.01	.14	"	5.01	.14	"
B201	5.72	.41	"	5.72	.41	"
B211	5.54	.47	"	5.54	.47	"
B220	6.92	26.95	"	6.98	(28.72	")
G10	———	———		352.	63.	cal/m
G01	———	———		1263.	108.	cal/m
G11	———	———		3320.	433.	"
G20	———	———		3366.	2334.	"

TABLE VI b

C. Model:

$$E \rightleftarrows E\cdot H_2O \rightleftarrows E\cdot NH_4^+ \rightleftarrows E\cdot 2NH_4^+ \rightleftarrows E\cdot 2H_2O$$

Residual Mean Square .00014997 not converged

	Estimate	±	S.D.	
B10	4.296		.025	ppm
B110	4.226		.059	"
B101	4.079		.593	"
B102	4.233		.056	"
B120	4.841		11.35	"
E10	-3600.		4200.	cal/m
E01	5600		8600.	"
E02	-1000		8100.	"
E20	7200		13000.	"
S10	-12.4		14.9	e.u.
S01	13.5		32.9	"
S02	-8.2		29.0	"
S20	-33.9		72.9	"
B20	4.52		.11	ppm
B210	5.02		.35	"
B201	5.92		3.25	"
B202	5.05		.18	"
B220	7.16		39.2	"

D. Model:

$$E \rightleftarrows E\cdot H_2O \rightleftarrows E\cdot 2H_2O \rightleftarrows E\cdot NH_4^+\cdot H_2O \rightleftarrows E\cdot NH_4^+ \rightleftarrows E\cdot 2NH_4^+$$

.000061434 not converged

	Estimate	±	S.D.	
B10	4.287		.009	ppm
B110	4.239		.020	"
B120	4.492		1.030	"
B111	4.091		.371	"
B101	4.194		.120	"
B102	7.310		41.09	"
E10	-1300.		3000.	cal/m
E20	-1900.		9700.	cal/m
E11	3300.		1500.	"
E01	4500.		3700.	"
E02	2900.		6700.	"
S10	-5.5		10.4	e.u.
S20	-17.0		35.5	"
S11	1.1		0.0	"
S01	12.7		15.3	"
S02	-7.6		25.8	"
B20	4.58		.04	ppm
B210	5.02		.14	"
B220	5.86		3.29	"
B211	6.68		3.43	"
B201	5.05		.52	"
B202	100.0		0.0	"

TABLE VI c

E. Model:

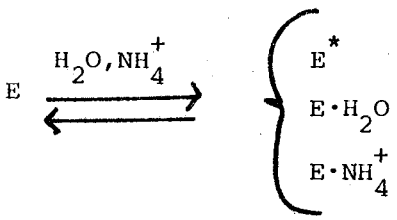

unstable, does not converge

F. Model:

$$E \rightleftarrows E \cdot H_2O \rightleftarrows E \cdot NH_4^+$$

Residual Mean Square .000091582

	Estimate	± S.D.	
B10	4.269	.006	ppm
B110	4.260	.018	"
B101	4.027	.015	"
E10	-7000.	1900.	cal/m
E01	1100	800.	"
S10	-26.5	7.9	e.u.
S01	-2.1	4.0	"
B20	4.43	.13	ppm
B210	6.26	1.82	"
B201	6.35	.99	"

G. Model:

$$E \rightleftarrows E \cdot H_2O \rightleftarrows E \cdot NH_4^+ \rightleftarrows E \cdot 2H_2O$$

.000075217

	Estimate	± S.D.	
B10	72.59	29.27	ppm
B110	4.220	.013	"
B101	4.167	.031	"
B120	5.352	.104	"
E10	-3900.	2800.	cal/m
E01	8500.	2700.	"
E20	10000.	0.0	"
S10	2.7	2.6	e.u.
S01	39.4	0.0	"
S20	-21.4	8.1	"
B20	-48.4	30.3	ppm
B210	4.56	.22	"
B201	5.58	.15	"
B220	5.98	1.27	"

Likewise, if B220 assumed its lowest range consistent with the standard deviation estimated, then $\delta^2_{obs}(T)$ would show an anomalous maximum. One concludes that all parameters associated with the formation of the double hydrate have standard deviations whose estimates are unreliable and too great, possibly because of outliers in the data.

Table VII presents a list of predicted dependent variables, the residues, the estimated standard deviation of the predicted value, the independent variables a_{H_2O}, $a_{\pm}(NH_4Cl)$, and T, and the observed chemical shifts, δ^K_{obs}. The agreement is good and most residues are within spectrometer error (±.005 ppm).

Table VIII shows the asymptotic correlation matrix of the parameters for the "correct" model, and a legend on the caption page that explains the symbolism. It is noted that, as expected, the ΔH_{ij} and ΔS_{ij} have a high error correlation. However, the ΔG values have relatively low intercorrelations. Thus, they may confidently be estimated independent of the errors of the others. In other words, the model gives a picture in which the four equilibria involved appear well-resolved. Among the δ estimates, the error correlations may be thought of as arising from coupling through the common reference, dioxane, or through coupling of errors in populations of reaction steps that are chained.

Figure 23 shows a plot of the predicted and observed values of δ^K, the ^{13}C chemical shift of C(1) and C(2) of 1,4-anhydroerythritol. The proximity of the predicted (P) and observed (O) values is immediately apparent. These values are grouped with the C(1) values appearing at the bottom of the graph and the C(2) values at the top. The co-ordinate axis

TABLE VII a

Independent, Observed and Predicted Variables of "True Model"

F	Y-F	STANDARD DEVIATION OF ESTIMATE	VARIABLES a_{H_2O}	$a_{\pm(NH_4Cl)}$	T, °C	$\delta^{K=1}_{obs}$
4.28117	0.00383	0.00484	0.22610	0.0	2.00000	4.28500
4.27716	-0.00116	0.00345	0.41375	0.0	11.00000	4.27600
4.27716	0.00184	0.00345	0.41375	0.0	11.00000	4.27900
4.26746	-0.00246	0.00322	1.19310	0.0	28.00000	4.26500
4.26633	-0.00133	0.00328	1.33921	0.0	30.00000	4.26500
4.25919	0.00381	0.00293	3.18329	0.0	46.00000	4.26300
4.25761	-0.00461	0.00240	4.96697	0.0	55.00000	4.25300
4.25756	0.00044	0.00237	5.20986	0.0	56.00000	4.25800
4.25756	0.00644	0.00237	5.20986	0.0	56.00000	4.26400
4.25869	0.00131	0.00246	8.25408	0.0	66.00000	4.26000
4.25958	-0.00458	0.00258	9.42003	0.0	69.00000	5.25500
4.26381	0.00619	0.00292	13.78591	0.0	78.00000	4.27000
4.26506	0.00694	0.00297	14.95883	0.0	80.00000	4.27200
4.27997	0.00003	0.00415	28.65968	0.0	97.00000	4.28000
4.28348	-0.00048	0.00501	31.98219	0.0	100.00000	4.28300
4.25140	-0.00140	0.00197	4.77089	0.68870	55.00000	4.25000
4.26526	-0.00426	0.00245	0.66293	0.70685	19.00000	4.26100
4.25813	-0.00013	0.00255	1.44260	0.70340	32.00000	4.25800
4.25177	0.00323	0.00216	3.92823	0.69192	51.00000	4.25500
4.25286	0.00314	0.00196	8.65759	0.67666	68.00000	4.25600
4.26002	-0.00202	0.00228	16.86263	0.65918	84.00000	4.25800
4.25216	-0.00016	0.00189	7.58022	0.67963	65.00000	4.25200
4.26065	-0.00065	0.00230	17.53966	0.65801	85.00000	4.26000
4.27314	-0.00014	0.00438	31.85628	0.63827	101.00000	4.27300
4.25431	0.00069	0.00227	1.03995	1.37267	27.00000	4.25500
4.24628	-0.00428	0.00212	3.59356	1.34836	50.00000	4.24200
4.24894	-0.00194	0.00190	10.77115	1.30276	74.00000	4.24700
4.24828	-0.00328	0.00186	9.89508	1.30716	72.00000	4.24500
4.25653	-0.00753	0.00262	20.43385	1.26461	90.00000	4.24900
4.25089	-0.00289	0.00348	0.60783	2.23673	19.00000	4.24800
4.23918	-0.00118	0.00228	3.95982	2.18914	53.00000	4.23800
4.24188	-0.00288	0.00224	10.24518	2.11951	74.00000	4.23900
4.24159	-0.00559	0.00220	9.82107	2.12333	73.00000	4.23600
4.23847	-0.00047	0.00371	1.11332	3.07183	30.00000	4.23800
4.23298	0.00502	0.00278	3.94185	3.00700	54.00000	4.23800
4.23420	-0.00020	0.00267	7.50398	2.94239	68.00000	4.23400
4.23782	0.00018	0.00352	13.49784	2.86352	82.00000	4.23800
4.24299	0.00701	0.00569	23.84517	2.76739	97.00000	4.25000
4.22746	0.00454	0.00444	1.81411	4.09749	40.00000	4.23200

TABLE VII b

F	Y-F	STANDARD DEVIATION OF ESTIMATE	VARIABLES a_{H_2O}	$a_{\pm(NH_4Cl)}$	T, °C	$\delta^{K=2}_{obs}$
4.63884	-0.00684	0.00649	0.22610	0.0	2.00000	4.63200
4.67079	0.00221	0.00392	0.41375	0.0	11.00000	4.67300
4.67079	0.01121	0.00392	0.41375	0.0	11.00000	4.68200
4.75645	-0.00445	0.00429	1.19310	0.0	28.00000	4.75200
4.76783	-0.00083	0.00417	1.33921	0.0	30.00000	4.76700
4.85991	-0.00691	0.00373	3.18329	0.0	46.00000	4.85300
4.90881	0.00419	0.00308	4.96697	0.0	55.00000	4.91300
4.91404	-0.00004	0.00302	5.20986	0.0	56.00000	4.91400
4.91404	-0.00404	0.00302	5.20986	0.0	56.00000	4.91000
4.96439	0.00361	0.00302	8.25408	0.0	66.00000	4.96800
4.97891	-0.00191	0.00322	9.42003	0.0	69.00000	4.97700
5.02160	0.00640	0.00381	13.78591	0.0	78.00000	5.02800
5.03102	-0.01802	0.00394	14.95883	0.0	80.00000	5.01300
5.11263	-0.01063	0.00482	28.65968	0.0	97.00000	5.10200
5.12813	0.01587	0.00550	31.98219	0.0	100.00000	5.14400
4.94133	-0.00433	0.00250	4.77089	0.68870	55.00000	4.93700
4.75585	-0.00085	0.00344	0.66293	0.70685	19.00000	4.75500
4.82313	-0.00213	0.00353	1.44260	0.70240	32.00000	4.82100
4.92168	0.01532	0.00278	3.92823	0.69192	51.00000	4.93700
5.00274	0.00626	0.00224	8.65759	0.67666	68.00000	5.00900
5.07734	0.00266	0.00316	16.86263	0.65918	84.00000	5.08000
4.98880	0.00920	0.00226	7.58022	0.67963	65.00000	4.99800
5.08210	0.00290	0.00328	17.53966	0.65801	85.00000	5.08500
5.16186	-0.00886	0.00636	31.85628	0.63827	101.00000	5.15300
4.83713	0.00087	0.00397	1.03995	1.37267	27.00000	4.83800
4.94775	0.00025	0.00347	3.59356	1.34836	50.00000	4.94800
5.05501	0.00499	0.00249	10.77115	1.30276	74.00000	5.06000
5.04605	0.00895	0.00243	9.89508	1.30716	72.00000	5.05500
5.12960	0.00640	0.00445	20.43385	1.26461	90.00000	5.13600
4.84830	-0.00530	0.00629	0.60783	2.23673	19.00000	4.84300
4.99819	-0.02319	0.00357	3.95982	2.18914	53.00000	4.97500
5.08481	-0.01881	0.00307	10.24518	2.11951	74.00000	5.06600
5.08054	-0.00854	0.00305	9.82107	2.12333	73.00000	5.07200
4.94132	0.00768	0.00432	1.11332	3.07183	30.00000	4.94900
5.03535	0.01365	0.00403	3.94185	3.00700	54.00000	5.04900
5.08776	0.00124	0.00407	7.50398	2.94239	68.00000	5.08900
5.14499	0.00501	0.00453	13.49784	2.86352	82.00000	5.15000
5.21347	0.00153	0.00712	23.84517	2.76739	97.00000	5.21500
5.02733	-0.00133	0.00628	1.81411	4.09749	40.00000	5.02600

TABLE VIII

Asymptotic Correlation Matrix of the Parameters

B10	-	δ^1_0			
B110	-	δ^1_{10}			
B101	-	δ^1_{01}			
B111	-	δ^1_{11}			
B120	-	δ^1_{20}			
E10	-	ΔH_{10}			
E01	-	ΔH_{01}			
E11	-	ΔH_{11}			
E20	-	ΔH_{20}			
S10	-	ΔS_{10}			
S01	-	ΔS_{01}			
S11	-	ΔS_{11}			
S20	-	ΔS_{20}			
B20	-	δ^2_0			
B210	-	δ^2_{10}			
B201	-	δ^2_{01}			
B211	-	δ^2_{11}			
B220	-	δ^2_{20}			
G10	-	ΔG_{10}	= ΔH_{10}	-	$300\Delta S_{10}$
G01	-	ΔG_{01}	= ΔH_{01}	-	$300\Delta S_{01}$
G11	-	ΔG_{11}	= ΔH_{11}	-	$300\Delta S_{11}$
G20	-	ΔG_{20}	= ΔH_{20}	-	$300\Delta S_{20}$

		B10	B110	B101	B111	B120	E10	E01	E11	E20
		1	2	3	4	5	6	7	8	9
B10	1	1.0000								
B110	2	-0.8546	1.0000							
B101	3	-0.0987	0.1075	1.0000						
B111	4	0.2447	-0.2864	-0.1419	1.0000					
B120	5	0.7041	-0.9342	-0.2042	0.2545	1.0000				
E10	6	-0.4478	0.5518	0.1265	-0.4196	-0.4504	1.0000			
E01	7	-0.2687	0.4509	0.7122	-0.0606	-0.5565	0.4643	1.0000		
E11	8	-0.4651	0.5694	0.2635	0.3999	-0.6626	0.0464	0.5961	1.0000	
E20	9	-0.7912	0.9765	0.1453	-0.2527	-0.9783	0.5166	0.4934	0.6406	1.0000
S10	10	-0.4363	0.5451	0.1279	-0.4216	-0.4468	0.9998	0.4672	0.0401	0.5104
S01	11	-0.2641	0.4444	0.7305	-0.0614	-0.5507	0.4539	0.9995	0.5911	0.4867
S11	12	-0.4827	0.5963	0.2578	0.3854	-0.6864	0.0878	0.6070	0.9988	0.6663
S20	13	-0.7760	0.9717	0.1584	-0.2578	-0.9856	0.5151	0.5109	0.6435	0.9992
B20	14	-0.4853	0.4915	0.1266	-0.3649	-0.3717	0.9449	0.4096	0.0613	0.4578
B210	15	-0.1175	-0.0435	-0.1804	0.3731	0.0632	-0.7676	-0.4228	0.2715	-0.0318
B201	16	0.1965	-0.2678	-0.9299	0.0690	0.3373	-0.1690	-0.7721	-0.3871	-0.2911
B211	17	0.2810	-0.3477	0.1048	-0.7129	0.3901	0.0930	-0.1956	-0.7971	-0.3998
B220	18	0.7049	-0.9306	-0.1997	0.2388	0.9992	-0.4212	-0.5434	-0.6767	-0.9778
G10	19	-0.3042	0.0359	-0.1268	0.2944	0.0582	-0.4803	-0.3583	0.2679	0.0308
G01	20	0.1360	-0.2509	-0.9301	0.0655	0.3516	-0.1896	-0.8176	-0.3984	-0.2841
G11	21	0.1107	-0.2333	0.2216	0.4412	0.1338	-0.7290	0.0695	0.4693	-0.1801
G20	22	0.6421	-0.8990	-0.2381	0.2804	0.9920	-0.4829	-0.6055	-0.6359	-0.9516

		S10	S01	S11	S20	B20	B210	B201	B211	B220
		10	11	12	13	14	15	16	17	18
S10	10	1.0000								
S01	11	0.4568	1.0000							
S11	12	0.0816	0.6014	1.0000						
S20	13	0.5094	0.5043	0.6694	1.0000					
B20	14	0.9404	0.3999	0.0962	0.4512	1.0000				
B210	15	-0.7785	-0.4152	0.2380	-0.0490	-0.6519	1.0000			
B201	16	-0.1684	-0.7908	-0.3838	-0.3014	-0.1703	0.1218	1.0000		
B211	17	0.0982	-0.1877	-0.8014	-0.3956	0.0894	-0.3438	0.0040	1.0000	
B220	18	-0.4172	-0.5379	-0.6992	-0.9846	-0.3468	0.0268	0.3338	0.4063	1.0000
G10	19	-0.4971	-0.3522	0.2402	0.0050	-0.2565	0.8730	0.0585	-0.2824	0.0268
G01	20	-0.1915	-0.8350	-0.3971	-0.2992	-0.1566	0.2078	0.9868	0.0143	0.3456
G11	21	-0.7349	0.0773	0.4257	-0.1805	-0.6061	0.7282	-0.2333	-0.2795	0.1046
G20	22	-0.4814	-0.5994	-0.6613	-0.9633	-0.3886	0.1611	0.3569	0.3514	0.9882

		G10	G01	G11	G20
		19	20	21	22
G10	19	1.0000			
G01	20	0.1811	1.0000		
G11	21	0.6230	-0.2017	1.0000	
G20	22	0.1662	0.3868	0.1757	1.0000

Figure 23 . Plot of activity of water versus predicted and observed variable, DELTA C13. Predicted - P, Observed - O, conincidence * .

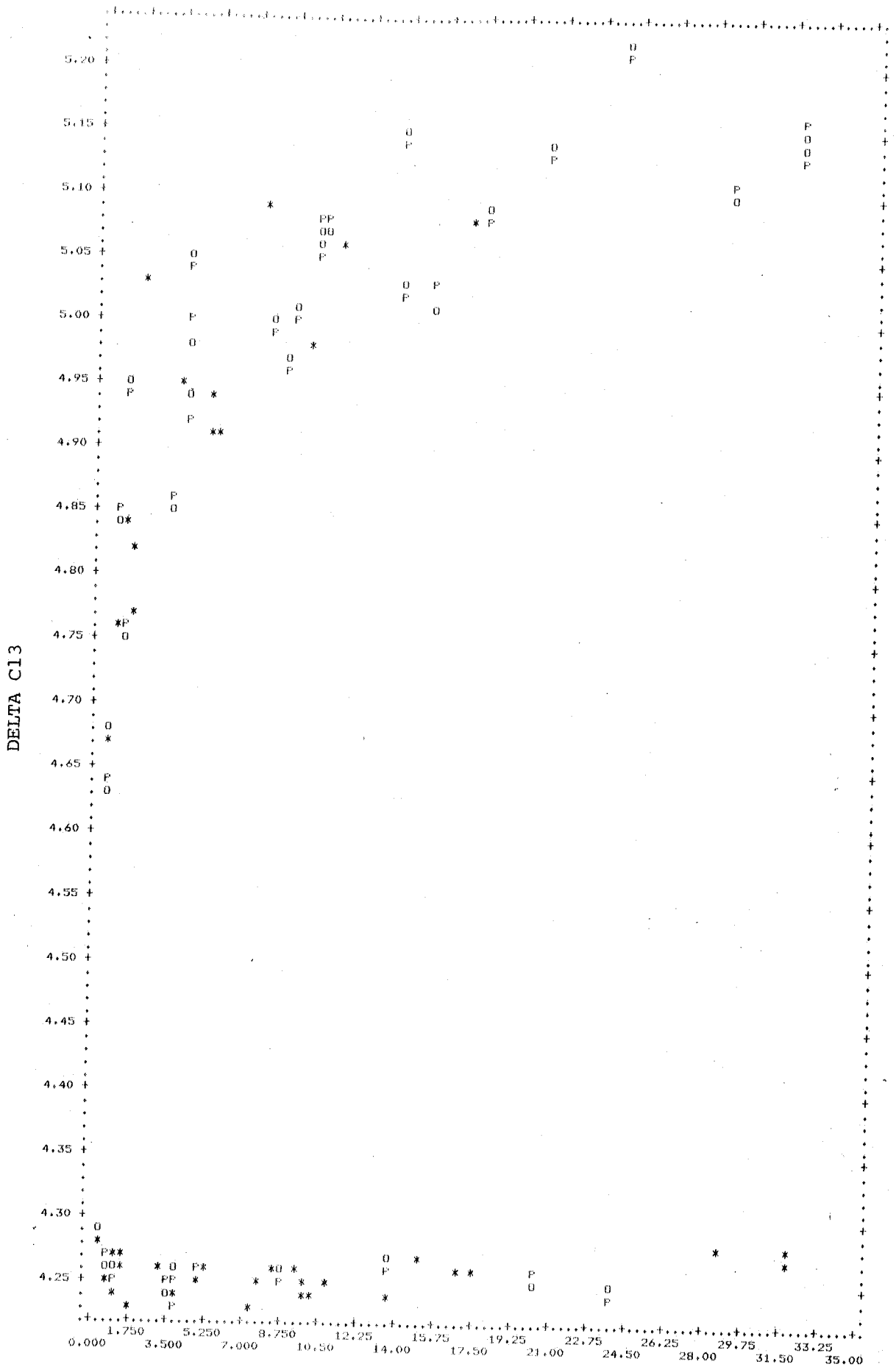
DELTA C13
5.20
5.15
5.10
5.05
5.00
4.95
4.90
4.85
4.80
4.75
4.70
4.65
4.60
4.55
4.50
4.45
4.40
4.35
4.30
4.25
0.000
1.750
3.500
5.250
7.000
8.750
10.50
12.25
14.00
15.75
17.50
19.25
21.00
22.75
24.50
26.25
28.00
29.75
31.50
33.25
35.00
a_{H_2O}

Figure 24. Plot of activity of ammonium ion versus predicted and observed variable, DELTA Cl3.

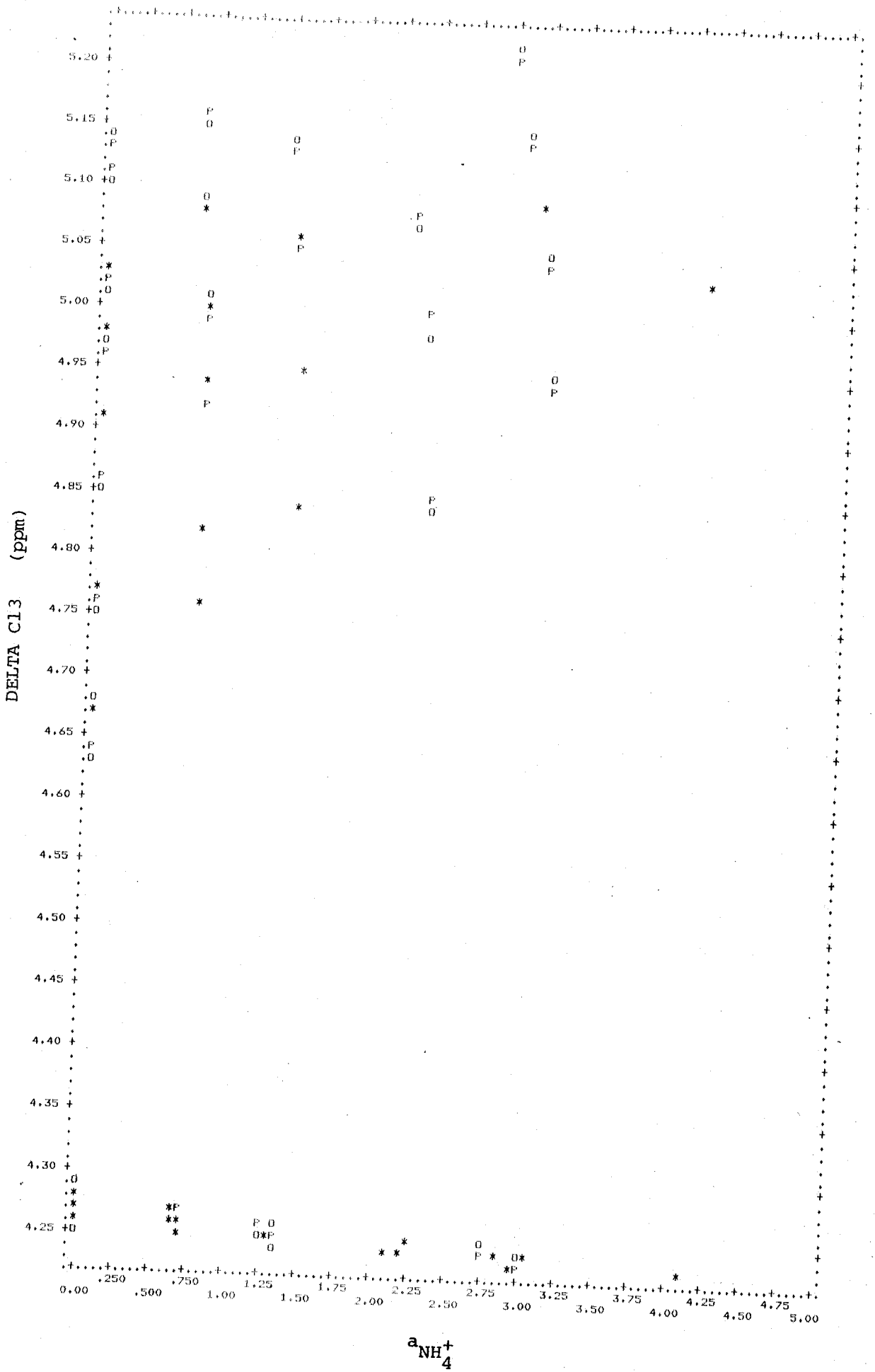
DELTA C13 (ppm)
5.20
5.15
5.10
5.05
5.00
4.95
4.90
4.85
4.80
4.75
4.70
4.65
4.60
4.55
4.50
4.45
4.40
4.35
4.30
4.25
0.00
.250
.500
.750
1.00
1.25
1.50
1.75
2.00
2.25
2.50
2.75
3.00
3.25
3.50
3.75
4.00
4.25
4.50
4.75
5.00
$a_{NH_4^+}$

Figure 25. Plot of temperature versus predicted and observed variable, DELTA C13.

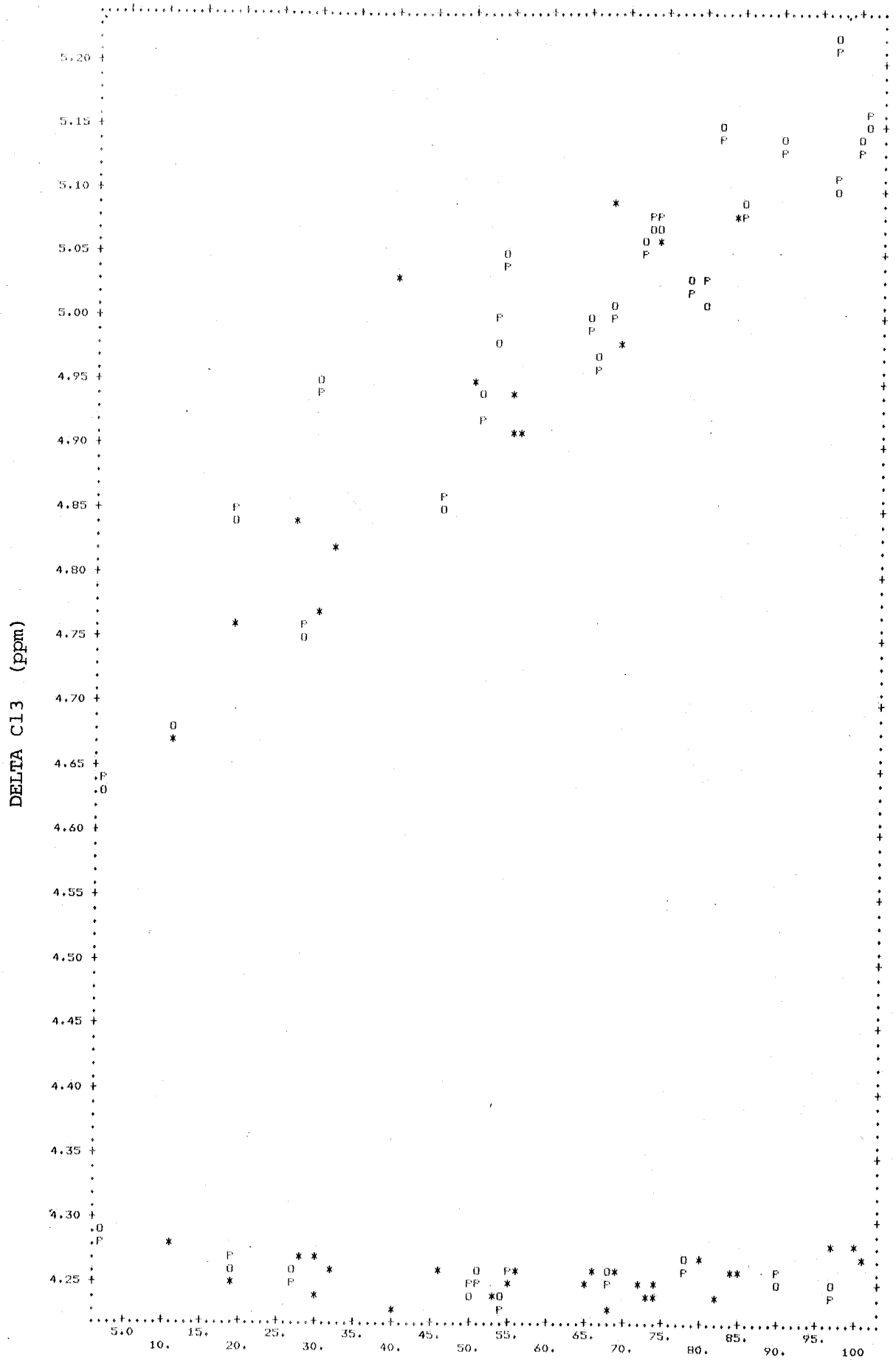
DELTA C13 (ppm)
5.20
5.15
5.10
5.05
5.00
4.95
4.90
4.85
4.80
4.75
4.70
4.65
4.60
4.55
4.50
4.45
4.40
4.35
4.30
4.25
5.0
10.
15.
20.
25.
30.
35.
40.
45.
50.
55.
60.
65.
70.
75.
80.
85.
90.
95.
100
Temperature, °C.

Figure 26. Plot of activity of water versus residuals.

1 - one point per grid point

2 - two points per grid point etc.

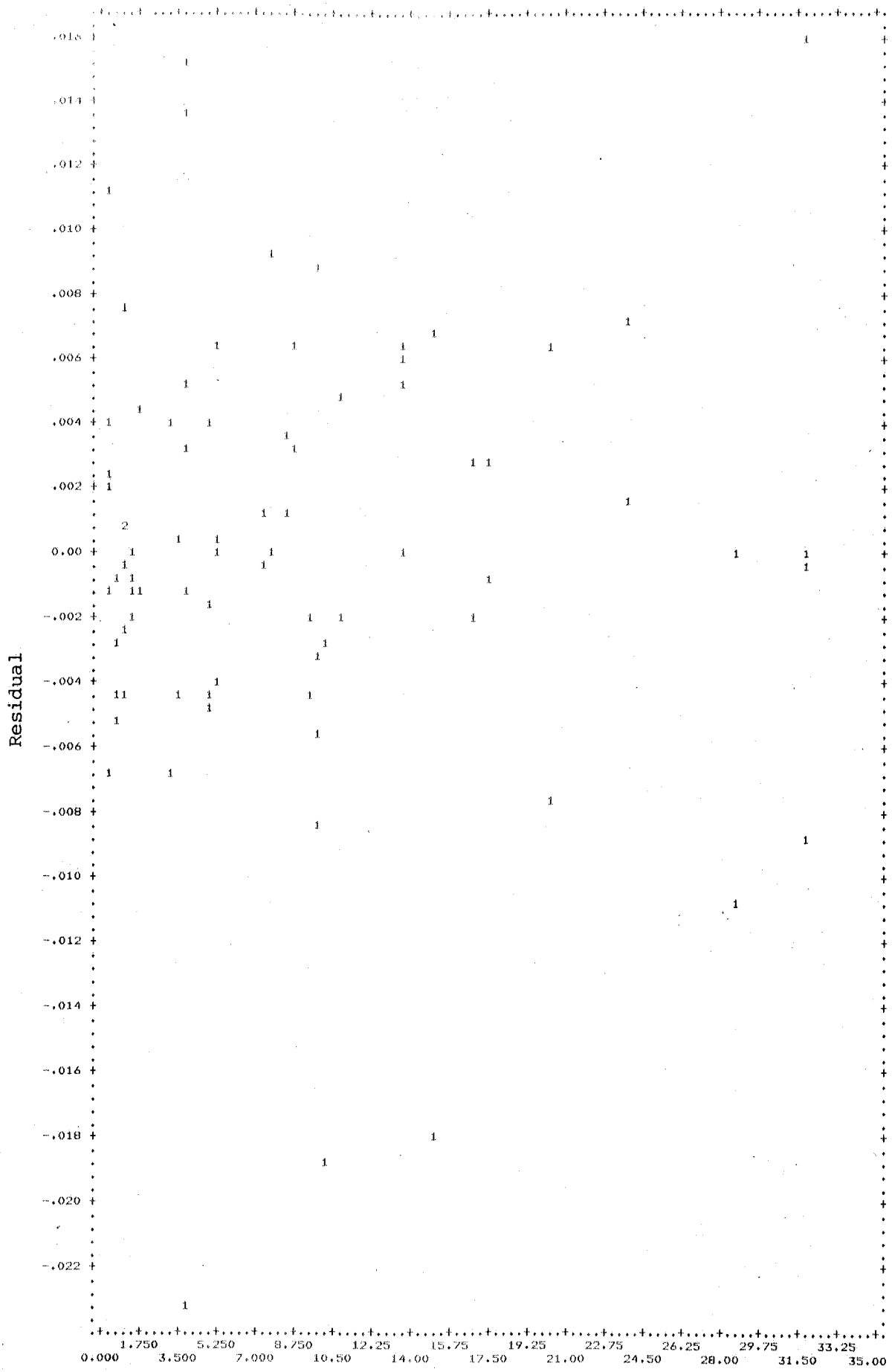
Residual
.016
.014
.012
.010
.008
.006
.004
.002
0.00
-.002
-.004
-.006
-.008
-.010
-.012
-.014
-.016
-.018
-.020
-.022
0.000
1.750
3.500
5.250
7.000
8.750
10.50
12.25
14.00
15.75
17.50
19.25
21.00
22.75
24.50
26.25
28.00
29.75
31.50
33.25
35.00
a_{H_2O}

Figure 27 . Plot of activity of ammonium ion versus residuals.

1 - one point per grid point

2 - two points per grid point

3 - three points per grid point etc.

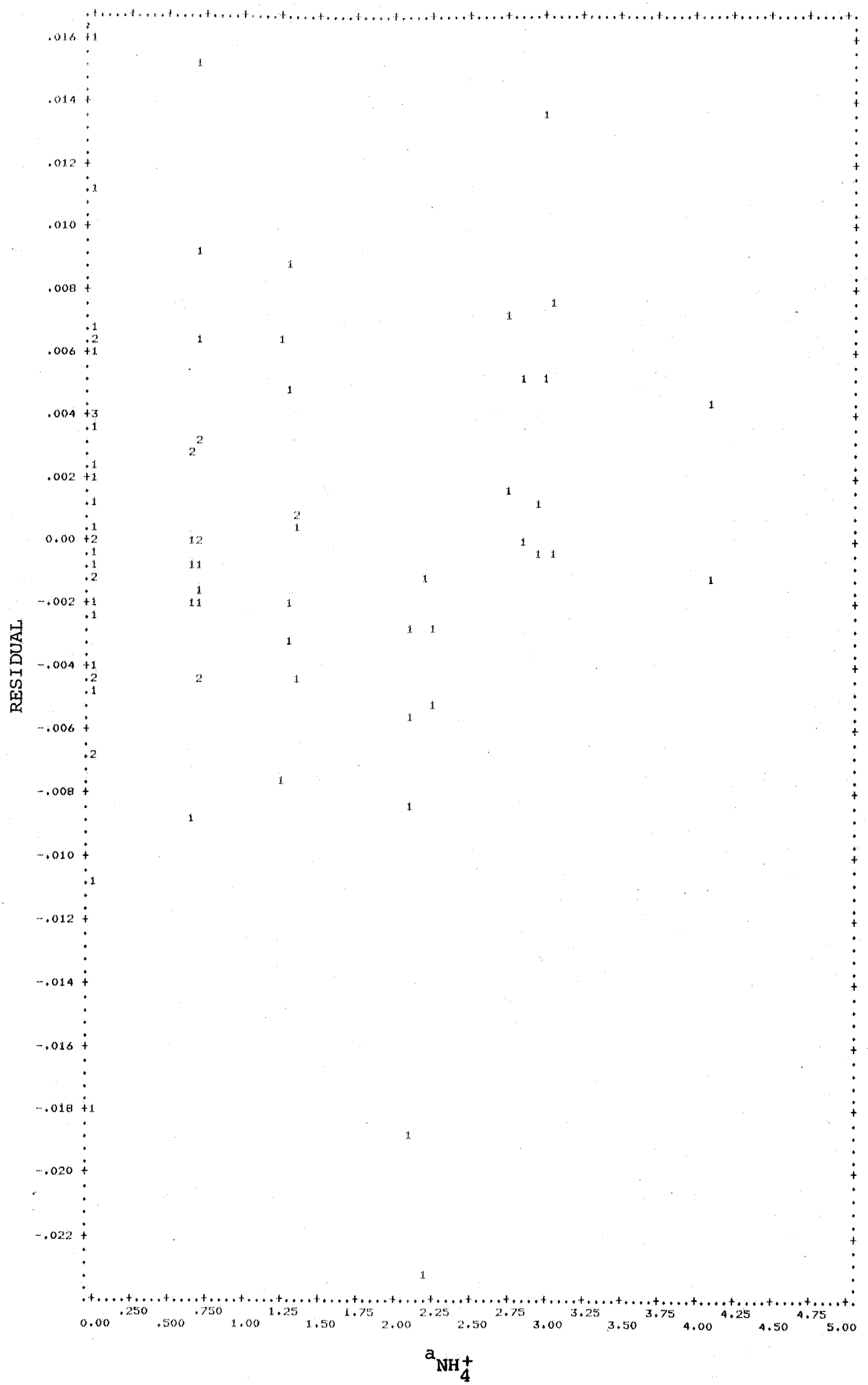
RESIDUAL
.016
.014
.012
.010
.008
.006
.004
.002
0.00
-.002
-.004
-.006
-.008
-.010
-.012
-.014
-.016
-.018
-.020
-.022
0.00
.250
.500
.750
1.00
1.25
1.50
1.75
2.00
2.25
2.50
2.75
3.00
3.25
3.50
3.75
4.00
4.25
4.50
4.75
5.00
$a_{NH_4^+}$

Figure 28 . Plot of temperature versus residuals.

1 - one point per grid point

2 - two points per grid point etc.

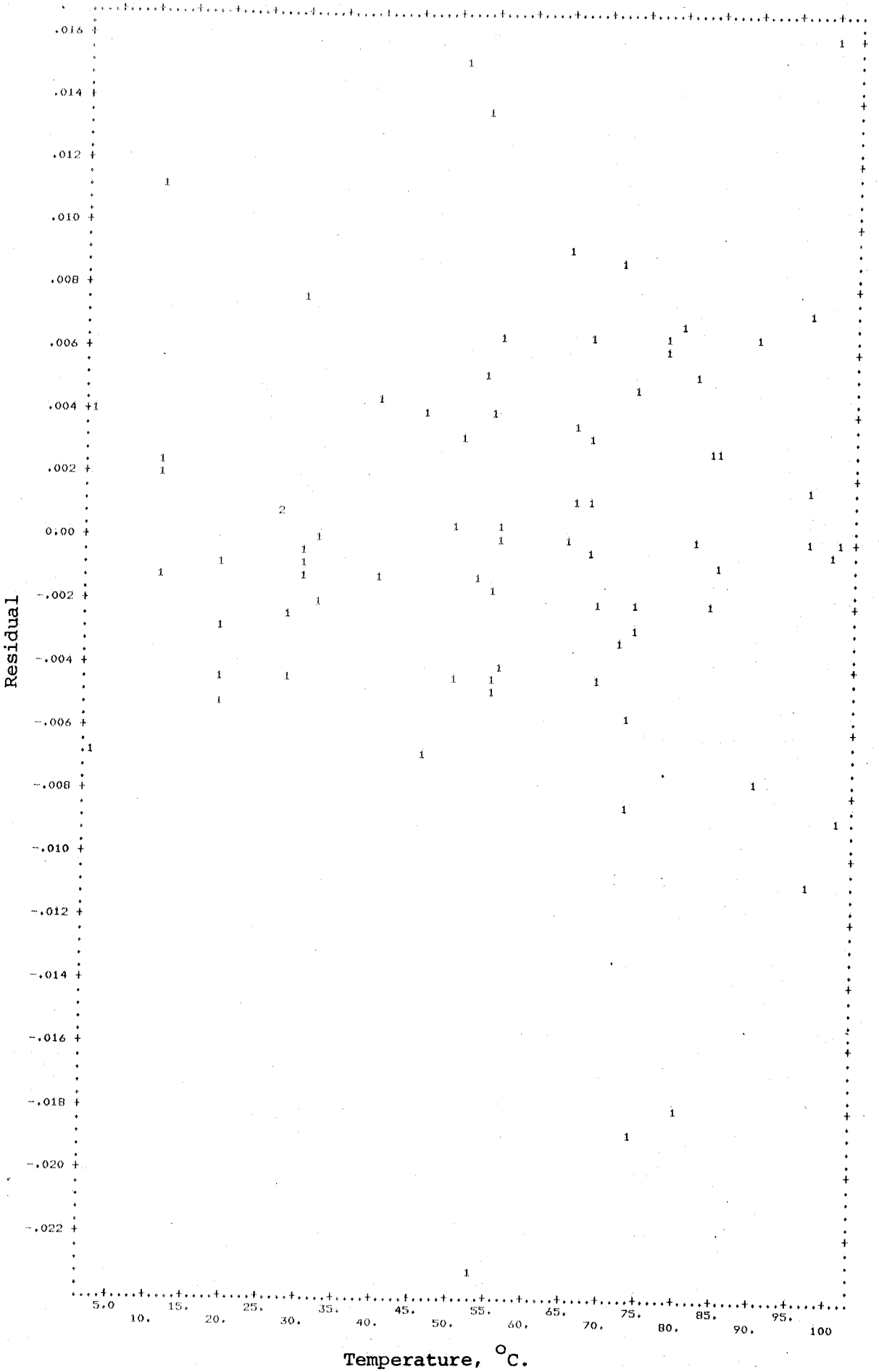
Residual
.016
.014
.012
.010
.008
.006
.004
.002
0.00
-.002
-.004
-.006
-.008
-.010
-.012
-.014
-.016
-.018
-.020
-.022
5.0
10.
15.
20.
25.
30.
35.
40.
45.
50.
55.
60.
65.
70.
75.
80.
85.
90.
95.
100
Temperature, °C.

Figure 29 . Plot of predicted variable DELTA C13 versus residuals.

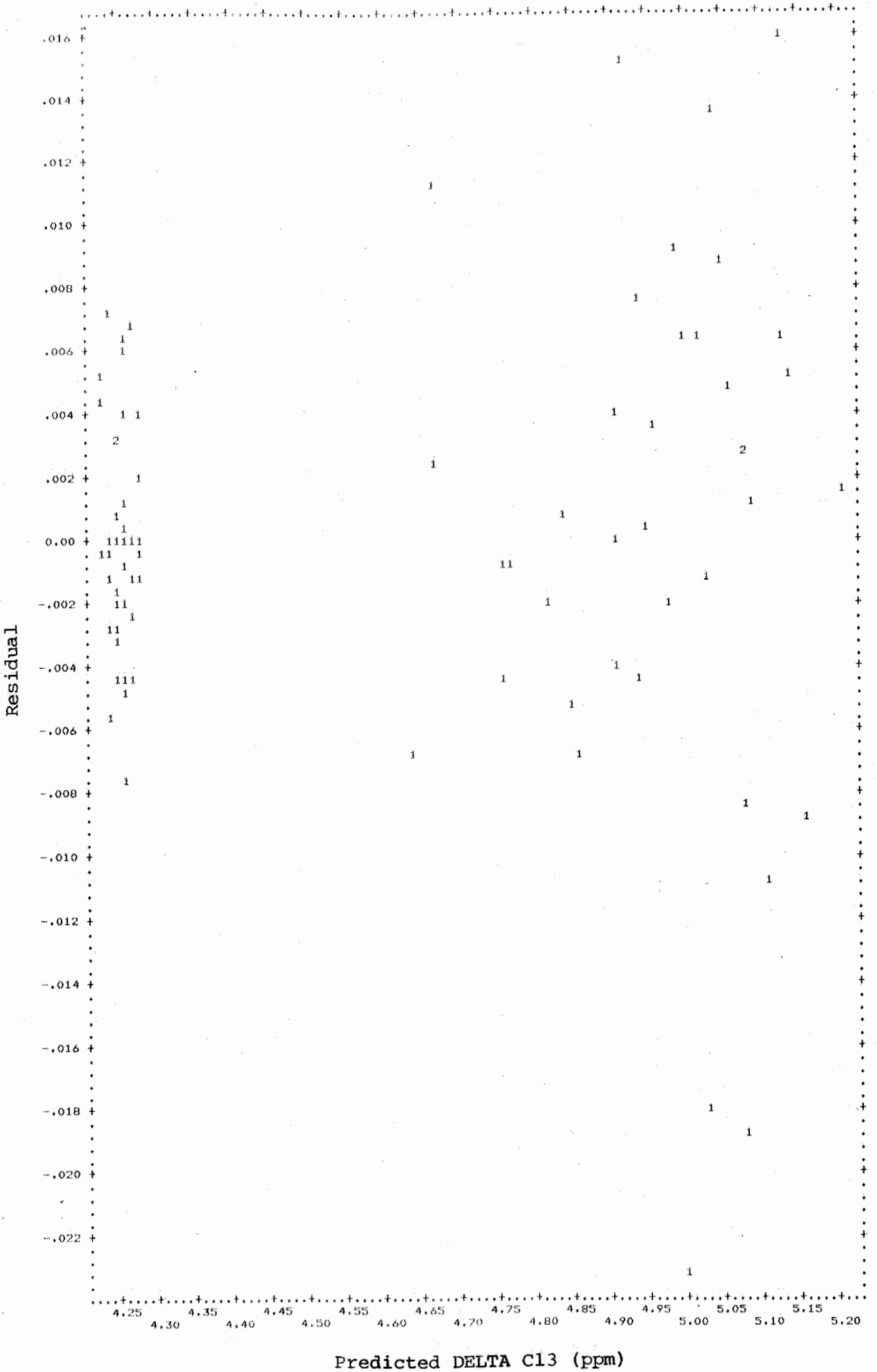
Residual
.016
.014
.012
.010
.008
.006
.004
.002
0.00
-.002
-.004
-.006
-.008
-.010
-.012
-.014
-.016
-.018
-.020
-.022
4.25
4.30
4.35
4.40
4.45
4.50
4.55
4.60
4.65
4.70
4.75
4.80
4.85
4.90
4.95
5.00
5.05
5.10
5.15
5.20
Predicted DELTA C13 (ppm)

Figure 30 . Plot of predicted variable DELTA C13 versus residuals squared.

1 - one point per grid point

2 - two points per grid point

3 - three points per grid point

4 - four points per grid point

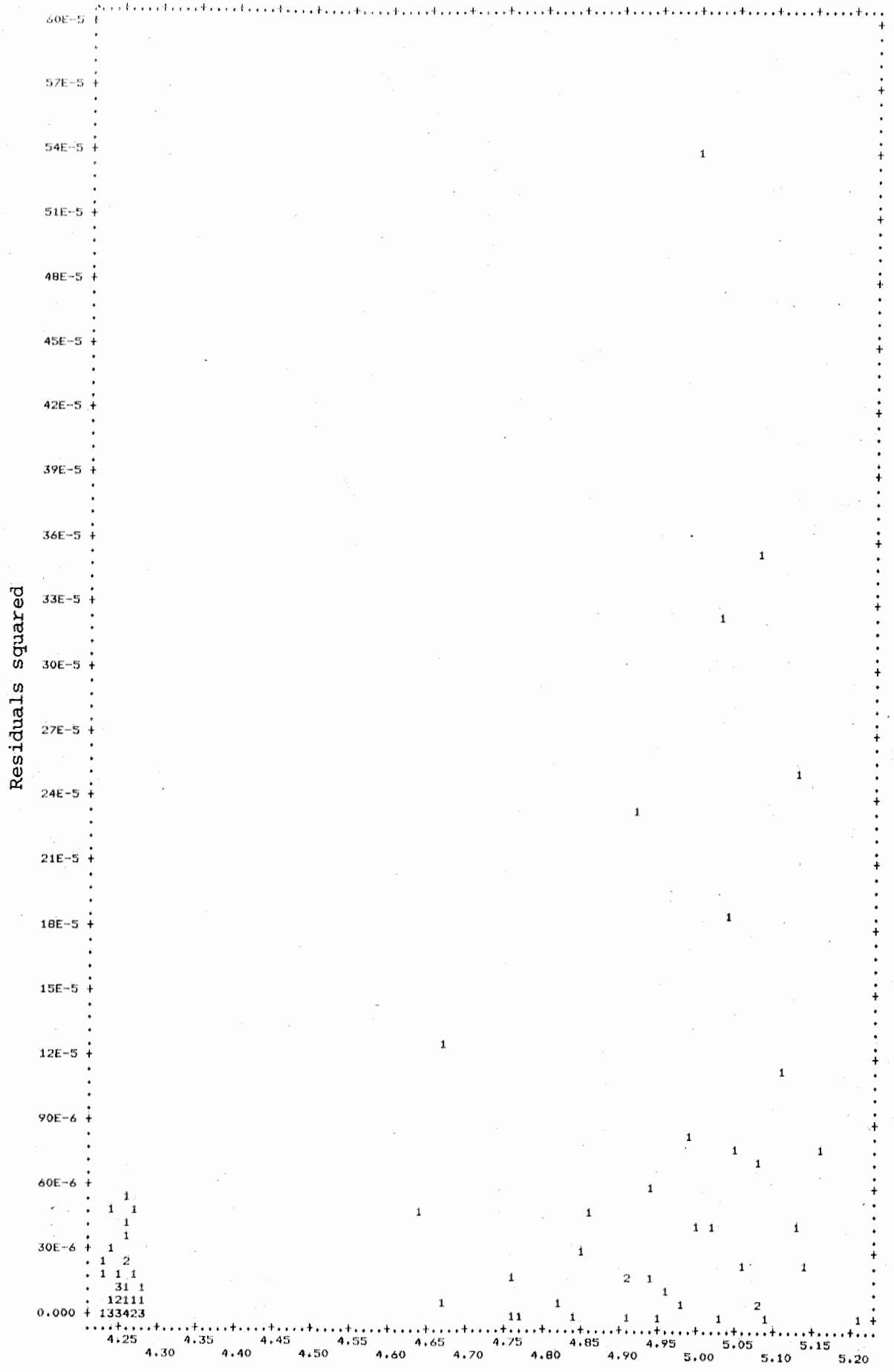
Residuals squared
60E-5
57E-5
54E-5
51E-5
48E-5
45E-5
42E-5
39E-5
36E-5
33E-5
30E-5
27E-5
24E-5
21E-5
18E-5
15E-5
12E-5
90E-6
60E-6
30E-6
0.000
4.25
4.30
4.35
4.40
4.45
4.50
4.55
4.60
4.65
4.70
4.75
4.80
4.85
4.90
4.95
5.00
5.05
5.10
5.15
5.20
Predicted DELTA C13 (ppm)

Figure 31 . Normal probability plot of residuals.

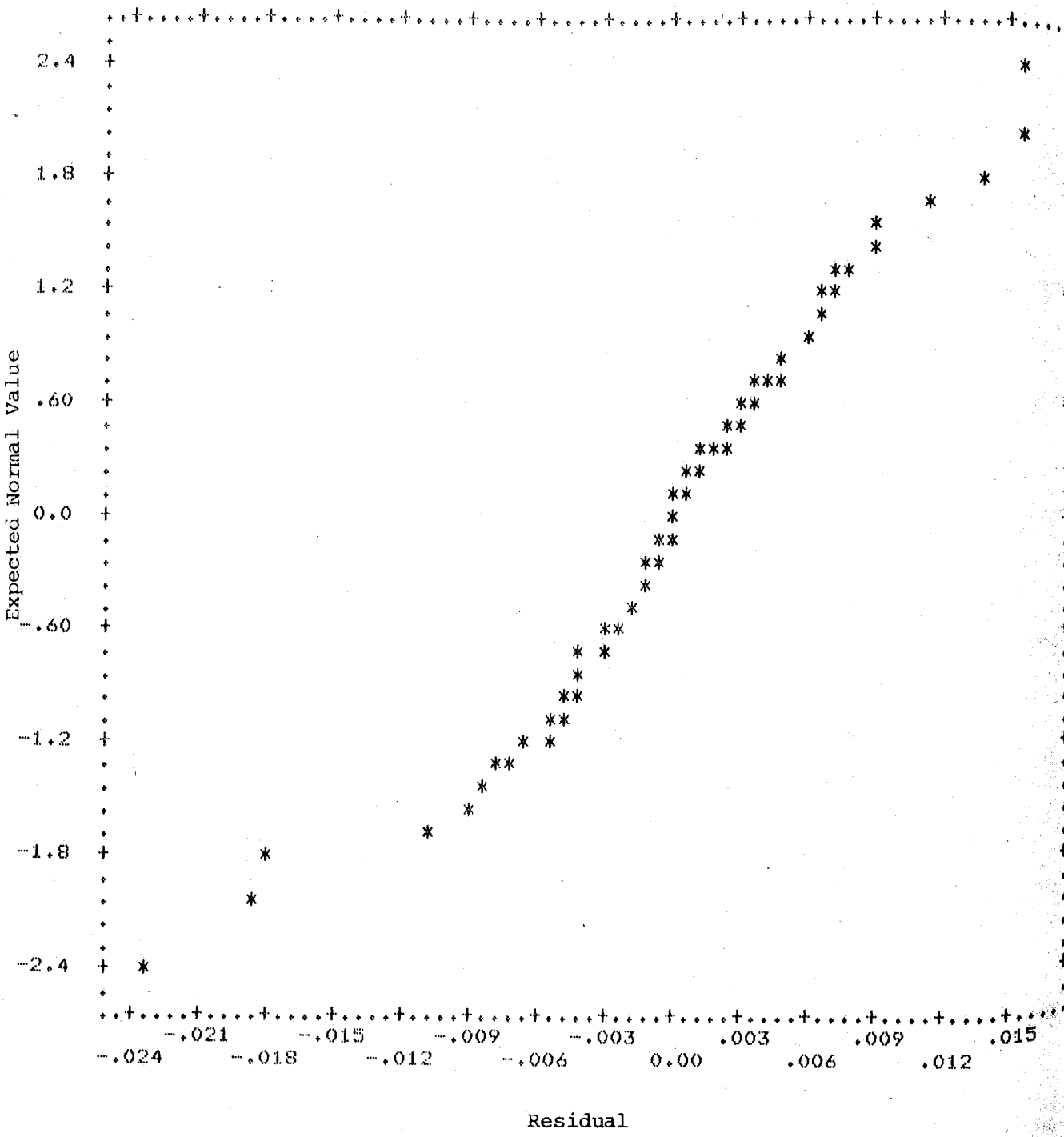
Expected Normal Value
2.4
1.8
1.2
.60
0.0
-.60
-1.2
-1.8
-2.4
-.024
-.021
-.018
-.015
-.012
-.009
-.006
-.003
0.00
.003
.006
.009
.012
.015
Residual

Figure 32 . Detrended normal probability plot of residuals.

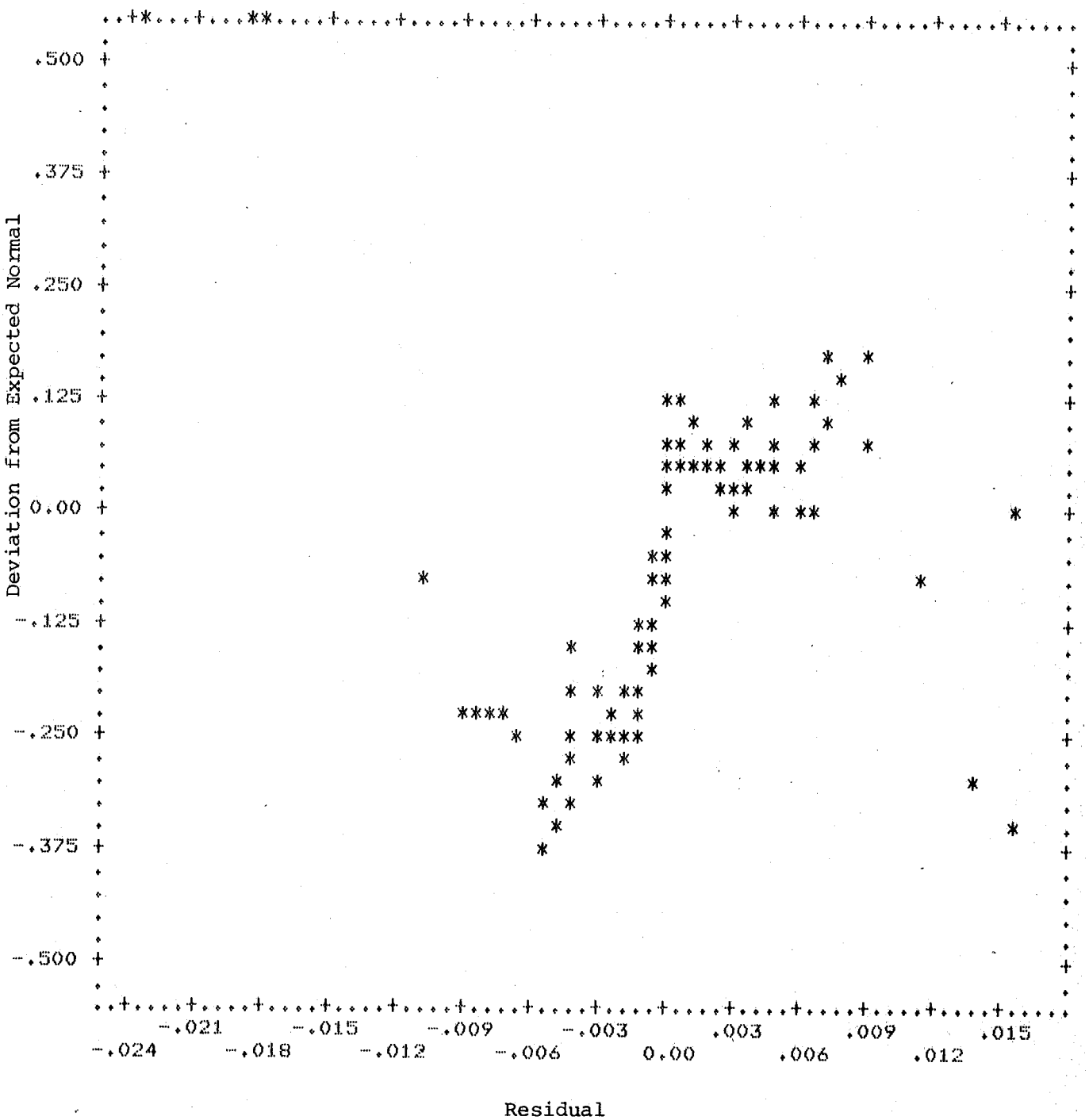
Deviation from Expected Normal
.500
.375
.250
.125
0.00
-.125
-.250
-.375
-.500
-.024
-.021
-.018
-.015
-.012
-.009
-.006
-.003
0.00
.003
.006
.009
.012
.015
Residual

is the activity of water. Because the other two independent variables, $a_{NH_4^+}$ and T, are projected onto the plot, the trend with respect to a_{H_2O} is not perfectly defined. However, C(2) defines some sort of curve and C(1) decreases and then increases. The greater number of coincidences (*) within grid points for the C(1) group indicates a smaller scatter as a group.

Figure 24 shows a similar plot where, now, the coordinate axis is the activity of ammonium. The C(1) and C(2) groups have their same relative positions as in Figure 23 . C(1), at bottom, appears to follow a straight line downward with a little scatter (due to T and a_{H_2O}). The great scatter of C(2), however, indicates that it is more sensitive to the influences of a_{H_2O} and T, which are projected onto the plot.

Figure 25 is a plot of δ^K versus temperature. It bears some resemblance to Figure 23 , since the activity of water is most sensitive to the temperature. In spite of projection of the other variables, the trend in C(1) appears to first decrease and then to increase with T. However, C(2) appears to scatter uniformly about a straight line upwards.

The plots of the residuals are useful for analyzing the extent of unexplained trends. Figure 26 depicts a plot of residuals versus the activity of water. The greatest number of residual values are seen to be between -.008 and +.008. The spatial density of points reflects the sampling inherent in the data. The likelihood of having a large residual value for a small value of a_{H_2O} appears to be about the same as that for a large value of a_{H_2O}. The likelihood of having a small residual value appears to be independent of the value of a_{H_2O}. Thus, the residual values appear not to be correlated with a_{H_2O}.

Figure 27 shows a plot of the residuals versus the activity of ammonium ion. Most points again (and consequently) fall between -.008 and +.008. As in Figure 26 a number of anomalously large or small residue values are apparent However, these values do not appear to be correlated in occurence with either large or small values of $a_{NH_4^+}$. Hence, the errors appear to be independent of $a_{NH_4^+}$. Most of the same arguments given for Figure 26 apply here. In particular, the likelihood of having a large residual value for a small value of $a_{NH_4^+}$ appears to be about the same as that for a large value of $a_{NH_4^+}$. Like-wise, the likelihood of having a small residual value appears to be independent of the value of $a_{NH_4^+}$.

Figure 28 gives the plot of the residual values versus the temperature, T. Similar arguments as given in the discussion of Figures 26 and 27 apply to Figure 28 . However, the largest and the smallest residue values lie on the extremes of the graph, between 53° and 80° C. These appear to be outliers, separated as they are from the rest of the dispersion. This may suggest an error in the temperature determination for these observations. Temperature measurements were obtained using a double junction copper-constantan thermocouple, which may be subject to failure by electrolytic corrosion.

Figure 29 shows the plot of the residuals versus the predicted ^{13}C chemical shifts. These are separated into two groups, the C(1) values to the left and the C(2) values to the right. It is clearly apparent that there are two error distributions. The errors associated with C(1) are smaller than those for C(2). This may be because the C(1) line positions are more accurately determined because it lies closest to the reference, dioxane. Or, alternately, since C(2) is more sensitive to changes in the

dependent variables, it may reflect more fully the errors in those values. A third hypothesis is that the C(2) carbon, with its hydroxyls protruding into the solution, is more sensitive to "impurity" effects such as those of residual dissolved oxygen or other unknown agents not readily controlled.

Figure 30 shows the magnitudes of the residuals, i.e. the residuals squared versus the predicted ^{13}C chemical shifts. Many of the considerations given for Figure 29 apply here. However, a trend is noticable. The magnitude of the residuals appears to correlate with the value of δ for C(2). This suggests that the predictability of δ^2_{obs} decreases for greater values of δ^2_{obs} where a_{H_2O}, $a_{NH_4^+}$, and T are greatest. This reflects the uneven sampling of data. There is less data for the larger values of the independent variable for which a prediction of δ^2_{obs} can be made. A greater sample size for the data would correct this flaw.

Figure 31 shows the normal probability plot of the residuals. Such graphical means may be used to investigate the probability distribution of the errors [49,56,60]. The expected normal value, i.e. the i^{th} ordered value selected from a normal distribution, with the computed mean and variance as the given set of residues, is plotted against the i^{th} residue. For a distribution of errors following a normal distribution, such a plot should approximate a straight line. The distribution is seen to be somewhat curved at the ends.

A detrended normal probability plot displays the deviation of the error from the straight line expected of a normal probability plot. Figure 32 shows the distribution to be grouped in the upper right hand quadrant and in the lower left hand quadrant. This is characteristic of a bimodal distribution. The residues associated with C(2) have a broader distribution than those of C(1).

6.1

Tests of Significance

1. The serial correlation, or autocorrelation (see page 99), of the residuals for the "true model" was calculated to be r = 0.231. Applying the t-test [52,56,77] for the hypothesis H_o: p = 0 gives the statistic

$$t = \frac{r\sqrt{N-2}}{\sqrt{1-r^2}} = 2.057 \tag{78}$$

for 77 degrees of freedoms, whereas $t_{.95} = 1.66$, while $t_{.99} = 2.36$. Thus, at the 5% level, we reject the hypothesis that the serial correlation is not significantly different from zero, whereas, at the 1% level, we cannot reject the hypothesis. Since p parameters have been determined, there are n residuals associated with only n - p degrees of freedom [56], and, therefore, there ought to be some correlation amongst the residuals. Thus, the calculation of the serial correlation does not reveal anything to be out of line.

2. The residuals are grouped into those for C(1) and for C(2). The correlation coefficient between these groups was calculated to be r = .04293. Applying the t-test as above shows that the null hypothesis cannot be rejected at the 1% probability level. Thus we could say that there is no correlation between the errors for the two different carbons and the model adequately represents each independently.

3. The standard deviations calculated for the residuals associated with C(1) and C(2) were .00360 and .00876, respectively. The F-test for one-sided alternatives [77,49] was applied to the hypotheses

$$H_o: \sigma_1^2 = \sigma_2^2 \quad , \quad H_1: \sigma_1^2 < \sigma_2^2 \quad .$$

Since (79) $\frac{S_2^2}{S_1^2} = 5.921 > F_{38,38,.01} = 2.02,$

we say that the difference is probably significant at the .01 level.

4. The significance of improvements in the error mean square due to changes in the model may be tested using partial or sequential F-tests or the R-factor ratio test [56,51,49]. The R-factor ratio for n observations and p parameters is distributed as

(80)
$$R_{p,n-p,\alpha} \equiv \left[\frac{p}{n-p} F_{p,n-p,\alpha} + 1\right]^{\frac{1}{2}} .$$

Thus, for the "true model" (n=78, p=18), an R-factor ratio (alternately, RMS ratio) of 1.311 is significant at the .005 level and 1.233 is significant at the .05 level. Model A, Table VI is then significantly improved over C. $R_1/R_o = 2.64.$

A reduced model with b_o fewer parameters may be given a test of signifcance with respect to a full model by comparing the R-factor ratio to $R_{b_o,n-p,\alpha}$. Thus, for F. ,

$$\left(\frac{.00091582}{.00056886}\right) = 1.6099 > R_{8,60,.005} = 1.191$$

and, so, Model F. would be rejected in favour of A. at the 0.5% level. Similarly, $R_1/R_o = 1.322 > R_{4,60,.005} = 1.130$ for Model G. and it too would be rejected in favour of A. at the 0.5% level.

In summary, then, the preponderence of evidence provided by the residual analysis and the tests of significance demonstrate to all but the unredeemed

skeptic that "true model" has indeed been shown. The value of this model in predicting the chemical shifts and the thermodynamic constants of all the species is limited only by the quality and quantity of the dataset used. In hindsight, then, a further refinement would be obtained by collecting additional data for higher concentrations and higher temperatures.

6.2
Normal Probability Plots [60]

The observed values are plotted along the horizontal axis. The data values are ordered before plotting: the vertical axis corresponds to the expected normal value based on the rank of the observation. Let $x_{(1)}, x_{(2)}, \ldots$ represent the data values after ordering from smallest to largest. The subscript (j) is the rank order of the observation. If N is the total frequency, the vertical plotting position corresponds to the expected normal value for the relative rank (j out of N) of the observation. The expected normal value is estimated as

(81) $$\Phi^{-1}[(3j-1)/(3N+1)],$$

the standard normal value corresponding to the probability (3j-1)/(3N+1). If the data are from a normal distribution, this line will be straight, except for random fluctuations. In addition the serial correlation of the residuals is printed. The serial correlation is defined as

(82) $$\frac{\Sigma\ (w_j w_{j-1})^{\frac{1}{2}}\ (y_j-\hat{y}_j)\ (y_{j-1}-\hat{y}_{j-1})}{\{\ \Sigma\ w_j(y_j-\hat{y}_j)^2\ \ \Sigma\ w_{j-1}(y_{j-1}-\hat{y}_{j-1})^2\ \}^{\frac{1}{2}}}$$

where the summation is for j=2 to N and w_j is the case weight for the j^{th} case (1.0 if there is no case weight). A large serial correlation indicates a pattern in the residuals. When the data are ordered, such as by time, the pattern can be a result of a change in the method of data collection or an omission of a variable from the regression equation.

Detrended Normal Probability Plot [60]

This is similar to the normal probability plot except that the linear trend is removed before the plot is printed. The vertical scale represents the differences between the expected normal values and the standardized values of the observations. That is, each observation is transformed into a standardized value by subtracting the mean and dividing by the standard deviation; i.e., $z_{(j)} = (x_{(j)}-\bar{x})/s$. We then compute

(83) $$\Phi^{-1}[(3j-1)/(3N+1)] - z_{(j)} \quad .$$

7.0

Calculation of the Activity Coefficient of Solute at various Temperatures from values at 25^{o} [75].

The chemical potential as defined by Gibbs [77,78].

$$\mu_i = \left(\frac{\partial G}{\partial n_i}\right)_{T,p,n_j} \quad , \tag{84}$$

is seen to be the partial molal Gibbs free energy for component i, with all other variables fixed. The activity, a_i, of a pure chemical species or constituent of a solution is given general definition by the equation

$$\mu_i = RT \ln a_i + \mu_i^{o} \tag{85}$$

in which μ_i^{o} is its chemical potential in some arbitrary standard state. The specific value of μ_i^{o} will depend on the concentrations scale and the standard state chosen for a_i .

It follows from (84) and (85) and the definition of the Gibbs free energy, G ≡ H - TS, that the dependence of the activity upon temperature is given by

$$\left(\frac{\partial \ln a_i}{\partial T}\right)_p = \frac{-(\bar{H}_i - \bar{H}_i^{o})}{R T^2} \tag{86}$$

where $\bar{H}_i^{o}$ is the partial molal enthalpy at the standard state. If we restrict ourselves to the solute (i=2) [75] and introduce the relative partial molal enthalpy, $\bar{L}_2 \equiv \bar{H}_2 - \bar{H}_2^{o}$, then

$$\left(\frac{\partial \ln a_2}{\partial T}\right)_p = \frac{-\bar{L}_2}{R T^2} \quad . \tag{87}$$

Differentiating $\bar{L}_2$ with respect to T serves to define the partial molal heat capacity, $\bar{c}_{p_2}$, and the relative partial molal heat capacity, $\bar{c}_{p_2} - \bar{c}^{o}_{p_2}$, at constant pressure. Thus

$$(88) \qquad \left(\frac{\partial \bar{H}_2}{\partial T}\right) - \left(\frac{\partial \bar{H}^{o}_2}{\partial T}\right) = \bar{c}_{p_2} - \bar{c}^{o}_{p_2} = \left(\frac{\partial \bar{L}_2}{\partial T}\right) \equiv \bar{J}_2 .$$

The stoichiometric mean ionic molal activity coefficient $\gamma_{\pm}$, or practical activity coefficient is defined for a uni-valent electrolyte of molality, m, as

$$(89) \qquad \gamma_{\pm} = (\gamma_+ \gamma_-)^{\frac{1}{2}} = (a_+ a_-)^{\frac{1}{2}} / m$$

and (85) becomes, with this definition,

$$(90) \qquad \mu_2 = 2 RT \ln \gamma_{\pm} m + \mu^{o}_2 .$$

We thus have

$$(91) \qquad \left(\frac{\partial \ln \gamma_{\pm}}{\partial T}\right)_{p,m} = \left(\frac{1}{2}\right)\left(\frac{-\bar{L}_2}{R T^2}\right) .$$

If small variations of $\bar{J}_2$ with temperature can be neglected and if $\bar{L}_2$ and $\bar{J}_2$ are known at some reference temperature, T_R, then a good approximation for $\bar{L}_2$ is

$$(92) \qquad \bar{L}_2 = \bar{L}_2(T_R) + \bar{J}_2(T_R)\ (T - T_R) .$$

From equation (91) and (92)

(93)

$$\left(\frac{\partial \ln \gamma_{\pm}}{\partial T}\right)_{p,m} = \frac{-\bar{L}_2 (T_R)}{2 R T^2} - \frac{\bar{J}_2 (T_R)}{2 R T} + \frac{\bar{J}_2 (T_R)\, T_R}{2 R T^2}$$

Integrating (93),

(94)

$$\ln \gamma_{\pm} = \frac{\bar{L}_2 (T_R) - \bar{J}_2 (T_R)\, T_R}{2 R T} - \frac{\bar{J}_2 (T_R)}{2 R} \ln T + I \quad ,$$

where I is an integration constant. If $\gamma_{\pm} (T_R)$ at the reference temperature T_R is given, then I may be determined

(95)

$$I = \ln \gamma_{\pm} (T_R) - \frac{\bar{L}_2 (T_R) - \bar{J}_2 (T_R)\, T_R}{2 R T_R} + \frac{\bar{J}_2 (T_R)}{2 R} \ln T_R \quad .$$

Thus, combining (94) and (95),

(96)

$$\ln \gamma_{\pm} = \ln \gamma_{\pm} (T_R) + \left(\frac{T_R - T}{2 R T T_R}\right) \bar{L}_2 (T_R) - \left(\frac{T_R - T}{2 R T} - \frac{1}{2R} \ln T_R / T\right) \bar{J}_2 (T_R) .$$

In conclusion then, we now have a relationship which allows us to determine the activity coefficient of a 1 :1 electrolyte at any temperature or concentration provided we have

1. the activity coefficient
2. the relative partial molal enthalpy

and 3. the relative partial molal heat capacity, as a function of concentration and at a given reference temperature.

The reference temperature most frequently chosen is 25^{o} C.

Comparison of activity coefficients for NaCl, calculated using (96), with values obtained from boiling point or electromotive force measurements showed agreement to ±.001 [25]. This demonstrates the validity of the Procedure.

7.1

Determination of Partial Molal Quantities from Apparent Molal Quantities [75].

The mathematic definition of $\bar{L}_2$ formally requires the infinitesimal change of the quantity of solute with other variables fixed and the determination of the resulting change in heat content. Thermochemical measurements of the molal enthalpy of solute are, however, in practice taken with finite changes in solute concentration with the addition of solvent. The heat of dilution of a binary solution, $\Delta H_D \ (c_1 \rightarrow c_2)$, is measured calorimetrically during the isothermal, isobaric addition of sufficient pure solvent to change the concentration of one mole of solute from c_1 to a final value, c_2. In high dilution of an electrolyte, ΔH_D is linear with the root molality, so linear extrapolation to zero molality gives the relative apparent molal enthalpy (sign convention of reference [75])

$$\phi_L = - \Delta H_D \ (c \rightarrow 0) \quad . \tag{97}$$

The relative heat content referred to the infinitely dilute solution, for a solution containing n_2 moles of solute in n_1 moles of solvent is thus

$$L = n_2 \phi_L \tag{98}$$

and

$$\bar{L}_2 \equiv \left(\frac{\partial L}{\partial n_2} \right)_{T,p,n_1} = \phi_L + n_2 \frac{\partial \phi_L}{\partial n_2} \quad . \tag{99}$$

For molal concentrations,

$$\bar{L}_2 = \phi_L + m \frac{\partial \phi_L}{\partial m} \quad \text{or} \quad \bar{L}_2 = \phi_L + \frac{\sqrt{m}}{2} \frac{\partial \phi_L}{\partial \sqrt{m}} \quad . \tag{100}$$

The total heat capacity of a binary solution may be expressed in terms of the molal heat capacity of the pure solvent, $\bar{c}_{p_1}^{\,o}$, and the apparent molal heat capacity of the solute, ϕ_{c_p},

$$(101) \qquad c_p = n_1 \bar{c}_{p_1}^{\,o} + n_2 \phi_{c_p}$$

for a solution containing n_1 moles of solvent and n_2 moles of solute. Equation (101) may be transformed into the convenient form

$$(102) \qquad \phi_{c_p} = \frac{(1000 + m M_2) c_p - 1000 c_p^{\,o}}{m}$$

where m is the molality of the solute of molecular weight M_2 and c_p and $c_p^{\,o}$ are the measured specific heats of the solution and the pure solvent, respectively. The partial molal heat capacity may be obtained from the apparent molal heat capacity as before,

$$(103) \qquad \bar{c}_{p_2} = \phi_{c_p} + m \frac{\partial \phi_{c_p}}{\partial m} \quad .$$

The relative partial molal heat capacity is given by the definition

$$(104) \qquad \bar{J}_2 = \bar{c}_{p_2} - \bar{c}_{p_2}^{\,o} \quad .$$

7.2

The Activity of Solvent at various Temperatures and Concentrations of Solute

When chemical equilibrium prevails, the chemical potential of a component is the same in every phase. Consequently, at constant temperature and pressure, the activity of a component of a system is the same in every phase provided that it is defined in each phase in reference to the same standard state. For a solvent A, containing a non-volatile solute, the total vapour pressure above the solution is equal to the partial pressure of the solvent. In the regime where corrections for non-ideality of solvent vapour are small, the activity of the solvent is given by

$$a_A = \frac{p_A}{p_A^o} \tag{105}$$

The standard state chosen for the definition of the activity of solvent in solvation equilibria is the pure solvent in equilibrium with its vapour pressure at a total pressure of one atmosphere and a temperature of 25^o C. Vapour pressures at various temperatures and concentrations of solute are readily obtained and activities computed.

7.3
Thermodynamic Data used when Solvent is Water, Solute is Ammonium Chloride

7.3.0 The Activity Coefficient of Aqueous NH_4Cl [74]

The isopiestic vapour pressure method [75,78,79]has been used to determine the activity coefficients of NH_4Cl at 25° C from 0.1 m to saturation at 7.39 m. The results are tabulated in TABLE IX . A representation of $\gamma_{\pm(NH_4Cl)}$ plotted against molality NH_4Cl is given in Figure 21 and of $\gamma_{\pm(NH_4Cl)}$ against $\sqrt{m\ NH_4Cl}$ in Figure 33 .

If two solutions of different salts are allowed to equilibrate through the vapour pressure, then, at the isopiestic point, the activity of water is the same in both solutions. One solution serves as a reference for which the activity and activity coefficients are well known. Pairs of isopiestic solutions for NH_4Cl with KCl and NaCl as reference are given in Table X

The following relation [75] allows determination of the unknown activity coefficient

$$(106) \qquad \ln \gamma_{\pm} = \ln \gamma_R + \ln \frac{m_R}{m} + 2 \int_0^{a_R} \left(\frac{m_R}{m} - 1 \right) \frac{d\sqrt{a_R}}{\sqrt{a_R}}$$

γ_R and a_R are the activity coefficients and activity reference and m_R and m are the molalities of the reference and the unknown in the isopiestic pairs. m_R / m may be plotted against m and the second term evaluated at round concentrations. A plot of $(m_R / m - 1)/\sqrt{a_R}$ versus $\sqrt{a_R}$ allows graphical integration of the third term.

7.3.1 . Relative Apparent Enthalpy and Apparent Heat Capacity of Aqueous NH_4Cl at 25° C [80]

The unit of energy used is the thermochemical calorie, defined by

TABLE IX

Isopiestic mean ionic activity coefficients $\gamma_{\pm}$ of NH_4Cl at 25° C; m, molality [79].

m	$\gamma_{\pm}$
0.1	0.770
0.2	0.718
0.3	0.687
0.4	0.665
0.5	0.649
0.6	0.636
0.7	0.625
0.8	0.617
0.9	0.609
1.0	0.603
1.2	0.592
1.4	0.584
1.6	0.578
1.8	0.574
2.0	0.570
2.5	0.564
3.0	0.561
3.5	0.560
4.0	0.560
4.5	0.561
5.0	0.562
5.5	0.563
6.0	0.564
6.5	0.565
7.0	0.566
7.390 (saturated)	0.566

Figure 33. Smoothed curve representing the mean ionic activity coefficient, $\gamma_{\pm}$, of aqueous ammonium chloride at 25° C as a function of the square root of the molality, $\sqrt{m}$. The points represent the tabulated values.

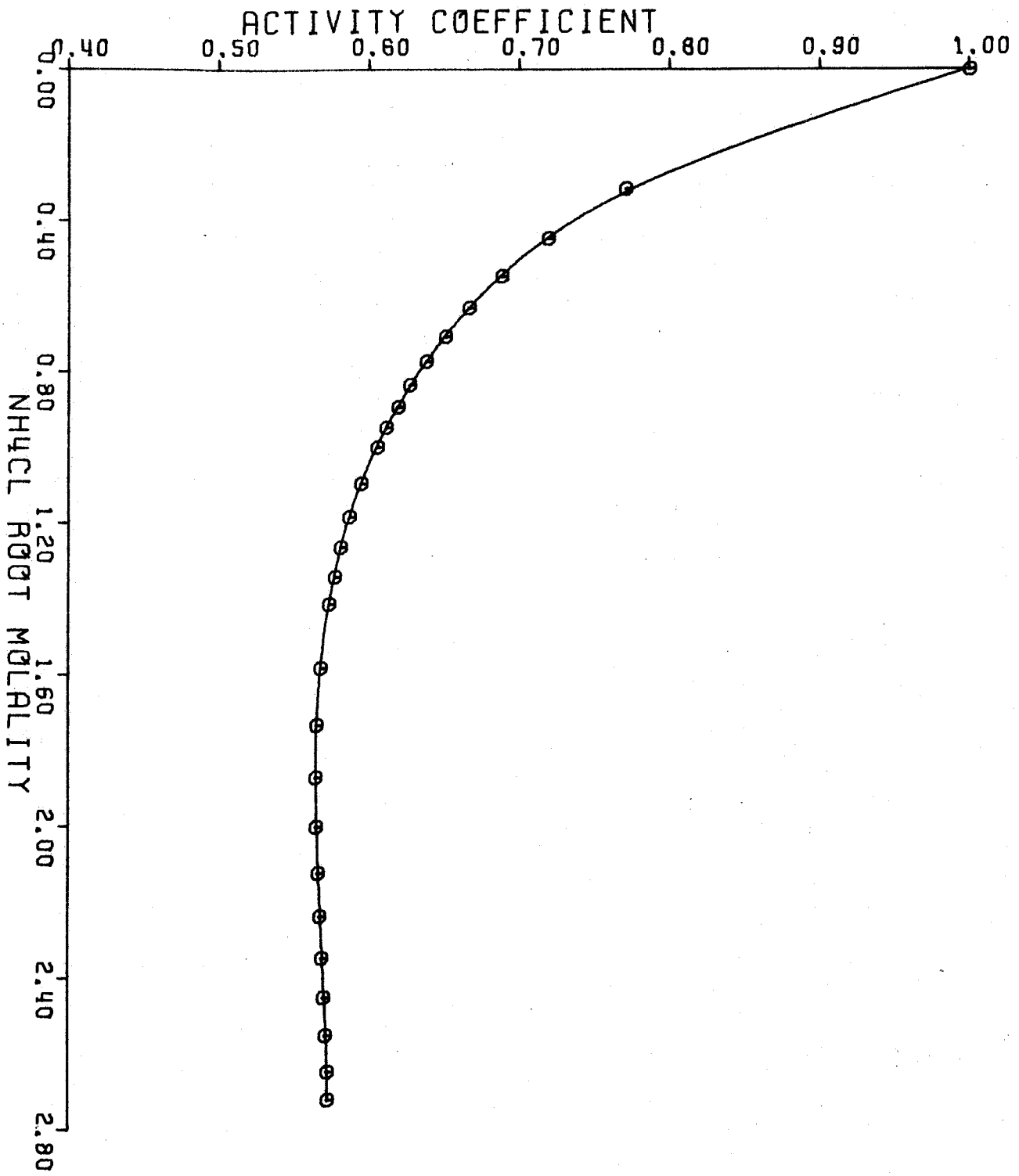

MEAN IONIC ACTIVITY COEFFICIENT OF AQUEOUS NH4CL AT 25 CELSIUS

TABLE X

Isopiestic pairs (reference KCl/NaCl, NH_4Cl), molal concentrations [79].

m_{KCl}	m_{NH_4Cl}	m_{KCl}	m_{NH_4Cl}	m_{KCl}	m_{NH_4Cl}
0.2029	0.2026	1.405	1.407	2.739	2.763
0.3830	0.3834	1.586	1.589	2.996	3.028
0.7134	0.7141	2.050	2.055	3.813	3.880
1.065	1.067	2.544	2.563	4.526	4.647
1.085	1.087	2.655	2.673	——	——

m_{NaCl}	m_{NH_4Cl}	m_{NaCl}	m_{NH_4Cl}	m_{NaCl}	m_{NH_4Cl}
4.268	5.043	5.278	6.580	5.732	7.328
4.398	5.244	5.323	6.659	5.768	7.390 (satd.)
4.472	5.352	5.485	6.919	——	——
4.871	5.943	5.661	7.209	——	——

1 cal = 4.1840 J, and 1961 atomic weights. ϕ_L is shown in Table XI and ϕ_C in Table XII for aqueous NH_4Cl at 25° C. ϕ_C and ϕ_L are represented in Figures 34 and 35 .

The chord-area method of Young et al. ([80] and references cited therein) is used to obtain values of ϕ_L. Chords $\Delta\phi_L / \Delta (m^{\frac{1}{2}})$ are plotted against $m^{\frac{1}{2}}$ on large scale graphs. Extrapolation to infinite dilution is made using the theoretical limiting value for $d\phi_L / d m^{\frac{1}{2}}$ of 472 cal/ mole $\frac{3}{2}$ [75]. A smooth curve is then drawn through all the data, giving greater weight to the more reliable data.

Values of ϕ_C are obtained from measurements of the specific heat of solutions [80]. The values for ϕ_C were plotted against $m^{\frac{1}{2}}$ on large scale graphs using $(d\phi_C / d m^{\frac{1}{2}})_{m^{\frac{1}{2}} \to 0}$ = 6.13 cal/deg mole $\frac{3}{2}$ for the limiting slope. A smooth curve is drawn through all the data.

7.3.2 Activity of Water [81]

Values of the measured vapour pressure of water for pure water and for various concentrations of NH_4Cl up to the solubility limit and at temperatures from 0° C to 110° C are given in Table XIII .

TABLE XI

Relative apparent molal enthalpy, ϕ_L (cal/mole), of NH_4Cl at 25° C (column 3); m, molality; n moles of H_2O containing one mole NH_4Cl [80].

n	m	NH_4Cl
∞	0.00	0
500,000	.000111	5
100,000	.000555	10
50,000	.00111	14
20,000	.00278	22
10,000	.00555	29
7,000	.00793	34
5,000	.01110	40
4,000	.01388	44
3,000	.01850	48
2,000	.02775	57
1,500	.03700	63
1,110	.05000	70
1,000	.05551	73
900	.0617	76
800	.0694	79
700	.0793	82
600	.0925	87
555.1	.1000	88
500	.1110	92
400	.1388	98
300	.1850	105
277.5	.2000	107
200	.2775	117
150	.3700	124
111.0	.5000	131
100	.5551	133
75	.7401	136
55.51	1.0000	136
50	1.1101	136
40	1.3877	134
37.00	1.5000	133
30	1.8502	128
27.75	2.0000	125
25	2.2202	120
22.20	2.5000	114

TABLE XI a continued

n	m	NH_4Cl
20	2.7753	108
18.50	3.0000	104
15.86	3.5000	93
15	3.7004	89
13.88	4.0000	82
12.33	4.5000	72
12	4.6255	69
11.10	5.0000	62
10	5.5506	53
9.5	5.8427	48
9.251	6.0000	45
9.0	6.1674	42
8.5	6.5301	36
8.0	6.9383	30
7.929	7.0000	29

TABLE XII

Apparent molal heat capacity, ϕ_C (cal/mol/^{o}), of NH_4Cl at 25^{o} C (column 3); m, molality; n moles of H_2O containing one mole NH_4Cl [80].

n	m	NH_4Cl
∞	0.00	-13.5
500,000	.000111	.....
100,000	.000555	-13.4
50,000	.00111	-13.3
20,000	.00278	-13.2
10,000	.00555	-13.1
7,000	.00793	-13.0
5,000	.01110	-12.9
4,000	.01388	-12.8
3,000	.01850	-12.7
2,000	.02775	-12.6
1,500	.03700	-12.4
1,000	.05551	-12.1
900	.0617	-12.0
800	.0694	-11.9
700	.0793	-11.8
600	.0925	-11.7
500	.1110	-11.6
400	.1388	-11.3
300	.1850	-11.0
200	.2775	-10.3
150	.3700	-9.7
100	.5551	-8.7
75	.7401	-7.8
50	1.1101	-6.2
40	1.3877	-5.3
30	1.8502	-3.9
25	2.2202	-2.9
20	2.7753	-1.6
15	3.7004	+0.3
12	4.6255	1.9
10	5.5506	3.4
9.5	5.8427	3.8
9.0	6.1674	4.3
8.5	6.5301	4.8
8.0	6.9383	5.3
7.5	7.4008	6.0

Figure 34 . Smoothed curve representing the apparent molal heat capacity ϕ_c (cal/mol/^{o}) of aqueous ammonium chloride at 25^{o} C as a function of the square root of the molality, $\sqrt{m}$. The points represent the tabulated values.

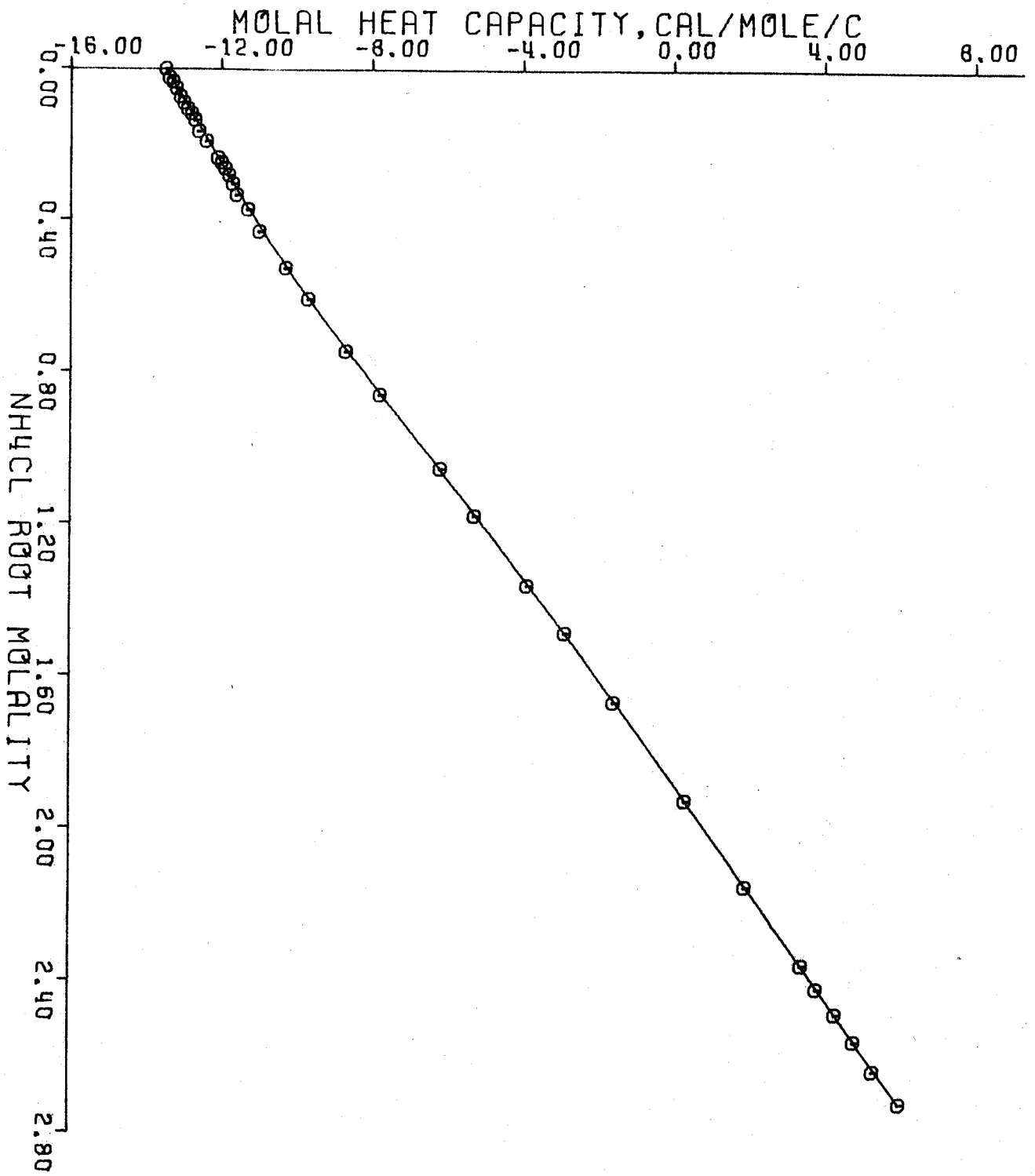

APPARENT MOLAL HEAT CAPACITY OF AQUEOUS NH4CL AT 25 CELSIUS

Figure 35. Smoothed curve representing the relative apparent molal enthalpy, ϕ_L (cal/mol), of aqueous ammonium chloride at 25° C as a function of the square root of the molality, $\sqrt{m}$. The points represent the tabulated values.

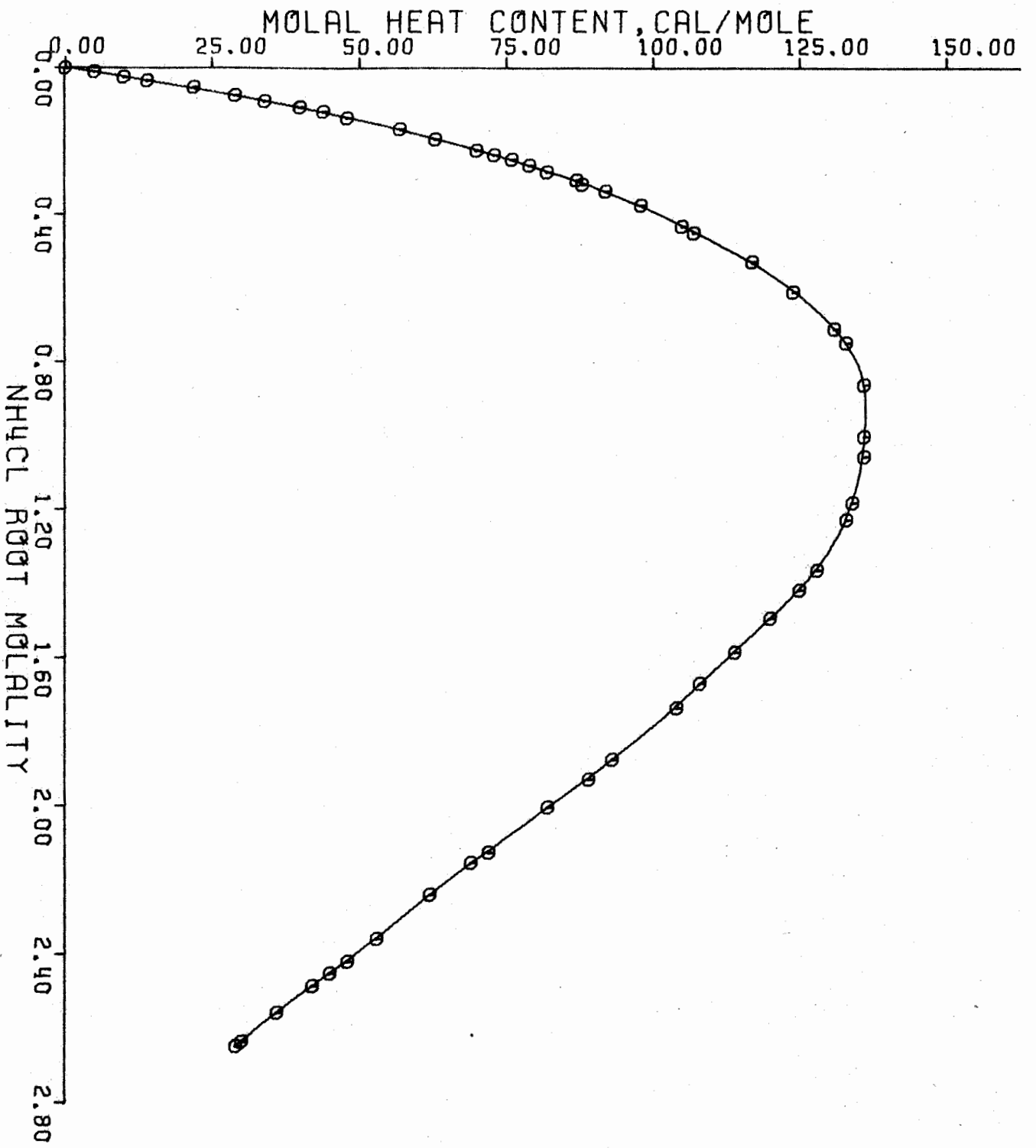

RELATIVE APPARENT MOLAL HEAT CONTENT OF AQUEOUS NH4CL AT 25 C

TABLE XIII

Vapour pressure (mm) of H_2O of aqueous NH_4Cl at concentrateion C (g NH_4Cl/ 100 g H_2O) and temperatures t, (^oC) [81].

t, ^oC \ C	p_{mm} 0.0	10.0	20.0	30.0	40.0	50.0	60.0	70.0	80.0
0	4.579	4.3	4.0	(3.8)					
10	9.210	8.6	8.1	7.6					
20	17.539	16.4	15.5	14.5	Saturated		solutions		
30	31.834	29.9	28.1	26.3	24.7				
40	55.34	51.9	48.9	45.8	42.9				
50	92.54	86.8	81.7	76.6	71.8	67.5			
60	149.46	140.2	132.0	123.6	116.0	109.0			
70	233.79	219.3	206.5	193.4	181.4	170.5	160.6		
80	355.47	333.5	314.0	294.1	275.9	259.3	244.2		
90	526.00	493.5	464.6	435.2	408.2	383.6	361.4	341.1	
100	760.00	713.0	671.2	628.7	589.8	554.3	522.1	492.9	
110	1074.5	1008	949	888.9	833.8	783.7	738.2	696.8	659.2

t, ^oC	p_{mm}	C
	α-NH_4Cl	
20	13.9	37.2
25	18.5	39.3
30	24.5	41.4

7.4
Computational Procedure

7.4.0 Interpolation, Approximation, Differentiation, and Smoothing using Cubic Splines and Bicubic Splines [82 - 88].

The preceeding discussion indicates the need to evaluate differential forms $Y + X \frac{d Y}{d X}$, where our knowledge of $Y(X)$ is restricted to tabulated values $\{(y_i, x_i)\}$ of experimentally determined values of finite precision only, approximating $Y(X)$ up to experimental error and to evaluate a function $F(X,Y)$ when we have only a table $\{(f_i, x_i, y_i)\}$ of experimentally determined values. Cubic spline functions have recently proven themselves useful for problems of this nature. A number of definitions are in order.

A cubic spline function is a piece-wise cubic polynomical function, S, defined for a given $\{(Y_i, X_i)\}$ such that $s(X_i) = Y_i$, which is continuous and has continuous first and second derivatives. The continuity conditions, plus two end conditions, $s''(X_o) = s''(X_n) = 0$ for natural cubic splines, are sufficient to determine the coefficients for the cubic in each subinterval $[X_i, X_{i+1}]$. Thus, $s(X) = Y_i + ((C_{i3} \cdot D + C_{i2}) \cdot D + C_{i1}) \cdot D$, where $X_i \leq X < X_{i+1}$ and $D = X - X_i$. Consequently, $s'(X) = (3 \cdot C_{i3} \cdot D + 2C_{i2}) \cdot D + C_{i1}$.

Cubic spline interpolation of a tabled function $\{(Y_i, X_i)\}$ involves the determination of the spline coefficients and evaluation of the spline function at a point in a given subinterval as in the last paragraph. When $\{(Y_i, X_i)\}$ contains experimental error, cubic spline interpolation gives a correspondingly poor approximation, $s(X)$. The approximation error is greater for $s'(X)$ and even greater for $s''(X)$.

Cubic spline smoothing of a tabled function $\{(Y_i, X_i)\}$ involves the determination of $\{(\hat{Y}_i, X_i)\}$ such that $s(X_i) = \hat{Y}_i$ and the corresponding spline

coefficients giving

(107) $$\int_{x_0}^{x_n} s''(x)^2\,dx \quad \text{, a minimum, and}$$

(108) $$\sum_{i=0}^{n} \left(\frac{s(X_i) - Y_i}{\delta Y_i} \right)^2 = S \quad \text{, where } \delta Y_i \text{ is an}$$

estimate of the standard deviation in Y_i and S is in the corresponding confidence interval $N - (2N)^{\frac{1}{2}} \leq S \leq N + (2N)^{\frac{1}{2}}$. Although the minimal integral second moment condition is satisfied for certain mathematical functions, this may not be so for physically derived functions. However, where this condition holds, it is shown that the approximation results in a reduced error for s(X), s'(X) and s"(X) [86].

Least squares approximation by cubic splines of a tabled function $\{(Y_i, X_i), i=0, n\}$, at a given set of knots $\{x_j, j=0, m \leq n\}$, where $X_o < x_o < x_m < X_n$, requires the evaluation of approximate $\{(y_j, x_j)\}$ such that $s(x_j) = y_j$ and the corresponding spline coefficients so that the mean squared error is at a minimum, i.e. $\sum_{i=0}^{n} (Y_i - s(X_i))^2 (X_{i+1} - X_i) / (X_n - X_0)$, a minimum. The least squares approximation is the most general procedure for minimizing the error due to approximation in s(X), s'(X), and s"(X). Note: In the FORTRAN program given in APPENDIX I the cubic spline smoothing method of approximation was chosen. the residual "wiggle" in $\bar{L}_2$ shown in Figure 36 suggests that this is a poor choice.

A bicubic spline function is a piece-wise bicubic polynomial in two independent variables defined in rectangular subregions of a rectangular region which has continuous first, second and mixed partial derivatives. Thus, if we have $F(X_i, Y_j)$, $\{X_0 < \ldots < X_n\} \times \{Y_0 < \ldots < Y_m\}$ an approximation s(X, Y)

Figure 36. Smoothed curve representing the relative partial molal enthalpy, $\bar{L}_2$ (cal/mol), of aqueous ammonium chloride at 25° C as a function of the square root of the molality, $\sqrt{m}$, as calculated by the computational procedue given as a FORTRAN program in APPENDIX I. The weighting function chosen was $(1 + \sqrt{m})^{-1}$.

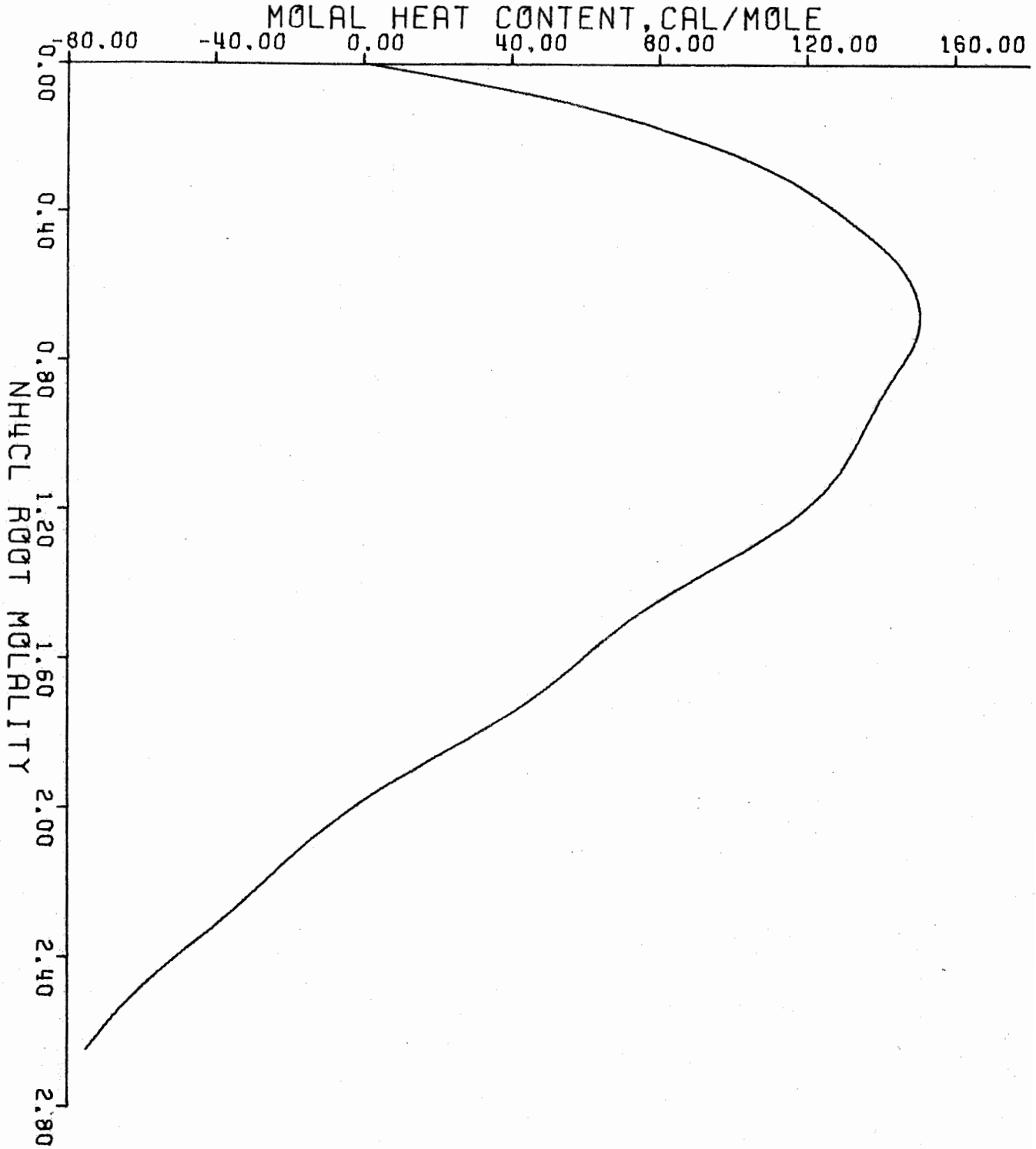

RELATIVE PARTIAL MOLAL HEAT CONTENT OF AQUEOUS NH4CL AT 25 C

Figure 37. Smoothed curve representing the partial molal heat capacity, $\bar{C}_{p2}$ (cal/mol/^{o}), of aqueous ammonium chloride at 25^{o} C as a function of the square root of the molality, $\sqrt{m}$, as calculated by the computational procedure given as a FORTRAN program in APPENDIX I.

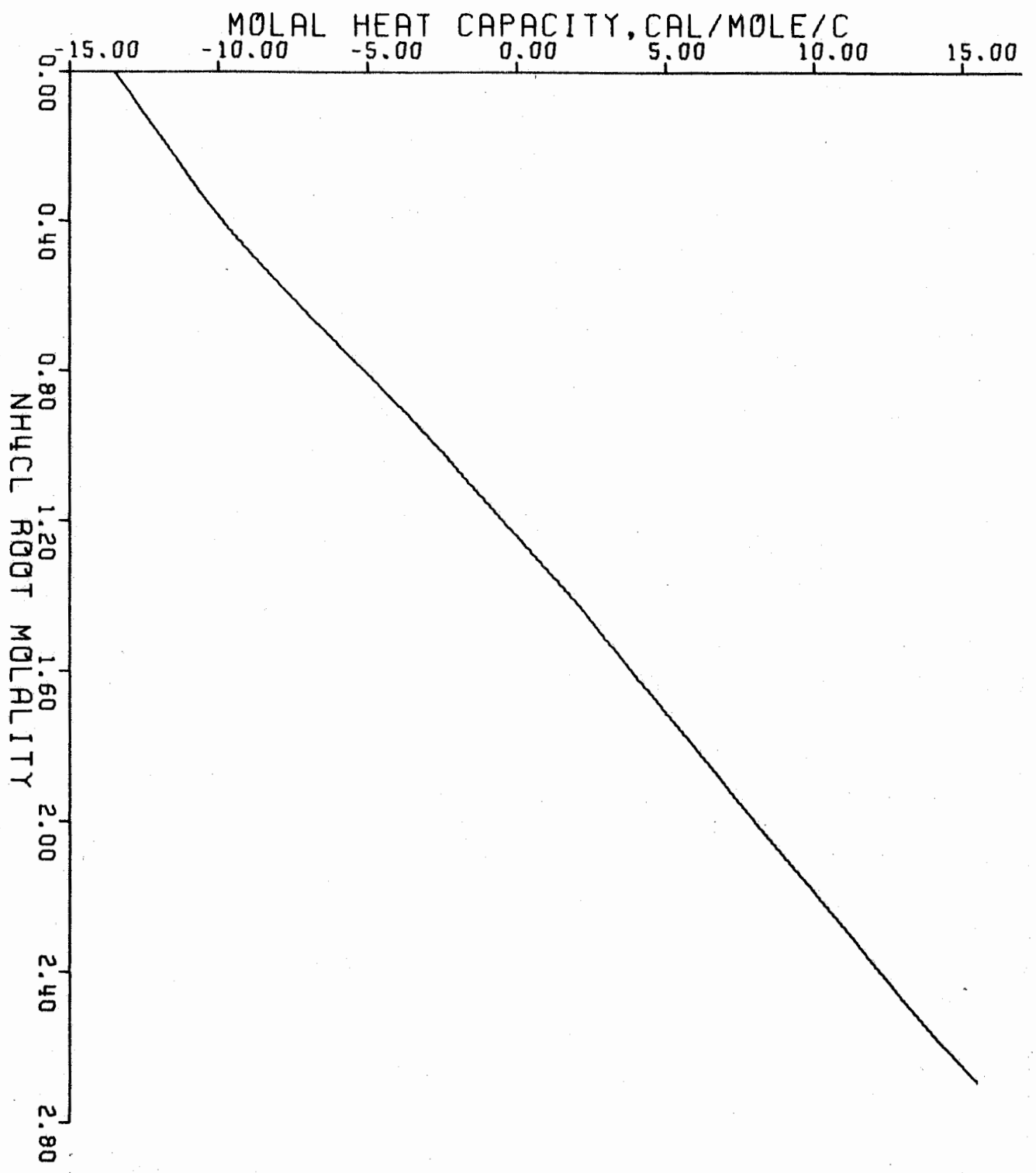

PARTIAL MOLAL HEAT CAPACITY OF AQUEOUS NH4CL AT 25 CELSIUS

may be obtained where

$$(109) \quad s(X, Y) = \sum_{i=0}^{3} \sum_{j=0}^{3} c_{ij} (X - X_K)^i (Y - Y_\ell)^j$$

for $X_K \leq X < X_{K+1}$, $Y_\ell \leq Y < Y_{\ell+1}$. The coefficients c_{ij} are determined by the required condition, of continuity etc.

7.4.1 The Problem

APPENDIX I lists the FORTRAN program which formally does the following. Tabulated values of ϕ_c, ϕ_L, $\gamma_\pm$ and V_A are read in, along with concentrations and temperatures for which calculations are to be performed. The following functions are constructed:

$$(110) \quad \bar{L}_2 = \phi_L + \frac{1}{2}\sqrt{m}\,\frac{d\,\phi_L}{d\sqrt{m}}$$

$$(111) \quad \bar{c}_{p_2} = \phi_c + \frac{1}{2}\sqrt{m}\,\frac{d\,\phi_c}{d\sqrt{m}}$$

$$(112) \quad \bar{J}_2 = \bar{c}_{p_2} - \bar{c}^{\,o}_{p_2}$$

$$(113) \quad a_A = V_A(m, T) \,/\, V_A\,(0, 25^o\,C)$$

$$(114) \quad \ln \gamma_\pm\,(m, T) = \ln \gamma_\pm\,(25^o) + \frac{1}{2}\left[\left(\frac{298.1 - T}{R \cdot 298.1 \cdot T}\right)\cdot \bar{L}_2 - \left(\frac{298.1 - T}{R \cdot T} - \frac{298.1}{T}\right)\cdot \bar{J}_2\right]$$

$$(115) \quad \gamma_\pm\,(m, T) = \exp\,(\ln \gamma_\pm)$$

$$(116) \quad a_\pm\,(m, T) = m\,\gamma_\pm\,(m, T)$$

Figure 38. Flowchart of Program given in APPENDIX I.

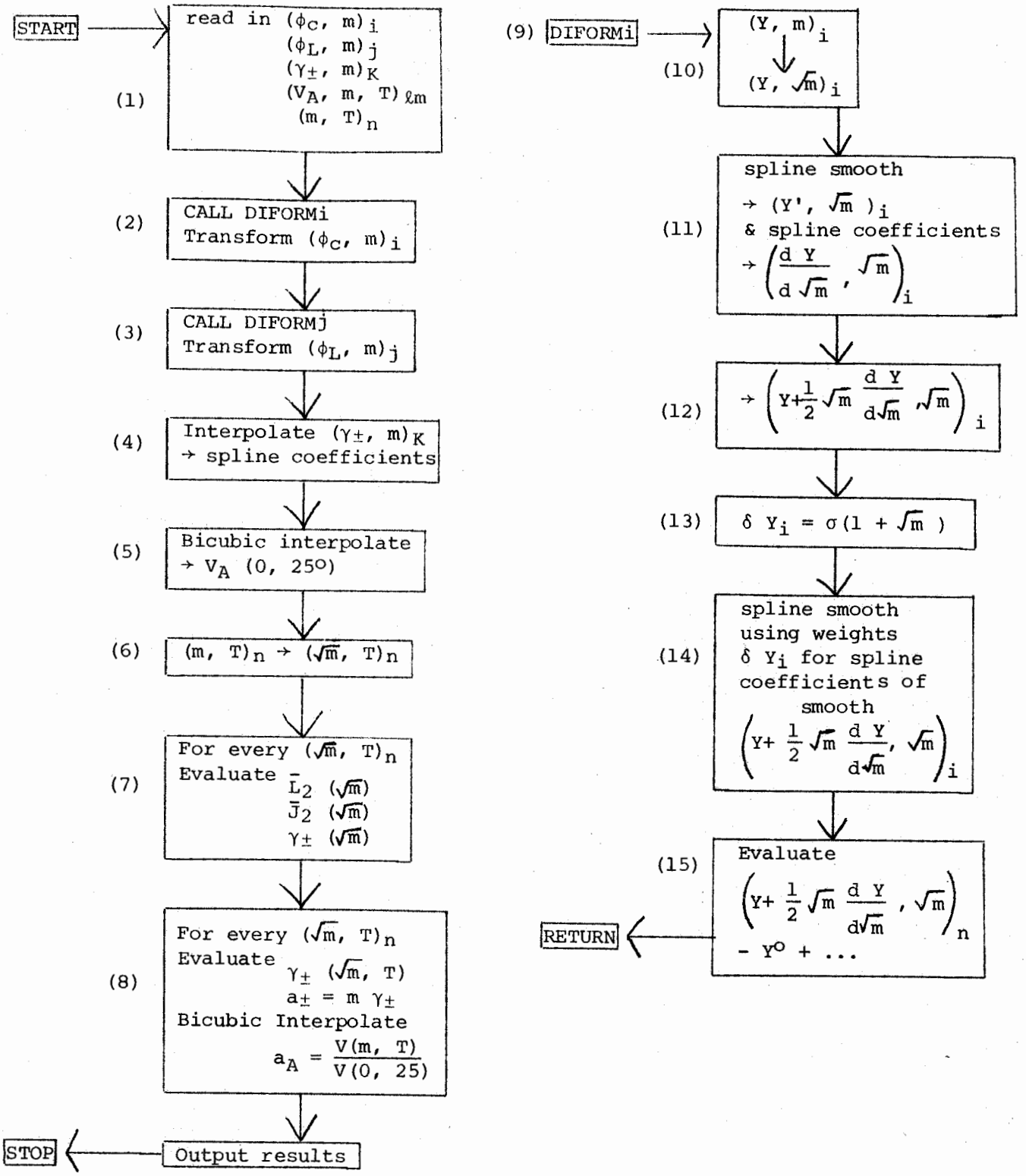

DATA

(16) $(\phi_c, m)_i$
(17) $(\phi_L, m)_j$
(18) $(\gamma_\pm, m)_K$
(19) $(V_A, m, T)_{\ell m}$
(20) $(m, T)_n$

TABLE XIV

Output of FORTRAN program given in APPENDIX I. Column 2,4,5 are the independent variables appearing in TABLE VII columns 4,5,6.

Molality NH_4Cl	Temperature	Mean Ionic Activity Coefficient NH_4Cl	Mean Ionic Activity NH_4Cl	Activity H_2O
0.0	2.000000	1.000000	0.0	0.226096
0.0	11.000000	1.000000	0.0	0.413748
0.0	11.000000	1.000000	0.0	0.413748
0.0	28.000000	1.000000	0.0	1.193101
0.0	30.000000	1.000000	0.0	1.339211
0.0	46.000000	1.000000	0.0	3.183289
0.0	55.000000	1.000000	0.0	4.966965
0.0	56.000000	1.000000	0.0	5.209857
0.0	56.000000	1.000000	0.0	5.209857
0.0	66.000000	1.000000	0.0	8.254076
0.0	69.000000	1.000000	0.0	9.420026
0.0	78.000000	1.000000	0.0	13.785914
0.0	80.000000	1.000000	0.0	14.958834
0.0	97.000000	1.000000	0.0	28.659683
0.0	100.000000	1.000000	0.0	31.982193
1.179999	55.000000	0.569523	0.672037	4.770890
1.179999	19.000000	0.599938	0.707927	0.662926
1.179999	32.000000	0.594111	0.701051	1.442597
1.179999	51.000000	0.574864	0.678339	3.928230
1.179999	68.000000	0.549797	0.648759	8.657592
1.179999	84.000000	0.521760	0.615677	16.862625
1.179999	65.000000	0.554636	0.654470	7.580222
1.179999	85.000000	0.519906	0.613489	17.539658
1.179999	101.000000	0.489174	0.577225	31.856277
2.370000	27.000000	0.578787	1.371725	1.039953
2.370000	50.000000	0.558469	1.323572	3.593560
2.370000	74.000000	0.521332	1.235557	10.771154
2.370000	72.000000	0.524858	1.243913	9.895076
2.370000	90.000000	0.491246	1.164253	20.433853
3.919999	19.000000	0.570813	2.237585	0.607829
3.919999	53.000000	0.546780	2.143378	3.959818
3.919999	74.000000	0.512551	2.009200	10.245176
3.919999	73.000000	0.514397	2.016436	9.821074
5.440000	30.000000	0.563886	3.067540	1.113316
5.440000	54.000000	0.540335	2.939420	3.941846
5.440000	68.000000	0.517364	2.814459	7.503985
5.440000	82.000000	0.490000	2.665602	13.497835
5.440000	97.000000	0.457655	2.489640	23.845169
7.339999	40.000000	0.554017	4.066487	1.814112

For all the pairs (m, T) the following is output: m, T, $\gamma_{\pm}$, $a_{\pm}$, a_A. An example of the output of the program is shown in Table XIV . Figure 38 contains a more detailed description of the procedure with correspondence numbers to the program listing in APPENDIX I . The external subroutines ICSICU, IBCIEU, ICSEVU, ICSSCU, and DCSEVU are the cubic spine routines. Explanations of these routines can be found in [89].

8.0
B.Differential Nuclear Shielding and Electronic Structure

Carbon-13 chemical shifts have been shown to be an effective means to estimate differential electronic densities and vice versa. The sensitivity of the method derives from the fact that, in the ^{13}C shielding constant tensor [90]

(117) $$\sigma = \sigma_d + \sigma_p + \sigma'$$

the paramagnetic term, σ_p, dominates and, hence, the large dispersion (~ 200 ppm) of ^{13}C shifts results. The "atom within a molecule" approximation [91] allows one to treat σ_d as a constant.

Pugmire and Grant have reported that carbons α- to the nitrogen in various five-membered nitrogen heterocycles are strongly shielded on protonation of the nitrogen, by about 9.0 ppm [92]. Explanations of this phenomenon differ; Grant has proposed a change in the N-C bond order, while Adam, Grimison, and Rodriguez have considered changes in the average excitation energy [93]. This protonation of a heterocycle has been envisioned as primarily a σ-bond change [94]. However, carbon-13 chemical shifts must be correlated with total (σ and π) electron density distributions [95,96].

8.1

Nuclear Shielding in Treatments due to Ramsey [97 - 106].

A review of the background of the theory of the nuclear shielding may give a foundation for the treatment of nitrogen heterocycles and anhydrosugars.

Ramsey has written the Hamiltonian for an electron in the Coulombic field of the nucleus, V, and a magnetic field $\vec{H}$ with vector magnetic potential, $\vec{A}$, as

$$(118) \qquad \mathcal{H} = \frac{1}{2m} \left(\frac{\hbar}{i} \vec{\nabla}_j + \frac{e}{c} \vec{A}(\vec{r}_j) \right)^2 + V ,$$

where, for zero guage, with respect to origin at the nucleus,

$$(119) \qquad \vec{A} = 1/2 \, (\vec{H} \times \vec{r}) + r^{-3} (\vec{\mu} \times \vec{r})$$

$$= (1/2 \, H + \mu r^{-3}) (-y \vec{i} + x \vec{j}) \quad .$$

Applying second order perturbation theory, where the unperturbed Hamiltonian is that of the system in the absence of a magnetic field allows the calculation of the shielding tensor. In the notation of dyadics

$$(120) \qquad \overleftrightarrow{\sigma} = \overleftrightarrow{\sigma}(d) + \overleftrightarrow{\sigma}(p)$$

where the diamagnetic term is

$$(121) \qquad \overleftrightarrow{\sigma}(d) = (e^2/2mc^2 a_o) \langle \psi_o | \Sigma_j (r_j^2 \overleftrightarrow{1} - \vec{r}_j \vec{r}_j)/r_j^3 | \psi_o \rangle$$

and the paramagnetic term is

$$\overleftrightarrow{\sigma}(p) = -(e^2/2m^2c^2a_o) \sum_{n\neq o} (E_n - E_o)^{-1} \Big(\langle \psi_o | \sum_j \vec{L}_j / r_j^3 | \psi_n \rangle \cdot$$

(122)

$$\langle \psi_n | \sum_k \vec{L}_k \psi_o \rangle + \langle \psi_o | \sum_j \vec{L}_k | \psi_n \rangle \langle \psi_n | \sum_j \vec{L}_j / r_j^3 | \psi_o \rangle \Big) .$$

In these equations $\overleftrightarrow{1}$ is the unit dyadic, $\vec{r}_j$ is the position vector of the j^{th} electron in units of Bohr radii ($a_o = 0.592$ Å), ψ_o is the ground state wave function with energy E_o, ψ_n is an excited state with energy E_n, and the angular momentum operator is $\vec{L}_j = -i\hbar\, \vec{r}_j \times \nabla_j$, coupling orbital angular momentum with the magnetic field.

At this point one may, with caution, introduce an average excitation energy ΔE in order to simplify using the closure relationship. Then, averaging over-all orientations, one obtains the scalar shielding

$$\sigma = (e^2/3mc^2a_o) \langle \psi_o | \sum_j 1/r_j | \psi_o \rangle$$

(123)

$$-(e^2h^2/3m^2c^2a_o^3)\,(\Delta E)^{-1} \langle \psi_o | \sum_{j,k} \vec{\ell}_j \cdot \vec{\ell}_k / r_j^3 | \psi_o \rangle ,$$

where $\vec{\ell}_j = i\,\vec{r}_j \times \nabla_j$.

We have, then, a closed analytical expression for the shielding constant that allows physical interpretation.

The first term is interpreted as the diamagnetic Lamb term. The second term represents the paramagnetic contribution to the shielding due to the deviation from spherical symmetry of the electronic environment of the nucleus. The paramagnetic term in the above form involves an empirically determined parameter, ΔE, the average excitation energy. This one parameter

summarizes the distribution of all low lying excited states. The availability of low lying excited states has been used to explain the paramagnetic $\delta^{13}C$ (downfield shift), in olefins and aromatics with respect to the corresponding alkanes.

Pople has suggested the following partition of the shielding constant

(124)
$$\sigma^{A} = \sigma^{AA}_{dia} + \sigma^{AA}_{para} + \sum_{B\neq A} \sigma^{BA} + \sigma^{A}_{deloc} + \sigma^{A}_{solv} \quad .$$

σ^{AA}_{dia} represents the contribution to the shielding of nucleus A of the electrons on A which are in an S orbital[100]. Similarly, σ^{AA}_{para} represents the paramagnetic contribution from electrons at A which are in p orbitals. $\sum_{B\neq A} \sigma^{BA}$ stands for a summation of contributions from intra-atomic currents induced in atoms B≠A and related to their magnetic anisotropy. σ^{A}_{deloc} is an inter-atomic contribution and may be associated with ring currents due to electron delocalization in cyclic molecules. σ_{solv} represents all the contributions of the solvent to the shielding of A. Accurate assessment of all the contributions to σ^{A} is quite difficult. Most work has stressed σ^{AA}_{p}, which is the largest contributor. However, the above partition is useful when explaining differential shielding.

In the context of LCAO-MO theory, Karplus and Pople have given an equation for σ^{AA}_{p} ,

125)
$$\sigma^{AA}_{p} = -\frac{e^2\hbar^2}{2m^2c^2} (\Delta E)^{-1} \langle r^{-3} \rangle_{2p} \sum_{B} q_{AB} \quad ,$$

where
(126)
$$q_{AB} = 1/3\ \delta_{AB}(P_{xx} + P_{yy} + P_{zz})_{AB}$$
$$-2/3\ (P_{yy}P_{zz} + P_{zz}P_{xx} + P_{xx}P_{yy})_{AB}$$

$$+ \ 2/3 \ (P_{yz}P_{zy} + P_{zx}P_{xz} + P_{xy}P_{yx})_{AB}$$

with $(P_{\mu\nu})_{AB} = 2 \sum_{i}^{occ} C^{A}_{\mu_i} C^{B}_{\nu_i}$

(127)

$C^{A}_{\mu_i}$ is the coefficient of the $2P_{\mu}$ ($\mu = x,y,z$) atomic orbital of carbon A in the i^{th} MO. Neglect of other atom contributions (i.e. , $q_{AB} = 0$, for $A \neq B$) gives the Karplus-Das equation for σ^{AA}_{p} [101]. Further reduction in the number of terms is obtained within a π approximation which neglects contributions from σ electrons for a planar π framework.

The principle simplifications in the Karplus-Pople formula, which is the link between the Ramsey treatment and even more approximate treatments, are the assumption of zero differential overlap, neglect of two center integrals, and the introduction of an average excitation energy, ΔE.

Pople has developed an expression for the neighbor anisotropy terms based on an independent electron guage invariant atomic orbital model

(128)

$$\sum_{B \neq A} \sigma^{BA} = -\frac{1}{3} N^{-1} \sum_{B \neq A} \sum_{\alpha\gamma} \chi^{B}_{\alpha\gamma} R_B^{-5} (R_B^2 \delta_{\gamma\alpha} - 3R_{B\gamma}R_{B\alpha}) .$$

$\chi^{B}_{\alpha\gamma}$ are the components of the magnetic susceptibility tensor centered at nucleus B. σ^{A}_{deloc} can be shown to be identically zero for acyclic molecules. For carbon chemical shifts the contribution due to delocalized ring currents is thought not to be large.

In the present formulation of nuclear shielding theory, differential nuclear shielding observed with changing substituents can be rationalized as

due to (a) diamagnetic effects from changes in S electron densities, (b) paramagnetic effects from changes in p electron distributions [107], or excitation energy changes or (c) magnetic anisotropy effects from other atoms. In atoms other than hydrogen, the diamagnetic effects may be ignored. Concentrating on the paramagnetic term in the nuclear shielding, equation (126) it is seen that there is a totally symmetric term $Q_{2p} = (P_{xx} + P_{yy} + P_{zz})_{AA}$, which relates to the charge density. This term indicates that an increase in charge density with symmetric distribution in the orbitals would result in decreased shielding. The other terms that enter into the paramagnetic term incorporate the opposite sign. On the basis of whether the observed shielding increases with increased calculated valence electron density, a symmetric redistribution of charge among the bonds may be distinguished from one unsymmetric among bonds.

8.2

Pyridines and Their N-Oxides

Table XV shows the ^{13}C chemical shifts with assignments [108] of pyridine, α,β,γ picoline, and their N-oxides. Table XVI shows the corresponding valence electron densities calculated by the CNDO/2 [109] molecular orbital program. In order to analyze the results, they have been classified according to atom type, as shown in Table XVII . There are five atom types: carbons in the α, β, or γ position, excluding those carbons directly bonded to methyl, and the methyl carbon.

Figures 40 to 44 show the plots of chemical shift versus charge density for the five chemically distinct carbon types. Least squares lines show an encouraging linearity. The calculated coefficients of correlation are excellent, the least shown by β carbons, with $\rho = -0.6934$, and the greatest for α, $\rho = -0.9772$. These trends can only be observed for the separated groups. In each group, each carbon has the same nearest neighbours, and only distant neighbours are changing.

Note the values of the shift per electron dependence given by the slope, -68.3, -32.5,-125.,-132., and 154. from Figures 40 to 44. Martin et al. [111] have compiled a number of the correlations between $\Delta\delta C$ and excess electronic charge, $\Delta Q(C)$. Perlin [112] has obtained the anomalously large value of -575 ppm/electron for the cyclanediols.

A significant observation can be obtained from the slopes of the linear regression lines. With the exception of that for the methyl carbons, they are all negative. This would suggest that, for the methyl, most of the increase in charge density goes into the C-C bond, giving a more asymmetric electronic distribution and a consequent downfield shift. In the aromatic carbon there would be a more symmetric distribution of charge between the σ and π systems. An alternative explanation might simply relate the changes

Figure 39. ^{13}C chemical shifts of pyridines and pyridine N-oxide derivatives. Assignments due to [108].

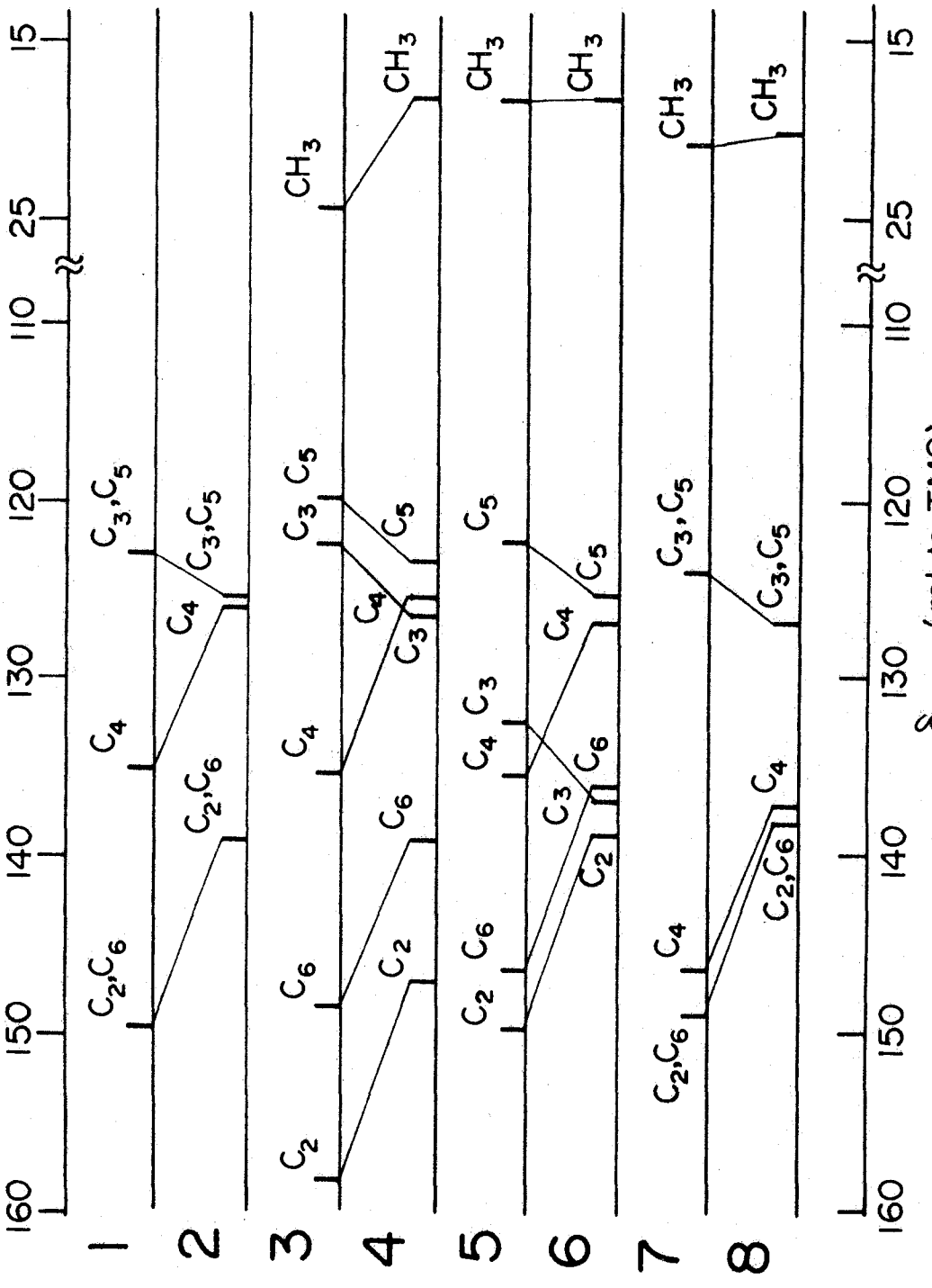
160
150
140
130
120
110
25
15
δppm (rel to TMS)
1
2
3
4
5
6
7
8
C2,C6
C4
C3,C5
CH3
C2
C6
C3

TABLE XV

^{13}C chemical shifts of pyridines and their N-oxides[a] [108]

Compound \ Position	2	3	4	5	6	Me
1	149.59	123.46	135.58	123.46	149.59	-
2	139.09	125.65	126.10	125.65	139.09	-
3	158.10	123.01	135.95	120.46	148.88	24.36
4	148.83	126.43	125.30	123.52	139.21	17.75
5	150.06	132.84	136.15	122.93	146.73	18.34
6	138.92	136.74	127.22	125.37	136.36	18.19
7	149.33	124.43	146.72	124.43	149.33	20.89
8	138.44	126.63	137.46	126.63	138.44	20.20

[a] Chemical shifts are downfield from internal TMS.

TABLE XVI

Valence electron densities calculated by CNDO/2[a]

Compound \ Position	2	3	4	5	6	Me
1	3.8450	4.0278	3.9304	4.0278	3.8450	--
2	3.9996	3.9497	4.0040	3.9497	3.9996	--
3	3.8422	4.0385	3.9276	4.0336	3.8432	3.9780
4	3.9704	3.9671	3.9978	3.9584	3.9944	3.9401
5	3.8574	4.0110	3.9428	4.0240	3.8517	3.9415
6	4.0148	3.9384	4.0172	3.9471	4.0068	3.9543
7	3.8420	4.0403	3.9215	4.0406	3.8420	3.9594
8	3.9949	3.9648	3.9834	3.9645	3.9944	3.9450

[a] Calculated using the Dobosh modification of the CNDO/2 [109] MO program on an IBM 370-155. Geometries from X-ray, microwave, or standard geometries were treated by PCILO [110] to give minimum energy geometries, as input for CNDO [108].

TABLE XVII

The structure of compounds 1-8 are given and the α, β, and γ carbons of pyridine, 1, are indicated. The ^{13}C chemical shifts (downfield from internal TMS) and the CNDO/2 valence electron densities are tabulated for α, β, γ, C-Me and methyl carbons. Standard numbering is shown.

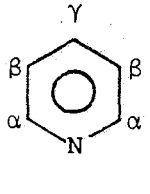

1

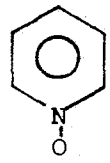

2

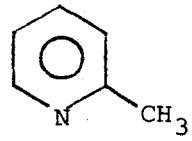

3

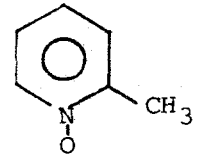

4

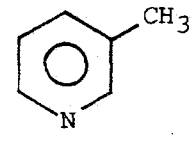

5

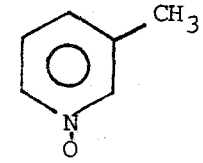

6

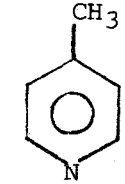

7

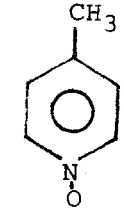

8

α	δ	Q_{2p}	β	δ	Q_{2p}	γ	δ	Q_{2p}	Me	δ	Q_{2p}	C-Me	δ	Q_{2p}
1-2,6	149.59	3.8450	1-3,5	123.46	4.0278	1-4	135.58	3.9304	3-Me	24.36	3.9780	3-2	158.10	3.8422
2-2,6	139.09	3.9996	2-3,5	125.65	3.9497	2-4	126.10	4.0040	4-Me	17.75	3.9401	4-2	148.83	3.9704
3-6	148.88	3.8432	3-3	123.01	4.0385	3-4	135.95	3.9276	5-Me	18.34	3.9415	5-3	132.84	4.0110
4-6	139.21	3.9944	3-5	120.46	4.0336	4-4	125.30	3.9978	6-Me	18.19	3.9543	6-3	136.74	3.9384
5-2	150.06	3.8574	4-3	126.43	3.9671	5-4	136.15	3.9428	7-Me	20.89	3.9594	7-4	146.72	3.9215
5-6	146.73	3.8517	4-5	123.52	3.9584	6-4	127.22	4.0172	8-Me	20.20	3.9450	8-4	137.46	3.9834
6-2	138.92	4.0148	5-5	122.93	4.0240									
6-6	136.26	4.0068	6-5	125.37	3.9471									
7-2,6	149.33	3.8420	7-3,5	124.43	4.0405									
8-2,6	138.44	3.9949	8-3,5	126.63	3.9646									

Figure 40. Plot of ^{13}C chemical shift of α carbons versus calculated valence electron densities, Q_{2p}. The solid line is represented by $\delta = a + b\ Q_{2p}$, where $a = 4.12 \times 10^{2}$ (S.D. = 1.93×10^{1}), $b = -6.83 \times 10^{1}$ (S.D. = 4.91). Coefficient of correlation, ρ, = -0.9772.

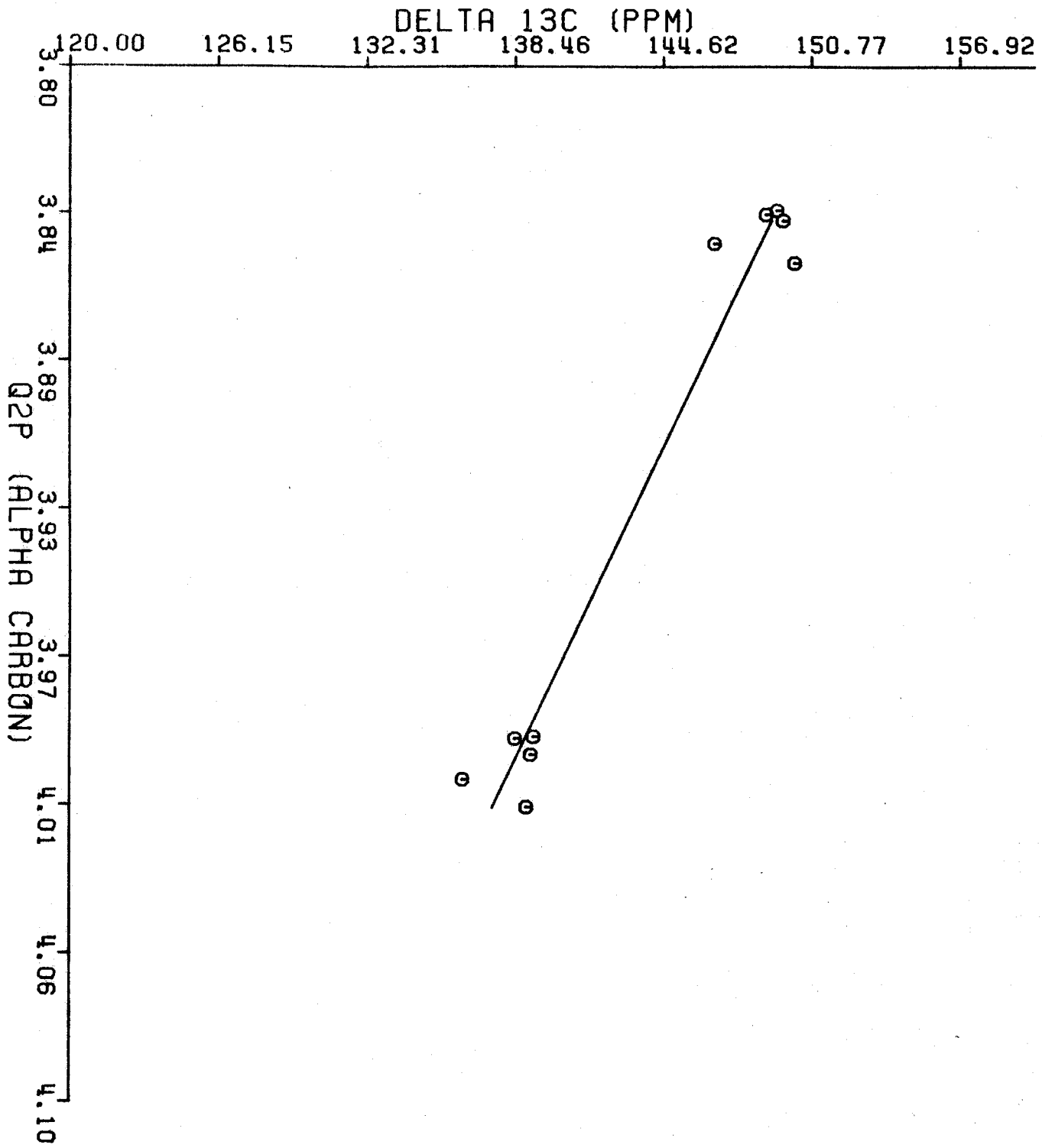

CHEMICAL SHIFT VERSUS CHARGE DENSITY (ALPHA)

Figure 41. Plot of ^{13}C chemical shift of β carbons versus calculated valence electron densities. The solid line is represented by $\delta = a + b\, Q_{2p}$, where $a = 2.54 \times 10^{2}$ (S.D. = 4.50×10^{1}), $b = -3.25 \times 10^{1}$ (S.D. = 1.13×10^{1}). Coefficient of correlation, ρ, = -0.6934.

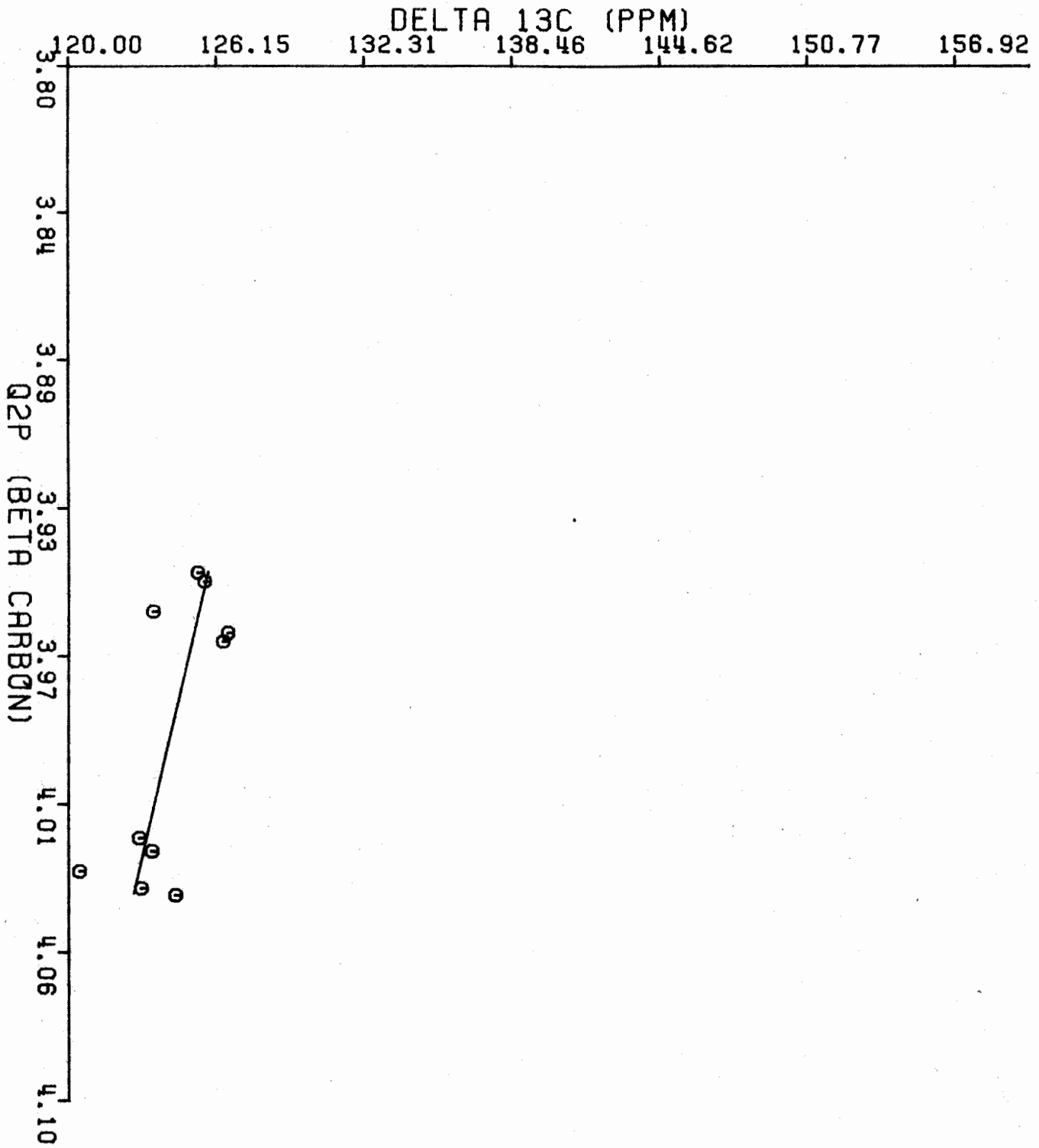

CHEMICAL SHIFT VERSUS CHARGE DENSITY (BETA)

Figure 42. Plot of ^{13}C chemical shift of γ carbons versus calculated valence electron densities. The solid line is represented by $\delta = a + b\ Q_{2p}$, where $a = 6.28 \times 10^{2}$ (S.D. = 7.09×10^{1}), $b = -1.25 \times 10^{2}$ (S.D. = 1.79×10^{1}). Coefficient of correlation, ρ, = -0.9527.

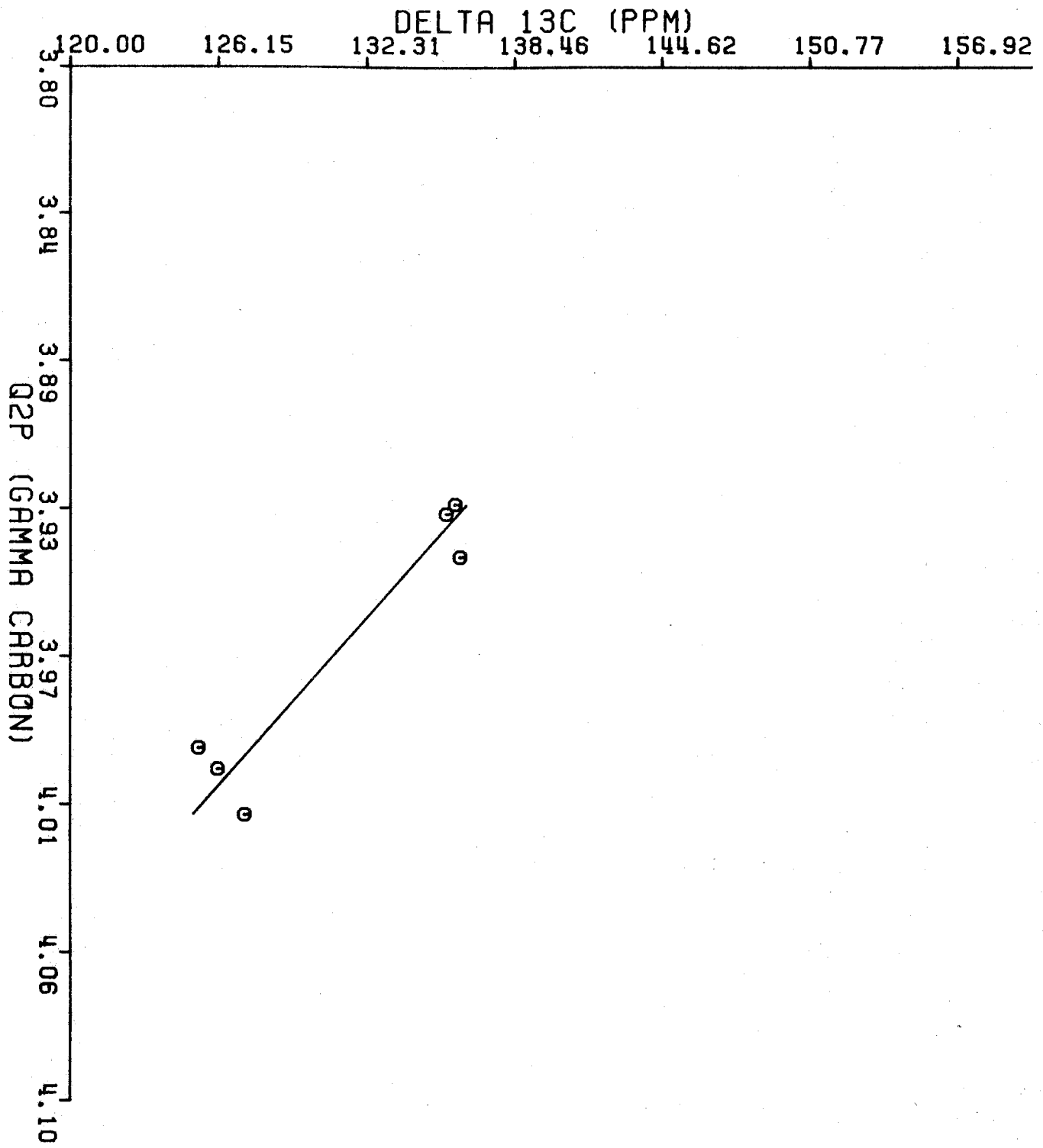

CHEMICAL SHIFT VERSUS CHARGE DENSITY (GAMMA)

Figure 43. Plot of ^{13}C chemical shift of carbon directly bonded to methyl, C-Methyl, versus calculated valence electron densities. The solid line is represented by $\delta = a + b\ Q_{2p}$, where $a = 6.65 \times 10^2$ (S.D. = 1.57×10^2), $b = -1.32 \times 10^2$ (S.D. = 3.98×10^1). Coefficient of correlation, ρ, = -0.8299.

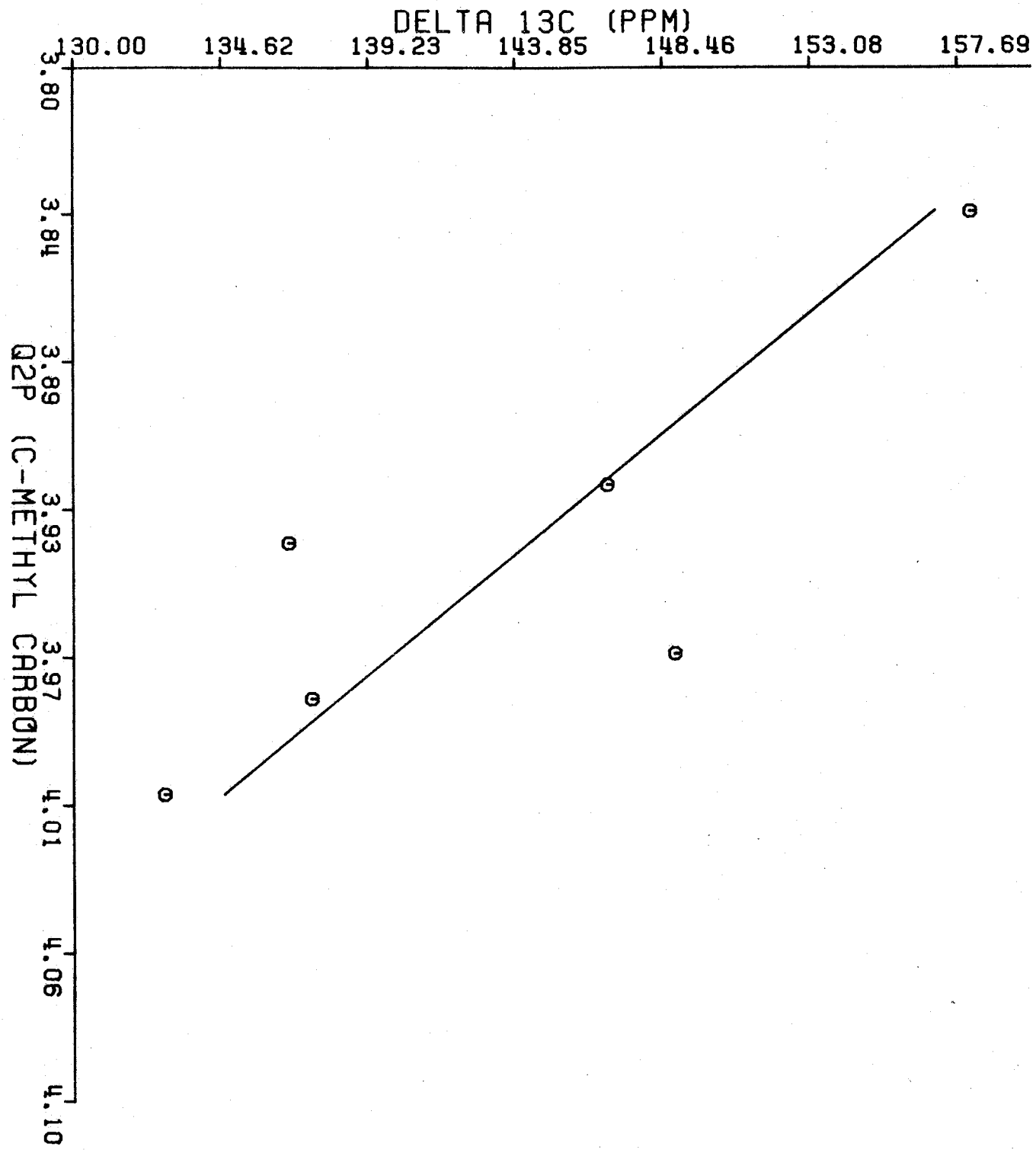

CHEMICAL SHIFT VERSUS CHARGE DENSITY (C-METHYL)

Figure 44. Plot of ^{13}C chemical shift of Methyl carbon versus calculated valence electron densities, Q_{2p}. The solid line is represented by $\delta = a + b\ Q_{2p}$, where $a = -5.89 \times 10^{2}$ (S.D. $= 1.39 \times 10^{2}$), $b = 1.54 \times 10^{2}$ (S.D. $= 3.53 \times 10^{1}$). Coefficient of correlation, ρ, = 0.8901.

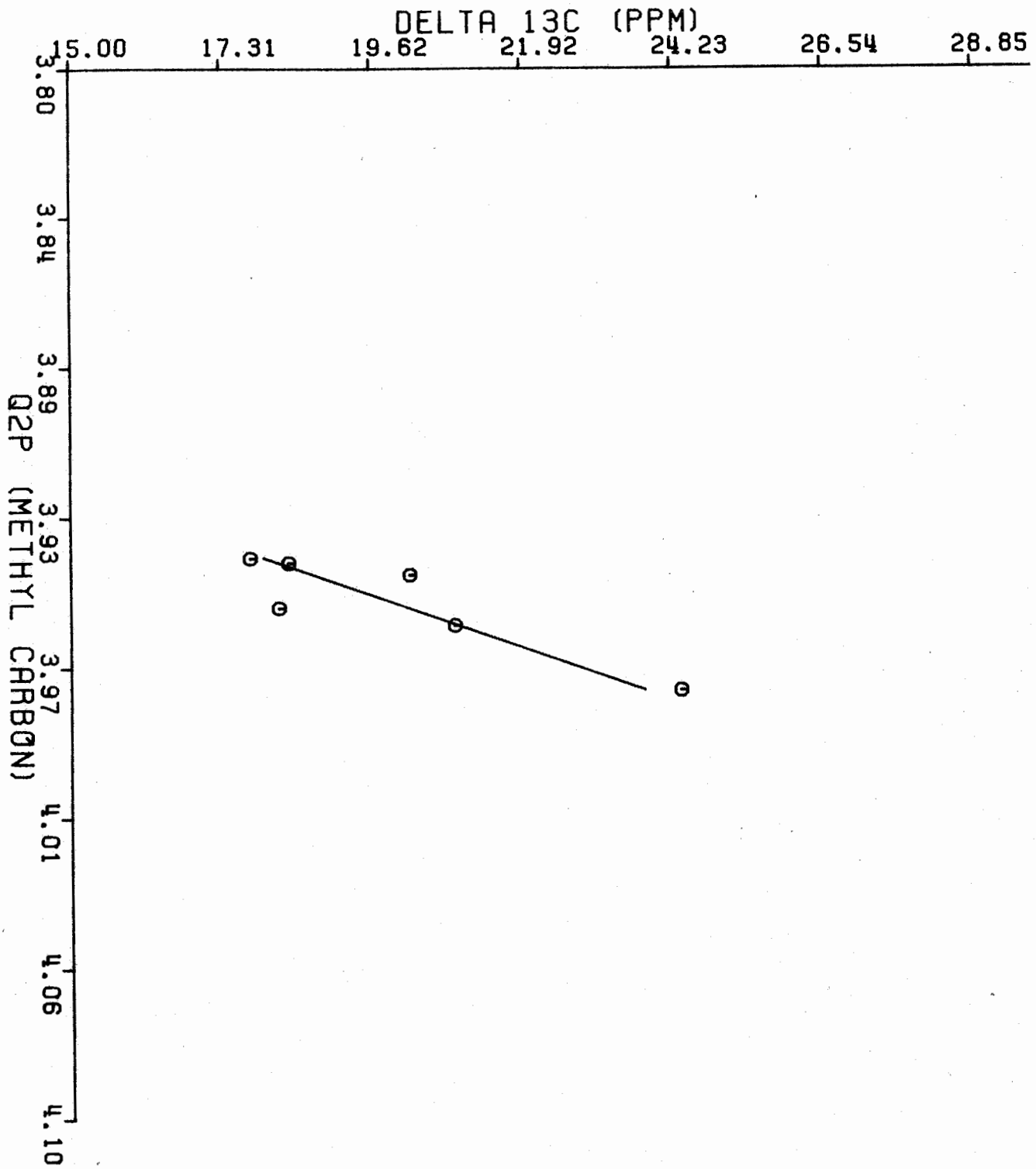

CHEMICAL SHIFT VERSUS CHARGE DENSITY (METHYL)

to the aromatic versus aliphatic distinction, the mechanism operating through a delocalized ring current [113].

In conclusion, this given scheme of classification is seen to be quite fruitful. Since linear interpolation is seen to give up to 97% of the differential chemical shifts in terms of the electronic changes, a predictive or interpretive method might be based on the "calibration" of the shift versus the charge. For the ^{13}C chemical shift of a given carbon in a given molecule, this calibration would entail the examination of the shifts of the corresponding carbon in derivative compounds in which nearest neighbors are not changed. Molecular orbital calculation would provide the densities. A favourable distribution of values would allow linear interpolation on the regression line. Two achievements could then be attained: (1) to interpret or assign a given resonance or to predict a priori and (2) since calculated densities are often based on ill-determined geometries, a given geometry could be tested according to the agreement provided.

8.3

The Conformational Manifold of Oxolane and Derivatives and the "Supermolecule" Problem

Molecular geometries are usually described in terms of spherical polar coordinates. Given three atoms, 1, 2, and 3, the position of a fourth is determined by constructing a coordinate system on 3, so that bond 2-3 is in the polar direction and the plane of 1, 2, 3 defines the zeroth meridian on the same side as 1. The bond to 4 is then defined by its distance and its azimuthal angle, known as the bond angle, and the polar angle, called the torsion or dihedral angle. Since the bond distance relates atoms which are bonded, since the bond angle relates non-bonded atoms separated by one atom, and since the torsion angle relates atoms separated by two atoms, the force constants can be placed in order of strength. The force constant for torsional distortions is so low that, at ordinary temperatures, a number of different conformations may be assumed by non-rigid molecules.

Ring closure of an acyclic molecule involves the loss of three degrees of freedom. In the furanoses, the five torsion angles are coupled and have only two degrees of freedom. The torsion angles, θ_j, may be related to pseudorotational coordinates which more adequately describe the continuous deformations of the molecule [114,115,116], i.e.

(129) $$\theta_j = \theta_m \cos (P + j\delta),$$

where $j = 0, 1, 2, 3, 4$ and $\delta = 144^{\circ}$.

The amplitude, θ_m, gives the degree of puckering or deviation from a planar structure. The phase angle, P, determines, for the various envelope or twist structures, which atoms are up and which are down with respect to an

average plane.

Large excursions of θ_m will lead to non-bonded interactions and increases in the electronic energy. Thus the electronic energy plotted for θ_m has the form of a trough. The phase angle P is a cyclic parameter, identical conformations occuring every 360° and conformations with inverted amplitude occuring every 180°. The shape of the electronic energy curve as a function of P may be such as to give preference to certain conformations [116,114,117]. Self-consistent field molecular orbital calculations have been used to elucidate the shape of the electronic energy surface over the conformational manifold of some five-member rings [118,119].

For the purposes of this study, the MINDO/3 molecular orbital program [120] was implemented in order to obtain approximate SCF-LCAO-MO ground state electronic energies for variations in geometry. Only the valence electrons are considered in the MINDO/3 approximation. MINDO/3 incorporates a DFP (see page 40) routine for the optimization of the calculated energy with respect to variations of the bond angle, bond lengths, and torsion angles. Optimization occurs at local minimum and, since there may be several local minima, only a thorough grid search of the parameter space can ensure that the global minimum has been found.

Since the program consumes a prodigious amount of CPU time and since the output of intermediate results during the course of the DFP minimization of the energy allows some insight into the energy surface in the absence of a thorough grid search, the program was implemented in a manner shown in Figure 45. In an interactive environment during the day, only 10 minute sequences of CPU time are available. Figure 45 shows how timing information from TIMEXP is relayed to the main program. When insufficient time for the next step is detected, the program creates the various output files. Also, if a fatal

Figure 45. Flow diagram to represent interactive operation of MINDO/3 molecular orbital program as implemented on IBM 370/155.

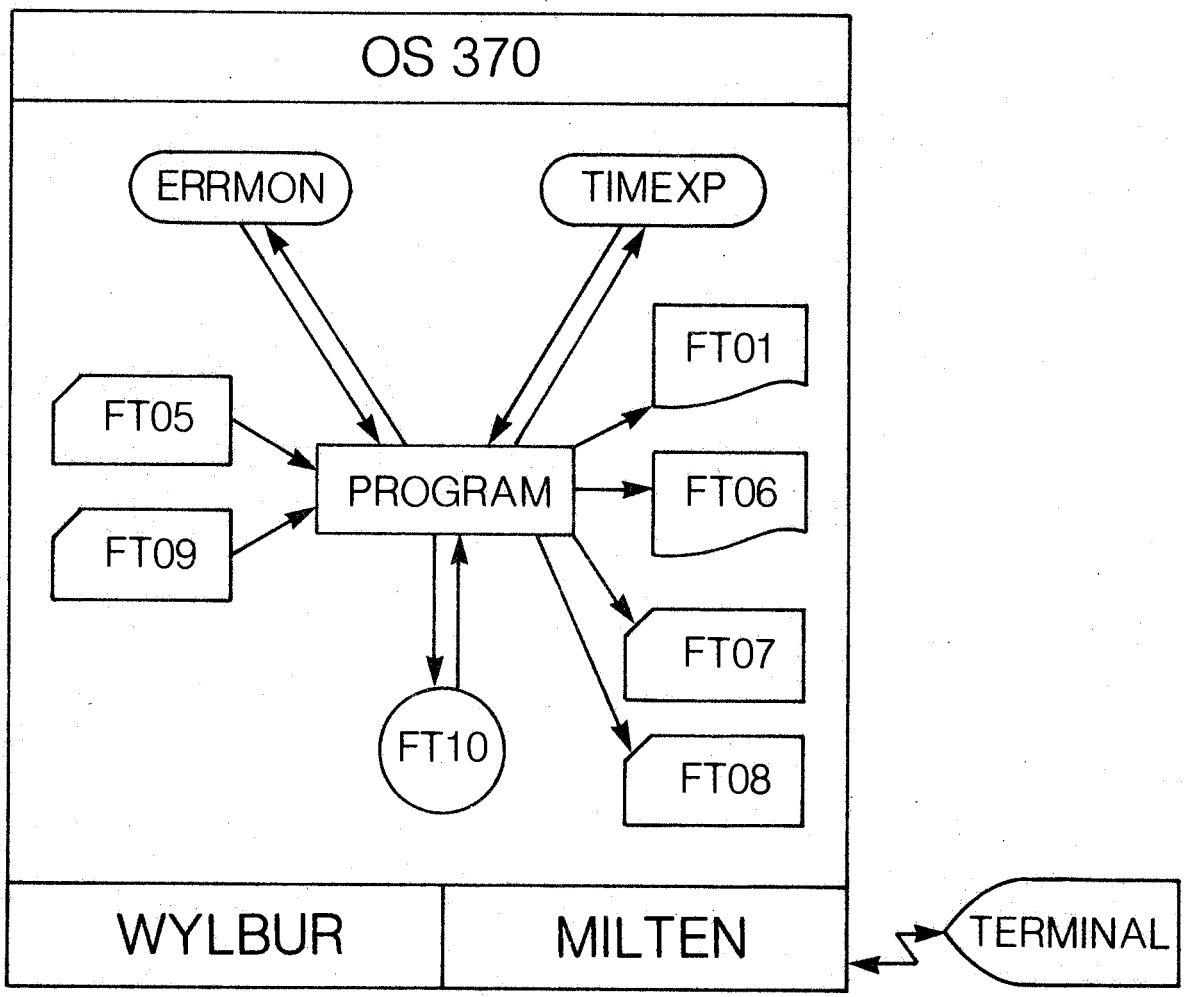
OS 370
ERRMON
TIMEXP
FT01
FT05
PROGRAM
FT06
FT09
FT07
FT10
FT08
WYLBUR
MILTEN
TERMINAL

execution time error is detected by ERRMON, the program does not "crash", instead the output files are created.

FT05 is the card input or input data file. FT09 is the geometry and orbitals information saved if the program is terminated by TIMEXP. FT01 gives a record of the progress of the DFP routine. FT06 outputs the energies, occupancy matrix, and geometry. FT07 gives the final cartesian geometry. FT08 is a save file for the geometry and orbital information. FT10 is a temporary disk file for storage of various matrix elements of the MO calculation. The program implemented in this fashion is executed in an interactive fashion. Commands are entered at a terminal to the WYLBUR/MILTEN system to set up the job. The job is then run under OS370. When a certain amount of CPU time has elapsed, the output files are created and these are examined with WYLBUR. FT08 is then assigned to FT09 for the continuation of the problem. The total CPU time required for the "optimization" of the geometry of tetrahydrofuran is of the order of 15-20 minutes, the time required for its 3,4-diol is 30 minutes.

TABLE XVIII shows the results of the MINDO/3 calculations for tetrahydrofuran. Constraints were put on the values of the torsion angles and the optimized geometries gave the pseudorotational parameters shown in the table. The symbolism for the conformations is that used in references [114,117]. Because of symmetry the envelope conformation V_o is the same as ^oV, and the twist conformations $^3T_2$ and $^2T_3$ are the same.

MINDO/3 gives energies as heats of formation, ΔH_f. TABLE XVIII indicates that the most stable structure is the pure planar form. A sharp debate has occured over the ability of MINDO/3 to calculate reliable equilibrium geometries of cyclic molecules [121-125]. The tendency of MINDO/3 to incorrectly favour energetically the planar conformation has been noted by other authors [121].

TABLE XIX shows the results of MINDO/3 calculations for cis- and trans-

TABLE XVIII

MINDO/3 calculations for tetrahydrofuran.

P, ^{o}	18. (V_o)			108. ($^3T_2$)		
	Θ_m, ^{o}	ΔH_f (kcal/mole)	Dipole moment (Debye)	Θ_m, ^{o}	ΔH_f (kcal/mole)	Dipole moment (Debye)
	0.935	-55.624	1.7878	3.806	-59.424	1.6514
	0.022	-60.8858	1.7571	1.324	-61.230	1.8003
	0.0189	-61.23921	1.8023	0.048	-61.23904	1.8034
	0.0063	-61.23925	1.8024	0.0226	-61.23874	1.8027
	0.0	-61.23923	1.8029	0.0	-61.23923	1.8029

TABLE XIX

MINDO/3 calculations for cis- and trans-oxolane 3,4-diol

Structure	cis - diol		trans - diol		
	V_o	V_o	^oV	$^2T_3$	V_3
Θ_o, °	3.820	10.0	-0.331	1.499	2.664
Θ_1, °	-3.922	-9.840	0.318	1.499	0.665
P, °	20.3	16.58	194.47	288.00	299.04
Θ_m, °	4.07	10.43	0.342	4.85	5.49
ΔH_f (kcal/mole)	-139.38	-141.79	-142.71	-111.42	-111.49
Dipole moment (Debye)	1.9602	1.9765	0.5713	0.0766	0.0964
electron densities C(1)	3.6851	3.6881	3.6864	3.7191	3.7188
electron densities C(2)	3.7333	3.7325	3.7192	3.7280	3.7279

oxolane 3,4-diol. θ_0 and θ_1 are the torsion angles about the ether oxygen. The conformations calculated for the cis-diol appear to be reasonable. ^3V has the ether oxygen moved away from the hydroxyls. The most stable cis form with ΔH_f = -141.79 Kcal has a puckering amplitude of 10.43^o, which is a significant departure from planarity. Symmetry relates ^3V to ^4V.

The ^oV conformation is calculated to be the most stable trans-diol, and its greater stability than that of the cis-diol is consistent with a greater O-O distance. The calculated V_3 and $^2T_3$ conformations have energies which appear to be on another potential energy surface. Anomalous energy minima given by MINDO/3 have been observed elsewhere [122] and have been related to level crossings which are not substantiated by full ab initio calculations. The most stable calculated conformation, ^oV, is seen to be almost planar, where θ_m = 0.342. This could be reasonable for the trans-diol since puckering would tend to move one of the two hydroxyls toward the ether oxygen. The $^2T_3$ conformation has the hydroxyl on the second and third carbon moved toward the equatorial direction. Symmetry relates V_0 to ^0V and V_3 to ^2V.

The numbering system used in TABLES XVIII and XIX is oxygen = 0, carbons sequential from 1 to 4. The pseudorotation values were calculated from the torsion angles about the ether oxygen by solving equation (129).

TABLE XIX also shows the calculated valence electron densities of the carbons. These might be of value in relating chemical shift values to conformations. Analysis of ^{13}C NMR results in this study showed, however, that conformational effects need not be invoked (page 75). The predominant effects are polar effects due to ligands.

Ideally, the best approach to rationalizing ^{13}C NMR chemical shifts

observed when known ligands participate is to employ MO calculations for a "supermolecule" in which the molecule and its ligand are brought together in a non-bonding interaction. The approach of this sort [126] was applied recently in the ^{13}C study of conformation changes of 2,3-naphtho-20-crown-6 caused by crown ether complexing cations. The chemical shifts observed in the naphthalene ring were related to the charge densities calculated by the semi-empirical INDO [127] MO program. Perturbing monopoles of charge +1 and +2 were modelled by placing "Li" and "Be" ions in the correct spatial relationship to the naphthalene system. A linear correlation coefficient $\rho = -0.943$ and a slope of -99 ppm/electron were obtained. Thus the calibration of the shift versus the charge is reasonably extended to the supermolecule MO calculation. The geometry of the complex had best be known, however. In the absence of, say, X-ray crystallographic structural knowledge of the complex, a geometric determination might be calculated using a DFP optimized equilibrium geometry for the complex.

Recently, a potential energy surface calculated for the ammonia-carbon dioxide complex was reported [128]. Optimized complex geometries and force constraints were calculated in an ab initio SCF scheme and were found to differ significantly from values obtained from the infrared spectrum of the Ar matrix-isolated complex.

The discrepancy was explained in terms of the superposition error. When the complex-forming molecules are brought together, their basis sets overlap. This leads to improvements in the descriptions of the individual molecules. The energy of complex formation is thus overestimated because of the superposition error for finite basis sets. Thus, one more known deficiency is added in an application of MINDO/3 to the "supermolecule" problem.

9. CONCLUSION

9.1 Thermodynamics

The present study was undertaken in order to demonstrate and elucidate that the complex formed between 1,4-anhydroerythritol and the ligands, water, and/or ammonium is a structure-forming effect in biochemical systems where ribonucleotides carry the essential moiety of the sugar and proteins carry the ammonium cation. It was necessary to consider the solvent isotope effect between light and heavy water [19] and the solvent isotope effect for ionic hydration [20], since the ^{13}C data was, by necessity, obtained using D_2O as aqueous solvent. D_2O was used as solvent since we required an internal deuterium field-frequency lock.

Thermodynamic data used to calculate the activities of water and ammonium at various concentrations and temperature was that for aqueous H_2O solutions. The calculated free energies for the formation of the various complex species apply only to aqueous D_2O solutions.

The solvent isotope effect between light and heavy water governs the thermodynamic differences between light and heavy water. The solvent isotope effect for ionic hydration governs changes in ionic activities observed for an ion which is transferred from H_2O to D_2O. Both of these effects can be neglected when considering the use of H_2O solutions data for the treatment of D_2O solutions experiments because in this study the ^{13}C data was properly reproduced in TABLE VII, which gives the predictions of Model A of TABLE VI. If these two effects were significant, the calculated thermodynamic functions would be so altered as to prevent a good fit. However, because D_2O is a common NMR solvent, more study is needed of the thermodynamic properties of this solvent and its electrolyte solutions.

Next, I have related the calculated free energy values to the H_2O system. The free energies for transfer of solvent and solute from D_2O to H_2O are known [129,130]. The free energy difference between heavy and light water is found in TABLE II, ΔG = 4.3 kcal/mole. This value was calculated from contributions from translations, vibrations and librations and was compared with the experimental value. The measured standard free energy of transfer of ammonium from D_2O to H_2O, ΔG = .164 kcal/mole, is from reference [130]. The free energies from transfer of 1,4-anhydro-erythritol in its fixed ligation states was assumed to be zero because hydration in the inner ligation sphere is defined and the outer hydration sphere is not susceptible to the ionic isotope effect for hydration, which is a microscopic effect. The outer hydration sphere is affected by macroscopic properties which change with different solvents for example, the dielectric constant. At 25°C, however, the dielectric constant of D_2O is 78.06 and that of H_2O is 78.54.

Thus, a Born-Haber cycle for the free energies at 25°C was constructed :

$$
\begin{array}{lll}
E_{(D_2O)} + D_2O_{\ell} \rightarrow E{\cdot}D_2O_{(D_2O)} & \Delta G = .35 \text{ kcal} \\
\downarrow \qquad\qquad \downarrow 4.3 \qquad\quad \downarrow & \qquad (130) \\
E_{(H_2O)} + H_2O_{\ell} \rightarrow E{\cdot}H_2O_{(H_2O)} & \Delta G = -3.95 \text{ kcal}
\end{array}
$$

$$
\begin{array}{lll}
E_{(D_2O} + ND_4^+{}_{(D_2O)} \rightarrow E{\cdot}ND_4^+{}_{(D_2O)} & \Delta G = 1.3 \text{ kcal} \\
\downarrow \qquad\qquad \downarrow -.164 \qquad\quad \downarrow & \qquad (131) \\
E_{(H_2O)} + NH_4^+{}_{(H_2O)} \rightarrow E{\cdot}NH_4^+{}_{(H_2O)} & \Delta G = 1.5 \text{ kcal}
\end{array}
$$

$$E_{(D_2O)} + ND_4^+{}_{(D_2O)} + D_2O_\ell \rightarrow E\cdot ND_4^+\cdot D_2O_{(D_2O)} \qquad \Delta G = 3.3 \text{ kcal}$$

(132) $\downarrow \qquad \downarrow -.164 \qquad \downarrow 4.3 \qquad \downarrow$

$$E_{(H_2O)} + NH_4^+{}_{(H_2O)} + H_2O_\ell \rightarrow E\cdot NH_4^+\cdot H_2O_{(H_2O)} \qquad \Delta G = -.84 \text{ kcal}$$

$$E_{(D_2O)} + 2D_2O_\ell \rightarrow E\cdot 2D_2O_{(D_2O)} \qquad \Delta G = 3.4 \text{ kcal}$$

(133) $\downarrow \qquad \downarrow 2\times 4.3 \qquad \downarrow$

$$E_{(H_2O)} + 2H_2O_\ell \rightarrow E\cdot 2H_2O_{(H_2O)} \qquad \Delta G = -5.2 \text{ kcal}$$

These derived values could be verified by doing experiments with a mixed H_2O/D_2O system and extrapolating to 100% H_2O, and such experiments should take precedence if further studies of this system are undertaken.

Thus it is seen that in D_2O, where the molecules have a greater structure-forming tendency, the extent of hydration is less than in H_2O. Also, the relative thermodynamic stabilities are altered in H_2O. In D_2O, in order of decreasing thermodynamic stability, the complexes are

$$E > E\cdot H_2O > E\cdot NH_4^+ > E\cdot NH_4^+\cdot H_2O > E\cdot 2H_2O \quad ,$$

while in H_2O

$$E\cdot 2H_2O > E\cdot H_2O > E\cdot NH_4^+\cdot H_2O > E > E\cdot NH_4^+ \quad .$$

An H_2O/D_2O study would verify this reordering of the stabilities.

9.2 ^{13}C Chemical Shifts

The thermodynamics appears to be more clear-cut than the ^{13}C NMR chemical shifts. Figure 46 is a representation of the C(1) and C(2) shifts relative to dioxane, given with idealizations of the topologies of the substrate-ligand complexes. Although only polar effects may be operating, rationalization of the shifts is not possible in the absence of defined geometries. Further studies are necessary in order to obtain valid structural information so that the ^{13}C NMR chemical shifts of these species may be understood.

The molecular orbital studies given in Sections 8.2 and 8.3 preceded the ^{13}C NMR studies given in Section 6.0. A noteworthy conclusion of this work is that theoretical studies may often fail to anticipate critically important results revealed by experiment (see quotation, page vi). The work wherein calculated charge densities were correlated with ^{13}C chemical shifts for the pyridine derivaties, Section 8.2, demonstrates that, underneath the gross electronic structural features which partly explain observed ^{13}C chemical shifts, there lie finer features. Thus, an attempt to explain observed phenomena in terms of the simplest possible theory is bound to ignore potentially important effects.

9.3 Proposals

A number of spectrometric methods are available for the study of aqueous equilibria discussed in this work. For these weak association complexes only techniques providing the highest resolution and sensitivity will be discussed.

Figure 46. Ligand substrate topologies and ^{13}C chemical shifts of 1,4-anhydroerythritol and species coordinated with water and ammonium.

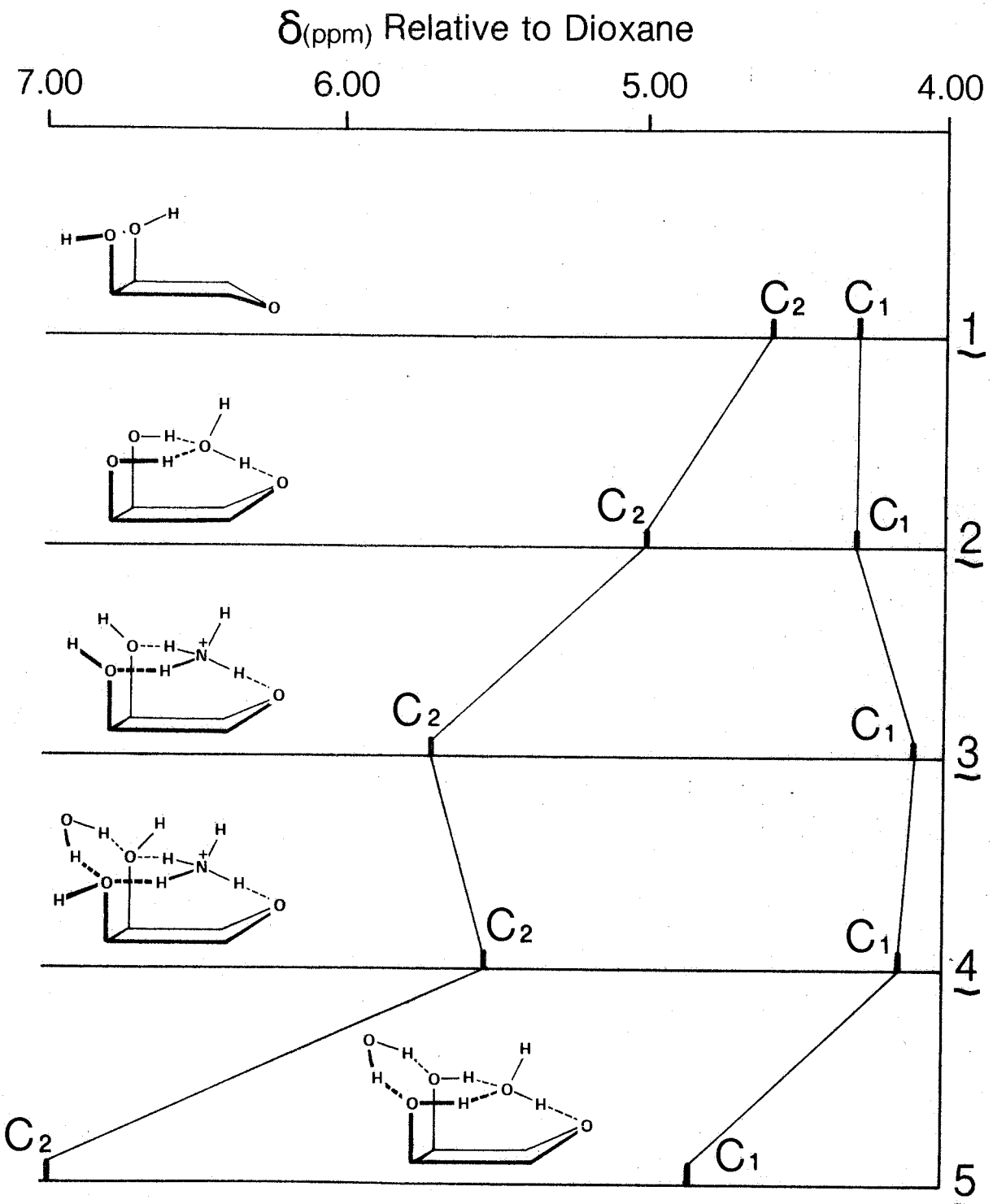
δ(ppm) Relative to Dioxane
7.00
6.00
5.00
4.00
C2
C1
1
2
3
4
5

Among the NMR techniques based on the magnetic nuclei of the reporter species, say 1,4-anhydroerythritol, double Fourier transformation, 2DFT[134], has been shown to give exceptional resolution. Experimentally, a linewidth of 0.08 Hz has been achieved on a spectrometer where the field inhomogeneity broadening is about 0.3 Hz for ^{13}C. 2DFT, J spectroscopy has been applied to proton-proton and carbon-proton spin coupling. Thus chemical shift information and coupling constants could be combined in an observed vector ($\delta^{i}_{^{13}C}$; $\delta^{j}_{^{1}H}$; $J_{C_iH_j}$; $J_{HH'}$) for a general least squares treatment of the kind illustrated in Chapter 6. The additional information provided would be the carbon and proton chemical shifts and coupling constants which would facilitate conformational analysis of species which cannot be isolated.

Other magnetic nuclei may be used, including ^{14}N (I=1), ^{15}N (I=½), and ^{17}O (I= 5/2) in an isotopically enriched substrate. Quadrupolar line broadening has its origin in the relaxation process involving the interaction of the quadrupole nucleus with the electric field gradients within the molecule. If the nucleus is surrounded by a highly symmetrical arrangement of substituents, such electric field gradients are small and quadrupolar line broadening is diminished. Thus NMR study of the exchange of $^{14}NH_4^+$ between the symmetrical water lattice and the unsymmetrical site on the sugar would give information on the dynamics of the process. NO_3^- could be used as a reference [135,136]. Similar information could be provided from the ^{17}O relaxation study of the sugar using H_2O as a reference [135,136]. Chemical shift information from a study with enriched $^{15}NH_4^+$ could be used in a Benesi-Hildebrand type treatment of the ammonium sugar complex.

Two infrared techniques are worth considering for application to this type of problem, laser Raman and Fourier transform spectroscopy.

Water is an excellent solvent for Raman spectroscopy since it scatters very weakly [137]. With moderately concentrated solutions, it is often possible to obtain spectra up to 3100 cm^{-1} which show no significant solvent background. With relatively little care in sample preparation, aqueous solution spectra can be obtained down to 150 cm^{-1}. With pure liquids, Raman line very close to the exciting frequency can be observed. Internal standards can be used where it is desirable to report intensities independent of instrumental effects. The perchlorate line at ca. 930 cm^{-1} arising from the totally symmetric breathing mode of ClO_4^- is most often used for work involving aqueous solutions because it forms no complexes in solution. Equilibrium studies may make use of intensity measurements because the Raman intensities are directly proportional to the molar concentrations.

The Raman spectra of pure water and of water in aqueous solutions provides information on the hydrogen bond-induced structure in the liquid. The broad bands centered at 175 cm^{-1}, 450 cm^{-1}, and 780 cm^{-1} are due to hydrogen bond stretching and libration and are effected by intermolecular interactions. With careful work the librations of the association complexes themselves may be seen very close to the exciting frequency. The number of lines observed for the association complexes of the sugar would give direct confirmation of the complexes proposed in this work. The observation of rotation structure rather than a broad featureless continuim in the low frequency region would prove the existence of relatively stable molecular aggregates. The thermodynamic stability of association complexes would be tested by temperature control work.

In the last decade IR FTS has gained some prominence [138]. Commercial instruments are available which provide a resolution of 0.067 cm^{-1} in the transmission mode. Aqueous spectra may be obtained by signal

averaging the Michelson interferogram in double precision and digitally subtracting the spectrum of pure water. The substitution of D_2O for H_2O may also provide additional windows free from H_2O absorbances.

The pseudorotational ring puckering mode of tetrahydrofuran was first observed using IR FTS [139]. Another vibrational mode that has been profitably studied using IR FTS is the OH torsional mode of alcohols. These two vibrational modes are features that are expected to be influenced by sugar ligand interactions and so should be studied by IR FTS.

Ordinary optical absorption spectrophotometry is severely limited in its resolution about an absorption bond. Circular dichroism or optical rotatory disperson provide inherently greater resolution because of the possibility that the CD or ORD spectrum may be positive or negative [140]. Thus overlapping absorption bands in the absorption spectrum of a molecule may be resolved with either CD or ORD. The phenomena of CD and ORD are different manifestations of the same underlying behaviour and are linked by the Kronig-Kramer relations. Since outside of the region of the absorption band the ORD is given by the Drude equation, it is sufficient to focus attention on CD as the most sensitive probe of perturbations to the electronic state. Even achiral molecules exhibit rotary behaviour in a magentic field, so MCD may be considered the most general technique.

A proposal for the optical study of the perturbation of electronic states caused by molecular associations of the type presented in this study would be based on adenosine, which presents a natural chirality and a chromophore, λ_{max} = 260 nm. The origin of the optical activity must be caused by the perturbation of the base by the asymmetric field of the sugar. The sign and magnitude of the near Cotton must be governed by the orientation of the base relative to the sugar and the conformation of the sugar. Thus, torsional and conformational changes may be probed using

CD. Theoretical predictions of CD and MCD effects given by MO calculation would give detailed insight into the effect of ligands on the orbitals.

Finally, a recent technique, extended X-ray absorption fine structure (EXAFS), has been applied to the accurate determination of interatomic distances, atomic types and coordination numbers of complexes in solution [141,142,143]. Carbon and nitrogen display absorption K edges at 43.648 and 30.990 Å respectively [70]. Since a $NaClO_4$ crystalline complex of 1,4-anhydroerythritol has been obtained [5], a NH_4ClO_4 complex might also be crystallized. X-ray diffraction then would provide interatomic distances that could be used for the calibration of the radial distribution functions provided by EXAFS based on the nitrogen K edge of ammonium and the carbon K edge of the sugar. This would solve the problems presented by a disordered system of a complex in equilibrium in solution.

APPENDIX I

This FORTRAN program is described in pages 122-125. External subroutine calls to IMSL routines for spline operations are included. Figure 38 shows the flowchart for the program and correspondence with the blocks shown there is obtained by using the correspondence numbers in the left-most column. The data, as described in pages 108-117, is given at the end where (16) is apparent molal heat capacity, (17) is relative apparent molal heat content, (18) is activity coefficients, (19) is vapour pressure data, and (20) is concentration and temperatures of experimental conditions, as described on page 75, second paragraph. The program output is shown in TABLE XIV.

APPENDIX I

```
//DGN514DS JOB (0508,G3966),'NAUGLER',MSGLEVEL=(1,1),MSGCLASS=R
/*JOBPARM  PSWD=NGD
//STEP2 EXEC FORTGCG
      DIMENSION X1(100),X2(100),X3(100),X4(100),Y1(100),Y2(100),Y3(100),
     .          Y4(100),BPAR(4),C1(99,3),C2(99,3),C3(99,3),CX(100),
     .          ACT(100),ACTM(100),TY(100),F(20,20),FL(20,20),AW(100),
     .          S1(100),S2(100),S3(100),FM(4),XX4(100)
      COMMON WK(714)
      DATA BPAR /0.,0.,0.,0./
      R=1.98717
C     READ IN  APPARENT MOLAL HEAT CAPACITY
      READ (5,101) NX1
      READ (5,100) (X1(I),Y1(I),I=1,NX1)
      READ (5,100) DFIN1,SM1
C     READ IN RELATIVE APPARENT MOLAL HEAT CONTENT
      READ (5,101) NX2
      READ (5,100) (X2(I),Y2(I),I=1,NX2)
      READ (5,100) DFIN2,SM2
C     READ IN ACTIVITY COEFFICIENTS
      READ (5,101) NX3
(1)   READ (5,100) (X3(I),Y3(I),I=1,NX3)
C     READ IN VAPOR PRESSURE DATA FOR WATER
      READ (5,101) IX
      READ (5,100) (CX(I),I=1,IX)
      READ (5,101) IY
      READ (5,100) (TY(I),I=1,IY)
      READ (5,103) (FM(I),I=1,4)
      READ (5, FM)((F(I,J),I=1,IX),J=1,IY)
C     READ IN CONCENTRATIONS AND TEMPURATURES
      READ (5,101) NX4
      READ (5,100) (X4(I),Y4(I),I=1,NX4)
(2)   CALL DIFORM(X1,Y1,NX1,DFIN1,SM1,Y1,C1)
(3)   CALL DIFORM(X2,Y2,NX2,DFIN2,SM2,Y2,C2)
(4)   CALL ICSICU(X3,Y3,NX3,BPAR,C3,99,IER)
(5)   CALL IBCIEU(F,20,CX,IX,TY,IY,0.,1,25.,1,FL,20,WK,IER)
      V25=FL(1,1)
(6)   DO 10 I=1,NX4
   10 XX4(I)=SQRT(X4(I))
```

```
      CALL ICSEVU(X1,Y1,NX1,C1,99,XX4,S1,NX4,IER)
(7)   CALL ICSEVU(X2,Y2,NX2,C2,99,XX4,S2,NX4,IER)
      CALL ICSEVU(X3,Y3,NX3,C3,99,XX4,S3,NX4,IER)
      DO 20 I=1,NX4
      T=Y4(I)+273.1
      XX=(298.1-T)/(R*298.1*T)
(8)   A=ALOG(S3(I))+(S2(I)*XX-S1(I)*(298.1*XX-ALOG(298.1/T)/R))*0.5
      ACT(I)=EXP(A)
      CALL IBCIEU(F,20,CX,IX,TY,IY,X4(I),1,Y4(I),1,FL,20,WK,IER)
      AW(I)=FL(1,1)/V25
   20 ACTM(I)=X4(I)*ACT(I)
      WRITE (6,102) (X4(I),Y4(I),ACT(I),ACTM(I),AW(I),I=1,NX4)
  100 FORMAT (10F8.4)
  101 FORMAT (I4)
  102 FORMAT (5F12.6)
  103 FORMAT(4A4)
      STOP
      END
      SUBROUTINE DIFORM(X,Y,NX,DFIN,SM,YY1,C)
      DIMENSION X(1),Y(1),YY1(1),C(99,3),DF(100),Y1(100),C1(99,3),
     .          DS(100),YY(100),XX(100)
(9)   COMMON WK(714)
      DO 19 I=1,NX
(10)  XX(I)=SQRT(X(I))
   19 DF(I)=DFIN
      CALL ICSSCU(XX,Y,DF,NX,SM,Y1,C1,99,WK,IER)
(11)  CALL DCSEVU(XX,Y1,NX,C1,99,XX,DS,NX,DDS,0,IER)
      CALL ICSEVU(XX,Y1,NX,C1,99,XX(NX),Y1(NX),1,IER)
      DO 20 I=1,NX
(12)  20 YY(I)=Y1(I)+XX(I)*DS(I)*0.5
      DO 21 I=1,NX
(13)  21 DF(I)=DFIN*(1.+X(I))
(14)  CALL ICSSCU(XX,YY,DF,NX,SM,YY1,C,99,WK,IER)
      Y0=YY1(1)
(15)  YY1(NX)=YY(NX)
      DO 22 I=1,NX
   22 YY1(I)=YY1(I)-Y0
      RETURN
      END
//GO.SYSIN DD *
```

```
                36
(16)  .00      -13.5   .000555  -13.4   .00111   -13.3   .00278   -13.2   .00555   -13.1
      .00793   -13.0   .01110   -12.9   .01388   -12.8   .01850   -12.7   .02775   -12.6
      .03700   -12.4   .05551   -12.1   .0617    -12.0   .0694    -11.9   .0793    -11.8
      .0925    -11.7   .1110    -11.6   .1388    -11.3   .1850    -11.0   .2775    -10.3
      .3700    -9.7    .5551    -8.7    .7401    -7.8    1.1101   -6.2    1.3877   -5.3
      1.8502   -3.9    2.202    -2.9    2.7753   -1.6    3.7004   +0.3    4.6255   1.9
      5.5506   3.4     5.8427   3.8     6.1674   4.3     6.5301   4.8     6.9383   5.3
      7.4008   6.0
      0.03     43.0
                52
      .00      0.      .000111  5.      .000555  10.     .00111   14.     .00278   22.
      .00555   29.     .00793   34.     .01110   40.     .01388   44.     .01850   48.
      .02775   57.     .037700  63.     .05000   70.     .05551   73.     .0617    76.
      .0694    79.     .0793    82.     .0925    87.     .1000    88.     .1110    92.
(17)  .1388    98.     .1850    105.    .2000    107.    .2775    117.    .3700    124.
      .5000    131.    .5551    133.    .7401    136.    1.000    136.    1.1101   136.
      1.3877   134.    1.500    133.    1.8502   128.    2.000    125.    2.2202   120.
      2.5000   114.    2.7753   108.    3.0000   104.    3.500    93.     3.7004   89.
      4.000    82.     4.5000   72.     4.6255   69.     5.000    62.     5.5506   53.
      5.8427   48.     6.0000   45.     6.1674   42.     6.5301   36.     6.9383   30.
      7.0000   29.     7.4      23.
      0.30     62.0
                27
      0.0      1.0     0.1      0.770   0.2      0.718   0.3      0.687   0.4      0.665
      0.5      0.649   0.6      0.636   0.7      0.625   0.8      0.617   0.9      0.609
(18)  1.0      0.603   1.2      0.592   1.4      0.584   1.6      0.578   1.8      0.574
      2.0      0.570   2.5      0.564   3.0      0.561   3.5      0.560   4.0      0.560
      4.5      0.561   5.0      0.562   5.5      0.563   6.0      0.564   6.5      0.565
      7.0      0.566   7.399    0.566
                5
      0.0      1.87    3.739    5.609   7.478
                12
      0.       10.     20.      30.     40.      50.     60.      70.     80.      90.
      100.     110.
      (5F8.0)
      4.579    4.3     4.0      3.8     3.6
      9.210    8.6     8.1      7.6     7.1
(19)  17.539   16.4    15.5     14.1    13.5
      31.824   29.9    28.1     26.3    24.7
      55.324   51.9    48.9     45.8    42.9
      92.51    86.8    81.7     76.6    71.8
      149.38   140.2   132.0    123.6   116.0
      233.79   219.3   206.5    193.4   181.4
      355.47   333.5   314.0    294.1   275.9
      525.76   493.5   464.6    435.2   408.2
      760.00   713.0   671.2    628.7   589.8
      1071.5   1008.   949.     888.9   833.8
                39
      0.       2.      0.       11.     0.       11.     0.       28.     0.       30.
      0.       46.     0.       55.     0.       56.     0.       56.     0.       66.
      0.       69.     0.       78.     0.       80.     0.       97.     0.       100.
(20)  1.18     55.     1.18     19.     1.18     32.     1.18     51.     1.18     68.
      1.18     84.     1.18     65.     1.18     85.     1.18     101.    2.37     27.
      2.37     50.     2.37     74.     2.37     72.     2.37     90.     3.92     19.
      3.92     53.     3.92     74.     3.92     73.     5.44     30.     5.44     54.
      5.44     68.     5.44     82.     5.44     97.     7.34     40.
      /*
```

APPENDIX II

FORTRAN subprogram encoded for modelling complex equilibria as expressed by equation (74). In the argument list of the subroutine FUN, F is the calculated function value, D is the array of first partial derivatives, P is the parameter array, and X the array of independent variables, the data matrix. Decision table logic for the assignment of parameters and specification of stoichiometry is represented in arrays IJK and NP. With the table initiated with the values shown here, the 18-parameter Model A, of Table VI, is evaluated. This subprogram was incorporated in the LINKEDIT step when using BMDX85 [59] or BMDX85/NAUGLER under IBM OS, or in BMDP3R by concatenating data sets when operating under MTS.

```
      SUBROUTINE FUN(F,D,P,X)
      IMPLICIT REAL*8 (A-H,O-Z)
      DIMENSION D(1),P(1),X(1)
      DIMENSION B(3,3),E(3,3),S(3,3),DB(3,3),DE(3,3),
     . DS(3,3),DVS(3,3),DVE(3,3),DUB(3,3),DUS(3,3),DUE(3,3),
     . CU1(3,3,3),CU2(3,3,3),IJK(3,27),K(2),NP(2,2)
      EQUIVALENCE (DB(1,1),DUB(1,1),CU2(1,1,1)),(DE(1,1),DUE(1,1),
     . CU2(1,1,2)),(DS(1,1),DUS(1,1),CU2(1,1,3)),(CU1(1,1,1),B(1,1)),
     . (CU1(1,1,2),E(1,1)),(CU1(1,1,3),S(1,1))
      DATA CU1,R/18*0.0D0,9*-1.0D3,1.98717D0/
C
C*************************************************************************
C
C        P(L)=B(I,J) K=1,   D(L)=DB(I,J) K=1,
C            =E(I,J) K=2,       =DE(I,J) K=2,
C            =S(I,J) K=3        =DS(I,J) K=3
C
C        '(I,J)'='E.(I-1)H2O.(J-1).NH4+'
C
C*************************************************************************
C
C    L               I J K
C    *               * * *
      DATA  IJK/     0,0,0,   2,1,1,
     2               1,2,1,   2,2,1,   3,1,1,
     3               2,1,2,   1,2,2,
     4               2,2,2,   3,1,2,
     5               2,1,3,   1,2,3,
     6               2,2,3,   3,1,3,
     7               0,0,0,   2,1,1,
     8               1,2,1,   2,2,1,   3,1,1,   27*0/
      DATA  NP/1,13,6,18/
C
      IFV=5
      ITHR=3
      KAPPA=IDINT(X(IFV)+0.499999D0)
      NP1=NP(1,KAPPA)
      NP2=NP(2,KAPPA)
      NPL=MAX0(NP(1,1),NP(2,1),NP(1,2),NP(2,2))
      DO 1 I=NP1,NP2
      IF(IJK(3,I).GT.0) GOTO 100
      BO=P(I)
      GOTO 1
  100 CU1(IJK(1,I),IJK(2,I),IJK(3,I))=P(I)
    1 CONTINUE
C
C
      U=BO
      V=1.0D0
```

```
      RINV=1.0D0/R
      RT=(X(ITHR)+273.1D0)*R
      DO 2 I=1,3
      DO 3 J=1,3
      K(1)=I
      K(2)=J
      G=-E(I,J)/RT+S(I,J)/R
      IF(G .GT. 174.0D0) G=165.0D0
      IF(G .LT. -180.0D0) G=-180.0D0
      DUB(I,J) = DEXP(G)
C
      DO 11 L=1,2
      KK=K(L)
      GOTO (11,12,13),KK
 13   DUB(I,J) = DUB(I,J)*X(L)
 12   DUB(I,J) = DUB(I,J)*X(L)
 11   CONTINUE
C
      DVE(I,J) = -1.0D0/RT*DUB(I,J)
      DVS(I,J) = RINV*DUB(I,J)
      DUS(I,J) = DVS(I,J)*B(I,J)
      DUE(I,J) = DVE(I,J)*B(I,J)
      U        = U+DUB(I,J)*B(I,J)
      V        = V+DUB(I,J)
 3    CONTINUE
 2    CONTINUE
      F=U/V
      DZ=1.0D0/V
      V2=V**2
      DO 4 I=1,3
      DO 5 J=1,3
      DB(I,J) = DUB(I,J)/V
      DE(I,J) = (DUE(I,J)*V-DVE(I,J)*U)/V2
      DS(I,J) = (DUS(I,J)*V-DVS(I,J)*U)/V2
 5    CONTINUE
 4    CONTINUE
C
C
      DO 50 I=1,NPL
 50   D(I)=0.0D0
      DO 6 I=NP1,NP2
      IF(IJK(3,I).GT.0) GOTO 60
      D(I)=DZ
      GOTO 6
 60   D(I)=CU2(IJK(1,I),IJK(2,I),IJK(3,I))
 6    CONTINUE
C
      RETURN
      END
```

APPENDIX III

Example of Program Control Information for BMDP3R [60] to do non-linear regression analysis with linear equality constraints. Parameter estimates obtained are shown in TABLE VI. B.

```
/PROBLEM  TITLE IS '1,4 ANHYDROERYTHRITOL-AMMONIUM COMPLEX , C13NMR SHIFTS'.
/INPUT    VARIABLES ARE 5.
          FORMAT    IS  '(5F12.6)'.
          CASES     ARE 78.
          UNIT      IS  3.
          REWIND.
/VARIABLE NAMES     ARE 'A(H2O)','A(+NH4)',TEMP,DELTAC13,'CARBON#'.
/PLOT     RESIDUAL.
          VARIABLES ARE 1,2,3.
          NORMAL.
          DNORMAL.
          SIZE      IS  100,100.
/REGRESS  DEPENDENT IS  DELTAC13.
          PARAMETERS ARE 22.
                     WEIGHT    IS 0.
                     CONSTRAIANTS ARE 4.
                     PRINT IS 1,2,3,5.
                     TITLE IS 'MULTICOMPONENT COMPLEX EQUILIBRIUM MODEL'.
                          ITERATION IS 1.
                          HALVING   IS 20.
/PARAMETER MAXIMUM ARE 5*1E2,  4*1E5,  9*1E2.
           MINIMUN ARE 5*-1E2, 4*-1E5, 9*-1E2.
            NAMES   ARE B10,B110,B101,B111,B120,
                        E10,E01,E11,E20,
                        S10,S01,S11,S20,
                        B20,B210,B201,B211,B220,
                        G10,G01,G11,G20,
            CONSTRAINT =5*0,1,3*0,-300,8*0,-1,3*0.  K=0.
            CONSTRAINT =6*0,1,3*0,-300,8*0,-1,2*0.  K=0.
            CONSTRAINT =7*0,1,3*0,-300,8*0,-1,0.    K=0.
            CONSTRAINT =8*0,1,3*0,-300,8*0,-1.      K=0.
               INITIAL ARE
               4.288679,4.230748,4.117557,4.170553,4.85321,
               -1284.178444,3056.228163,7612.447529,-3709.101927,
-5.452387,5.978147,14.308868,-23.58456,
               4.582278,5.005167,5.720235,5.541095,6.979743,
               351.53766,1262.784063,3319.787129,3366.266073.
/END
/FINISH
```

BIBLIOGRAPHY

[1] C. Detellier, J. Grandjean, and P. Laszlo. J.A.C.S. 98. 3375 (1976).

[2] A.P.G. Kieboom, A. Sinnema, J.M. van der Toorn, and H. van Bekkan. J. R. Neth. C. S. 96. 35 (1977).

[3] T. Spoonmaker, A.P.G. Kieboom, A. Sinnema, J.M. van der Toorn, and H. van Bekkan. Tet. Lett. 1974. 3713.

[4] A.H. Haines, K.C. Synes, and A.G. Wells. Carbohydrate Res. 41. 85 (1975).

[5] R.E. Ballard, A.H. Haines, E.K. Norris, and A.G. Wells. Acta Cryst. B 30. 1590 (1974).

[6] E.M. Arnett, H. Chung Ko, and C.E. Chao. J.A.C.S. 94. 4776 (1972).

[7] G.L. Eichhorn in "Inorganic Biochemistry." Vol. 2
Ch. 34

[8] A.L. Lehninger. In "Biochemistry", 2nd Ed. Worth Publishers. 1975.

[9] M. Nomura, A. Tissières, and P. Lenzyel. In "Ribosomes". Cold Spring Harbor Laboratory. 1974.

[10] Ref. [7]. Ch. 33.

[11] R.P. Agarwal and I. Feldman. J.A.C.S. 90. 6635 (1968).

[12] M. Gabriel, D. Larcher, J.C. Boubel, A.A. Peguy, and M. Torreilles. Inorganica Chimica Act. 26. 77 (1978).

[13] A. Saika and C.P. Slichter. J. Chem. Phys. 23. 26 (1954).

[14] C. Deverell. Mol. Phys. 18. 319 (1970).

[15] E.D. Becker. In "High Resolution NMR". Academic Press. New York. 1969.

[16] J.W. Emsley, J. FeeneY, and L.H. Sutcliffe. In "High Resolution Nuclear Magnetic Resonance." Vol. 1.

[17] S. Lewin. In "Displacement of Water and its Control of Biochemical Reactions". Academic Press. New York. 1974.

[18] J. Donohue. Proc. Natn. Acad. Sci. U.S.A. 42. 60 (1956).

[19] C.J. Collins and N.S. Bowman. In "Isotope Effects in Chemical Reactions". A.C.S. monograph 167. 1970.

[20] F. Franks. In "Water, a Comprehensive Treatise." Vol. 3. Plenum Press. New York. 1973.

[21] "Zahlenwerte und Funktionen aus Physik, Chimie, Astronomie, Geophysik, and Technik". 6th Ed. Springer Verlag. Berlin. 1950.

[22] G.E. Maciel and D.D. Traficante. J.A.C.S. 88. 220 (1966).

[23] S.N. Vinogradov and R.H. Linnel. In "Hydrogen Bonding". Van Nostrand Reinhold. 1971.

[24] R. Mathur, E D. Becker, RB Bradley, and NC Li. J. Phys. Chem. 67. 2190 (1963).

[25] E.R. Norris and C.J. Benoit. J. Biol. Chem. 158. 443 (1945).

[26] C. Neuberg. Bull. Res. Council Israel 4. 12 (1954).

[27] M.S. Fish, W.M. Johnson, E.P. Lawrence, and E.C. Horning. Biochem. Biophys. Acta 18. 564 (1955).

[28] B.B. Brodie, J.R. Gillette, and S.N. LaDu. Ann. Rev. Biochem. 27. 427 (1958).

[29] K.N. Murray, J.E. Watson, and S. Chayki. J. Biol. Chem. 241. 4798 (1966).

[30] J.K. Lanquist. J. Chem. Soc. 2816 (1953).

[31] S.M. Kupchan and M.J. Suffness. J. Pharm. Sci. 56. 541 (1967).

[32] A.D. Buckingham, T. Schaefer, and W.G. Schnieder. J. Chem. Phys. 32. 1227 (1960).

[33] R.K. Harris. In "Nuclear Magnetic Resonance". Vol. 3. The Chemical Society. Burlington House. London.

[34] J.W. Emsley, J. Feeney, and L.H. Sutcliffe. In "High Resolution Nuclear Magnetic Resonance". Vol. I.

[35] Ref. [34]. p. 483.

[36] H.M. McConnell. J. Chem. Phys. 28. 430 (1958).

[37] H.S. Gutowsky and A. Saika. J. Chem. Phys. 21. 1688 (1953).

[38] A. Carrington and A.D. McLachlan. In "Introduction to Magnetic Resonance". Harper and Row. New York. 1967.

[39] F.J.C. Rossotti and H. Rossotti. In "The Determination of Stability Constants". McGraw-Hill. 1961.

[40] R.D. Green and J.S. Martin. J.A.C.S. 90. 3659 (1968).

[41] H.A. Benesi and J.H. Hildebrand. J.A.C.S. 71. 2703 (1949).

[42] R.L. Scott. Rec. Trav. Chim. Pays-Bas 75. 787 (1956).

[43] S.N. Vinogradov and R.H. Linnell. In "Hydrogen Bonding". Van Nostrand. New York. 1971.

[44] V.S.Griffiths and G.Socrates. J. Mol. Spect. 21. 302 (1966).

[45] M.W. Hanna and D.G. Rose. J.A.C.S. 94. 2601 (1972).

[46] T.L. Hill. In "An Introduction to Statistical Mechanics". Addison Wesley. 1960.

[47] W.J. Moore. In "Physical Chemistry". 4th ed. Prentice-Hall. 1972.

[48] W.H. Ray and J. Szekely. In "Process Optimization". John Wiley & Sons. 1973.

[49] Y. Bard. In "Nonlinear Parameter Estimation". Academic Press. New York. 1974.

[50] R. Deutsch. In "Estimation Theory". Pretice Hall. 1965.

[51] W.C. Hamilton. In "Statistics in Physical Sciences". Ronald Press. 1964.

[52] M.R. Spiegel. In "Theory and Problems of Statistics". McGraw-Hill. 1961.

[53] P. Wiener. In "Unconstrained Nonlinear Optimization Techniques and their Application to Semiempirical Molecular Orbital Calculations". Univ. of Texas. Austin. 1975. Diss. Ab. 76-8123.

[54] W.W. Cooley and P.R. Lohnes. In "Multivariate Data Analysis". Wiley & Sons. 1971.

[55] R.J. Harris. In "A Primer of Multivariate Statistics". Academic Press. New York. 1975.

[56] N.R. Draper and H. Smith. In "Applied Regression Analysis". Wiley & Sons. 1966.

[57] D.W. Marquardt. J. Soc. Indust. Appl. Math. 11. 431 (1963).

[58] H.O. Hartley. Technometrics 3. 269 (1961).

[59] W.J. Dixon. In "BMD, Biomedical Computer Programs". Univ. of Calif. Press. Los Angeles. 1973.

[60] W.J. Dixon and M.B. Brown. Eds. "BMDP-77 Biomedical Computer Programs P-Series". Univ. of Calif. Press. 1977.

[61] M.J.S. Dewar and H.S. Rzepa. J. Am. Chem. Soc. 100. 58 (1978).

[62] M.J.S. Dewar et al., QCPE 10. 309 (1976)

[63] F.H. Otez and C.L. Mehltretter. J . Org. Chem. 26. 1673 (1961).

[64] S. Peat. Adv. Carb. Chem. Biochem. 2. 37 (1957).

[65] R.G.S. Ritchie, N. Cyr, B. Korsch, H.J. Koch, and A.S. Perlin. Can. J. Chem. 75. 1424 (1975).

[66] P.A.J. Gorin and M. Mazurek. Carb. Res. 27. 325 (1973).

[67] F.W. McLafferty. In "Interpretation of Mass Spectra, An Introduction". W.A. Benjamin. New York. 1967.

[68] T.A.W. Koerner, Jr., and E.S. Younathan. J. Biol. Chem. 249. 5749 (1974).

[69] B.C. Bera, A.B. Foster, and M. Stacey. J. Chem. Soc. 4531 (1956).

[70] R.C. Weast. Ed. "Handbook of Physics and Chemistry". 50th Ed. The Chemical Rubber Co., Cleaveland. 1969.

[71] P.K. Glasoe and F.A. Long. J. Phys. Chem. 64. 188 (1960).

[72] D.P. Shoemaker and C.W. Garland. In "Experiments in Physical Chemistry". 2nd ed. McGraw-Hill. 1967.

[73] J.D. Roberts and M.C. Caserio. In "Basic Principles of Organic Chemistry". W.A. Benjamin Inc. 1968.

[74] H.S. Harned and R.A. Robinson. In "Multicomponent Electrolyte Solutions". Pergamon Press. London. 1968.

[75] H.S. Harned and B.B. Owen. In "The Physical Chemistry of Electrolytic Solutions". A.C.S. Monograph Series no. 137. 3rd ed. 1958.

[76] E.L.Eliel N.L. Allinger, S.J. Angyal, and G.A. Morrison. In "Conformational Analysis". J. Wiley & Sons. 1965.

[77] J.E. Freund. In "Mathematical Statistics". 2nd Ed. Prentice-Hall, Inc. 1971.

[78] W.J. Moore. In "Physical Chemistry". Prentice Hall. 1972.

[79] B.F. Wishaw and R.H. Stokes. Trans. Faraday Soc. 49. 27 (1953).

[80] V. Parker. In "Thermal Properties of Aqueous Uni-univalent Electrolytes". U.S.G.P., NSRDS-NBS2. 1965.

[81] F.C. Kracek. In "International Critical Tables". Vol. III. 1928.

[82] J.H. Ahlberg, E.N. Nilsen, and J.L. Walsh. In "The Theory of Splines and Their Applications". Academic Press. New York. 1967.

[83] S. Wold. Technometrics 16. 1 (1974).

[84] R.D. Larsen. Comp. and Chem. 1. 23 (1976).

[85] T. Lyche and L.L. Schumaker. SIAM J. Numer. Anal. 10. 1027 (1973).

[86] C.H. Reinsch. Numer. Math. 10. 177 (1967).

[87] C. De Boor and J.R. Rice. C.S.D. TR Purdue 20. (1968).

[88] C. De Boor and J.R. Rice. C.S.D. TR Purdue 21. (1968).

[89] In "IMSL Library 1", Edition 6. International Mathematical and Statistical Libraries Inc. 1977.

[90] A. Saika and C.P. Slichter. J. Chem. Phys. 23. 26 (1954). same as 13.

[91] C. Deverell. Mol. Phys. 18. 319 (1970). same as 14.

[92] R.J. Pugmire and D.M. Grant. J. Am. Chem. Soc. 90. 697 (1968).

[93] W. Adam, A. Grimison, and G. Rodriguez. Tetrahedron 23. 2513 (1967).

[94] W. Adam, A. Grimison and G. Rodriguez. J. Chem. Phys. 50. 645 (1969).

[95] J.E. Bloor and D.L. Breen. J. Am. Chem. Soc. 89. 6835 (1967).

[96] T. Tokuhiro, N.K. Wilson, and G. Fraenkel. J. Am. Chem. Soc. 90. 3622 (1968).

[97] N.F. Ramsey. Physical Review 78. 699 (1950); ibid , 86. 243 (1952).

[98] B.V. Cheney and D.M. Grant. J. Am. Chem. Soc. 89. 5319 (1967).

[99] D.L. Beveridge and K. Miller. Mol. Phys. 14. 401 (1968).

[100] J.A. Pople. Proc. Roy. Soc. (London) Ser. A 239. 541 (1957).

[101] M. Karplus and T.P. Das. J. Chem. Phys. 34. 1683 (1961).

[102] M. Karplus and J.A. Pople. J. Chem. Phys. 38. 2803 (1963).

[103] J.A. Pople. J. Chem. Phys. 37. 53 (1962).

[104] J.A. Pople. Mol. Phys. 7. 301 (1964).

[105] J.E. Bloor and D.L. Breen. J. Am. Chem. Soc. 89. 6835 (1967).

[106] T. Yonezawa, I. Morishima, and H. Hato. Bull. Chem. Soc. Japan 39. 1398 (1966).

[107] K. Seislman and G.E. Maciel. J.A.C.S. 99. 3254 (1977).

[108] R.J. Cushley, D. Naugler, and C. Ortiz. Can. J. Chem. 53. 3419 (1975).

[109] P.A. Dobosh. In "CNINDO Molecular Orbital Program, Quantum Chemistry Exchange Program 141". Carnegie-Mellon University, Pittsburgh, Pa.

[110] P. Claverie et al. In "Perturbation Configuration Interation using Localized Orbitals Method (PCILO)." Quantum Chemistry Exchange Program 220/221.

[111] G.J. Martin, M.L. Martin, and S. Odiot. Org. Mag. Reson. 7. 2 (1975).

[112] N. Cyr, A.S. Perlin, and M.A. Whitehead. Can. J. Chem. 50 814 (1972).

[113] Ref. [15].

[114] C. Altona and Sundralingan. J.A.C.S. 94. 8205 (1972).

[115] D. Cremer and J.A. Pople. J.A.C.S. 97 . 1354 (1975).

[116] L.D. Hall, P.R. Steiner, and C. Pedersen. Can. J. Chem. 48. 1155 (1970).

[117] O. Röder, H. Lüdem, and E. Von Goldam. Eur. J. Biochem.53. 517 (1975).

[118] A. Saran, D. Perahia, and B. Pullman. Theoret. Chim. Acta (Berl.) 30. 31 (1973).

[119] D. Cremer and J.A. Pople. J.A.C.S. 97. 1558 (1975).

[120] M.J.S. Dewar. In "MINDO/3, Molecular Orbital Program. Quantum Chemistry Program Exchange Program 309". University of Texas. Austin.

[121] L.L. Coombs and M. Rossies Jr. J. Mol. Struct. 32. 1 (1976).

[122] L.L. Coombs and M. Rossies Jr. Spect. Lett. 9. 495 (1976).

[123] J.A. Pople. J.A.C.S. 97. 5306 (1975).

[124] W.J. Hehre. J.A.C.S. 97. 5308 (1975).

[125] M.J.S. Dewar. J.A.C.S. 97. 6591 (1975).

[126] L.R. Sousa and M.R. Johnson. J.A.C.S. 100. 344 (1978).

[127] J.A. Pople and D.L. Beveridge. J.Chem. Phys. 47. 2026 (1967).

[128] B. Jönsson and B. Nelender. Chem. Phys. 25. 263 (1977).

[129] S. Lewin. In "Displacement of Water and Its Control of Biochemical Reactions".

[130] C.J. Collins and N.S. Bowman. In "Isotope Effects in Chemical Reactions". ref. [19].

[131] A. Abragam. In "The Principles of Nuclear Magnetism". Oxford University Press. Oxford. 1961.

[132] A. Carrington and A.D. McLachlan. In "Introduction to Magnetic Resonance". Harper and Row. 1967.

[133] J.C. MacDonald. J. Mag. Res. 34. 207 (1979).

[134] G. Bodenhausen, R. Freeman, R. Niedermeyer and D.L. Turner. J. Mag. Res. 26. 133 (1977).

[135] J.W. Emsley, J. Feeney, and L.H. Sutcliffe. In "High Resolution Nuclear Magnetic Resonance", vol. 2. Pergamon Press. 1966.

[136] E.D. Becker. In "High Resolution NMR". Academic Press. 1969.

[137] A. Anderson. In "The Raman Effect, Volume 2: Applications". Marcel Dekker, Inc. 1973.

[138] P.R. Griffiths. In "Chemical Infrared Fourier Transform Spectroscopy". John Wiley and Sons. 1975.

[139] W.J. Lafferty, D.W. Robinson, R.V. St. Louis, J.W. Russell, and H.L. Strauss. J. Chem. Phys. 42. 2915 (1965).

[140] F. Ciardelli and P. Salvadori, eds. In "Fundamental Aspects and Recent Developemnts in Optical Rotary Dispersion and Circular Dirchromism". Heydon and Sons. 1973.

[141] D.R. Sandstron and H.W. Dodgen. J. Chem. Phys. 67. 473 (1977).

[142] B.M. Kincaid, P. Eisenberger, K.O. Hodgson, and S. Doniach. Proc. Nat. Acad. Sci. U.S.A. 22. 2340 (1975).

[143] S.P. Cramer, J.H. Dawson, K.O. Hodgson, and L.P. Hager. J.A.C.S. 100. 7282 (1978).